

General Disclaimer

One or more of the Following Statements may affect this Document

- This document has been reproduced from the best copy furnished by the organizational source. It is being released in the interest of making available as much information as possible.
- This document may contain data, which exceeds the sheet parameters. It was furnished in this condition by the organizational source and is the best copy available.
- This document may contain tone-on-tone or color graphs, charts and/or pictures, which have been reproduced in black and white.
- This document is paginated as submitted by the original source.
- Portions of this document are not fully legible due to the historical nature of some of the material. However, it is the best reproduction available from the original submission.

ASI-TR-75-21
(NASA CR 132651)

(NASA-CR-132651) A SPIRAL GUIDANCE APPROACH
CONCEPT FOR COMMERCIAL VTOL OPERATIONS
Final Report (Aerospace Systems, Inc.,
Burlington, Mass.) 128 p HC \$5.75 CSCL 01C

N76-10140

Unclas
G3/08 39380

A SPIRAL GUIDANCE APPROACH CONCEPT FOR COMMERCIAL VTOL OPERATIONS

FINAL REPORT

William C. Hoffman
Walter M. Hollister

May 1975

Contract No. NAS 1-12199

National Aeronautics and Space Administration
Washington, D. C. 20546

ASI

AEROSPACE SYSTEMS, INC.

ONE VINE BROOK PARK • BURLINGTON, MASS. 01803

(CORNER MIDDLESEX TURNPIKE AND LEXINGTON STREET)

TELEPHONE (617) 272-7517

ASI-TR-75-21

NASA CR 132651

A SPIRAL GUIDANCE APPROACH CONCEPT
FOR COMMERCIAL VTOL OPERATIONS

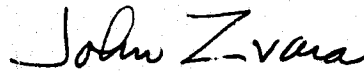
FINAL REPORT

by

William C. Hoffman
Walter M. Hollister

AEROSPACE SYSTEMS, INC.
One Vine Brook Park
Burlington, Massachusetts 01803

Approved



John Zvara
Technical Director

Prepared under
Contract No. NAS 1-12199

for

National Aeronautics and Space Administration
Washington, D. C. 20546

May 1975

FOREWORD

This report was prepared by Aerospace Systems, Inc. (ASI), Burlington, Massachusetts, for the National Aeronautics and Space Administration (NASA) under Contract No. NAS 1-12199. The study was sponsored by the Flight Instrumentation Division, Navigation and Guidance Research Branch, the NASA Langley Research Center (LaRC), Hampton, Virginia. Mr. Henry J. E. Reid, Jr. served as Technical Monitor on the contract.

This is a final technical report which documents the results of research performed during the period July 1974 to March 1975. It covers activity conducted under Modification 5 to the original contract.

The effort was directed by Mr. John Zvara, President and Technical Director of ASI. Mr. William C. Hoffman served as Project Engineer. Dr. Walter M. Hollister of the Department of Aeronautics and Astronautics at the Massachusetts Institute of Technology (MIT) contributed to the study as technical consultant and co-investigator. Dr. Robert W. Simpson, Director of the MIT Flight Transportation Laboratory and Dr. Arthur E. Bryson, Jr., Chairman of the Department of Aeronautics and Astronautics, Stanford University, also served as technical consultants.

TABLE OF CONTENTS

<u>Section</u>		<u>Page</u>
	FOREWORD	iii
	LIST OF ILLUSTRATIONS	ix
	LIST OF TABLES	xiii
1	INTRODUCTION	i
2	OPERATIONAL CONSIDERATIONS	5
	2.1 VTOL All-Weather Operations	5
	2.2 Basic Spiral Parameters	8
3	SPIRAL GUIDANCE FORMULATION	15
	3.1 Basic Concept	15
	3.2 Equations of Motion	16
	3.3 Spiral Angle as Independent Variable	17
	3.4 Time in Spiral for Arbitrary Turn Angle	18
	3.5 Nominal Spiral Specification	22
	3.6 Wind Effects on Nominal Spiral	23
	3.7 Feedback Guidance Laws	25
4	PERTURBATION GUIDANCE ANALYSIS	27
	4.1 Simplified 3D Guidance Without Wind	27
	4.1.1 Horizontal Plane Guidance	28
	4.1.2 Vertical Plane Guidance	30
	4.1.3 Example	31

PRECEDING PAGE BLANK NOT FILMED

v

TABLE OF CONTENTS (Continued)

<u>Section</u>	<u>Page</u>
4.2 4-D Guidance.....	32
4.3 Guidance Gains	42
4.4 Error Sensitivity	45
5 WIND ESTIMATION	47
5.1 Kalman Wind Estimator Formulation	47
5.2 Simplified Wind Estimator	50
5.3 Wind Estimator Dynamics	55
6 PHASE PLANE ANALYSIS	59
6.1 The Phase Plane	59
6.2 Guaranteed Spiral Capture	61
6.2.1 Right Hand Turns	61
6.2.2 Left Hand Turns	64
7 SPIRAL TRANSITION SEGMENTS	67
7.1 Nominal Path for Entry Transition to Spiral	67
7.1.1 Right-Hand Spiral Entry	67
7.1.2 Left-Hand Spiral Entry	69
7.2 Nominal Path for Exit Transition from Spiral	70
7.2.1 Right-Hand Spiral Exit	70
7.2.2 Left-Hand Spiral Exit	72
7.3 Transition Segment Guidance Law	72
7.4 Hover and Touchdown Phase	74

TABLE OF CONTENTS (Continued)

<u>Section</u>	<u>Page</u>
8	SIMULATION 77
8.1	Interactive Simulation 77
8.2	Program VALT Simulation 78
8.2.1	Initialization Calculations 80
8.2.2	Calculating Nominal Parameters 83
8.2.3	Wind Estimates 88
8.2.4	Guidance Laws 89
8.2.5	Measurements 90
8.3	Spiral Approach Example 92
9	SUMMARY AND CONCLUSIONS 109
10	RECOMMENDATIONS FOR ADDITIONAL RESEARCH 113
10.1	Spiral Guidance Flight Test Program 113
10.1.1	Purpose of Test 113
10.1.2	Test Equipment and Facilities 113
10.1.3	Flight Procedures 114
10.1.4	Data Obtained 114
10.1.5	Data Analysis 115
10.2	Guidance for Spiral Exit and Landing 115
10.3	Wind Estimation in the VALT Flight Program 116
	REFERENCES 119

LIST OF ILLUSTRATIONS

<u>Figure No.</u>		<u>Page</u>
1	Noninterfering VTOL Approach to Conventional Airport	6
2	Example Spiral Descent for JFK Int'l Airport	7
3	Spiral Descent Approach to CTOL Airport	9
4	Spiral Descent Approach to Heliport	10
5	Nominal Spiral Parameters - No Wind	11
6	Effect of Wind on Spiral with Constant Airspeed	12
7	Block Diagram of Spiral Guidance Concept	15
8	Nomenclature for Spiral Descent	16
9	Nomenclature for Determining $t^*(\theta)$	19
10	Nomenclature for Spiral Descent Guidance Scheme	27
11	Linearized Block Diagram of Horizontal Guidance System	33
12	Spiral Guidance Response for Various Sets of Gains	43
13	Effect of Finite Bank Rate	44
14	Nomenclature for Wind Analysis	47
15	Estimated Wind Speed with Simplified Estimator	52
16	Estimated Wind Direction with Simplified Estimator	53
17	Radial Position Accuracy with Simplified Wind Estimator	54
18	Linear Signal Flow Diagram for Wind Estimator	56
19	Wind Estimator in a Steady Shear	57
20	Linear Signal Flow Diagram for Wind Estimator During Transition Segment	58
21	Phase-Plane Plot of Guidance Law	59
22	Phase-Plane Performance of Horizontal Spiral Guidance Law	60

PRECEDING PAGE BLANK NOT FILMED

LIST OF ILLUSTRATIONS (Continued)

<u>Figure No.</u>		<u>Page</u>
23	Phase-Plane Examples	62
24	Modified Guidance Law	63
25	Example of Modified Guidance Law for $\Delta\psi_{\max} = 60^\circ$ and 90° ...	64
26	Independent Variables for Straight Segments and Circular Arcs...	67
27	Entry Transition to Right-Hand Spiral	68
28	Entry Transition to Left-Hand Spiral	69
29	Exit Transition from Spiral	70
30	Modified Transition Segment Guidance in Phase Plane	73
31	Pad-Centered Frame for Hover and Touchdown	74
32	Overall Flow Diagram of Program VALT	79
33	Segments of Nominal Spiral	80
34	Overall Flow Diagram of Spiral Guidance Algorithm	81
35	Rotated Coordinate Frame for Spiral Entry	84
36	Rotated Coordinate Frame for Spiral Exit	86
37	Example Spiral Approaches to JFK	93
38	Nominal Spiral Approach to JFK - Position Error Histories	95
39	Nominal Spiral Approach to JFK - Velocity Error Histories	96
40	Initial Crosstrack Error of -1 nm	99
41	Initial Along-Track Error of 1 nm	100
42	Initial Groundspeed Error of 20 kts	101
43	Initial Altitude Error of -300 ft.....	102
44	Initial Ground Track Error of -30 Deg	103
45	Constant Wind Direction Error of -90 Deg	104

LIST OF ILLUSTRATIONS (Continued)

<u>Figure No.</u>		<u>Page</u>
46	Wind Direction Shear Error of -90 Deg/100 Ft	105
47	Nominal Wind Speed Error of -15 kt	106
48	Nominal Wind Direction Error of -90 Deg	107
49	Possible Heliport Locations Relative to the Descent Spiral	115

LIST OF TABLES

<u>Table No.</u>		<u>Page</u>
1	Constant Groundspeed Versus Constant Airspeed	13
2	Operational Procedures for 3-D and 4-D Guidance	14
3	Approximate Solution to Elliptic Integral of the Second Kind	21
4	Wind Effects on 360° Turns ($V = 60$ kt, $r = 2000$ ft)	24
5	Nominal Turn With Bank Control Only	35
6	Effect of Initial Radial Error With Bank Control Only	35
7	Effects of Initial Heading Error With Bank Control Only	36
8	Effects of Airspeed Error With Bank Control Only	36
9	Effect of 5-Knot Wind With Bank Control Only (90°)	37
10	Effect of 5-Knot Wind With Bank Control Only (180°)	37
11	Effect of 20-Knot Wind With Bank Control Only	38
12	Effect of Including Wind Estimate in Nominal Calculation	38
13	Effects of Airspeed Error With Coupled Bank & Throttle Control	40
14	Effects of Airspeed Error With Uncoupled Bank & Throttle Control	40
15	Effects of Wind With Coupled Bank & Throttle Control	41
16	Effects of Wind With Uncoupled Bank & Throttle Control	41
17	Recommended Values for Guidance Gains	91
18	Spiral Guidance Parametric Analyses	97
19	Results of Parametric Analyses	98

PRECEDING PAGE BLANK NOT FILMED

SECTION 1 INTRODUCTION

Vertical takeoff and landing (VTOL) systems have been recommended by many experts in the aeronautical and transportation fields, including members of the President's Scientific Advisory Committee, as the logical form of transportation for the high-density, short-haul transportation markets in the 1980s. Such systems span a broad range of operations, from the intra-urban to the inter-city shuttles operating between downtown or nearby vertiports as well as to conventional airports.

Before a viable VTOL system can become a reality, technology developments are needed in several areas. For example, the technology for an economical, 150-passenger class VTOL with reasonably high cruise speed and acceptable passenger ride qualities for the inter-city market must be developed. At the other end of the spectrum, advanced helicopter development is needed to improve ride comfort and reduce maintenance requirements for the very short-haul, medium-density market. These vehicle design areas are receiving considerable attention in various programs sponsored by NASA, the U.S. Army, and the aircraft industry. However, to effectively utilize these vehicles, and to exploit their unique characteristics for minimizing noise and both air and ground space requirements, corresponding advances must be made in handling qualities, operating procedures and techniques, and avionics.

The NASA Langley Research Center (LaRC) has undertaken a research program to develop the navigation, guidance, control, and flight management technology base needed by Government and industry in establishing systems design concepts and operating procedures for VTOL short-haul transportation systems in the 1980s time period. The VALT (VTOL Automatic Landing Technology) program encompasses the investigation of operating systems and piloting techniques associated with VTOL operations under all-weather conditions from downtown vertiports; the definition of terminal air traffic and airspace requirements; and the development of avionics including navigation, guidance, controls, and displays for automated takeoff, cruise, and landing operations.

Aerospace Systems, Inc. (ASI) is conducting a research effort for LaRC in support of the VALT program. In a previous report (Reference 1), ASI analyzed the navigation and guidance requirements for commercial VTOL operations in the takeoff,

cruise, terminal area, and landing phases of flight in weather conditions up to and including Category III. The study was limited to two types of rotorcraft vehicles (pure helicopter and compound helicopter) and three types of services (intra-urban, inter-city, and conventional airports) were considered. Applicable navigation technology and systems (such as Omega, Loran, inertial, and microwave landing systems) were examined to define present system shortcomings, to identify areas where technology advances are required, and to select candidate systems and conceptual approaches. A multi-configuration "straw-man" system design was prepared, and representative operational procedures and trajectories defined. A limited flight evaluation program was conducted to investigate VTOL operational procedures and current navigation systems and to verify analytical results. A comprehensive digital computer simulation (Program VALT) was developed to provide a means for evaluation of VTOL guidance and navigation system performance.

One of the conclusions reached in Reference 1 was that curved decelerating approaches will be required for safe, efficient, and independent VTOL operations. To facilitate these maneuvers, a spiral descent technique was proposed as a possible standard VTOL approach procedure. The spiral descent uses minimal airspace, accommodates arrivals from any direction, and can service multipad landings. The spiral approach also provides the benefits of a vertical descent, but avoids the vortex ring state, maintains a stable airspeed, and uses less fuel. Flight evaluations were conducted for several spiral descents, and demonstrated the concept feasibility in terms of ride quality, vehicle capability and pilot workload.

As a result, Reference 1 recommended that additional research should be conducted to define the navigation and guidance system requirements for IFR VTOL spiral descents in the presence of winds. It suggested a study effort to establish recommended values for airspeed, bank angle, descent rate and protected airspace; to formulate a number of feasible guidance laws for spiraling flight; and to develop filtering algorithms for navigation during this phase. The guidance and navigation algorithms could be evaluated with the simulation Program VALT. The necessary commands to display on a flight director and/or the signals to feed an automatic pilot should be established. Finally, one or more spiral guidance laws should be recommended for further evaluation in the LaRC VTOL real-time simulation, and eventual implementation in the VTOL flight test program.

Subsequently, NASA LaRC decided to pursue the spiral guidance approach concept with additional research. The present report describes the results of ASI's investigation of the guidance and navigation requirements for VTOL spiral descents in the presence of winds. Models have been developed to describe the spiral maneuver and candidate guidance laws have been formulated and analyzed. An important element of the guidance scheme is a unique wind estimator which uses the perturbations in bank angle and heading to improve the knowledge of the winds. Finally, recommendations for additional research, including a flight program, have been outlined to evaluate the spiral guidance concept.

SECTION 2 OPERATIONAL CONSIDERATIONS

2.1 VTOL ALL-WEATHER OPERATIONS

The achievement of efficient all-weather VTOL commercial service to conventional airports requires that VTOL aircraft be operated essentially independent of existing CTOL aircraft route structures and procedures. The establishment of such independent VTOL operations during the takeoff and landing phases must take into account noise restrictions, obstacle clearance, VTOL aircraft performance capabilities, and interaction with CTOL air traffic. Previous studies of navigation and guidance requirements for VTOL operations at CTOL airports (Reference 1) have suggested the use of spiral descents by VTOL aircraft as a means of achieving efficient, safe operations that are independent of CTOL aircraft route structures and procedures.

At the present time, IFR operations of CTOL aircraft create a wall of airspace along the active runway that is typically 10 miles long, 1500 feet high and some hundreds of feet wide. The protected airspace is utilized by CTOL aircraft making ILS approaches, departures and missed approaches; it creates a problem for VTOL traffic desiring to cross the active runway with no interference to the CTOL traffic flow. A suggested noninterfering VTOL approach to a conventional airport is illustrated in Figure 1. Under this concept the airspace directly over the active runway is partitioned such that the CTOL traffic remains below 500 feet AGL over the runway, and VTOL traffic has free access to cross over the runway perpendicular to the CTOL traffic at 1000 feet AGL. Failure to allow IFR crossing of the CTOL runway in this way would necessitate an approach capability to both sides of each CTOL IFR approach course, followed by an air taxi across active runways. Such operations across active runways would have to be conducted under CTOL air traffic control, which could cause excessive delays and would make the VTOL traffic dependent on the CTOL operations.

After the 1000 feet crossing, the VTOL will take 2 minutes to descend at a rate of 500 ft/min. To expedite the approach, it is desirable to begin the turn to the pad as soon as possible. Using a standard turn rate (3 deg/sec) at an airspeed of 60 knots, the approach will consist of a spiral descent with turn radius of about 2000 feet, which fits conveniently into the typically available airspace. For example, Figure 2 illustrates a 2000 ft spiral superimposed on a diagram of New York's Kennedy

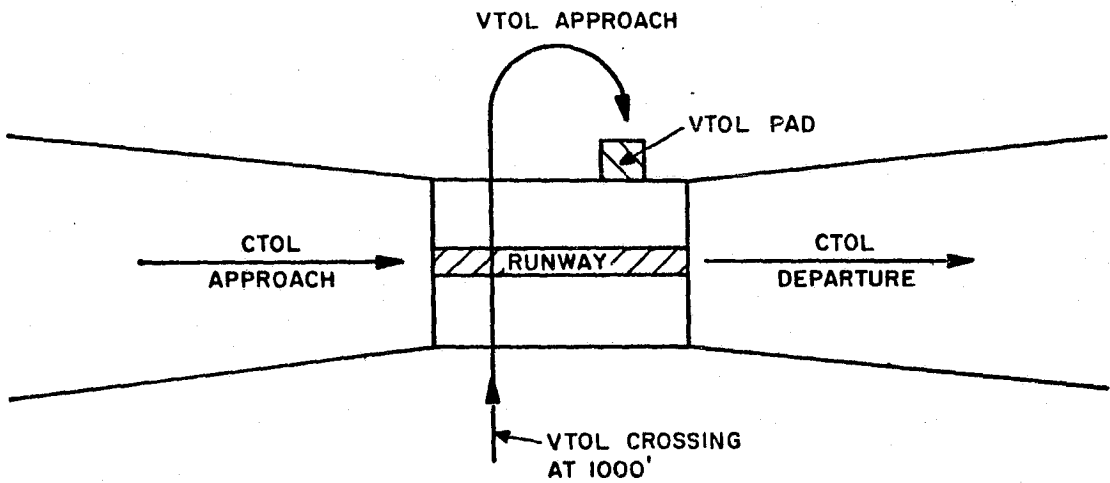
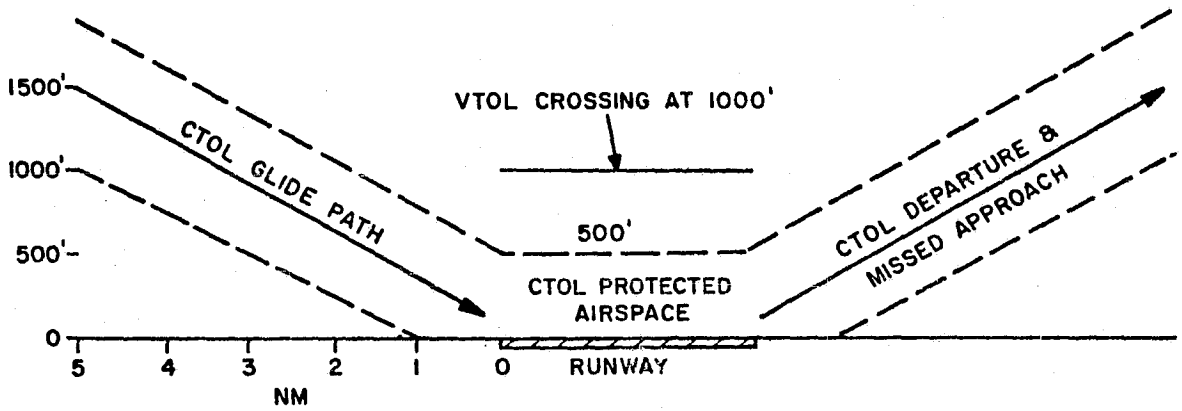


Figure 1. Noninterfering VTOL Approach to Conventional Airport.

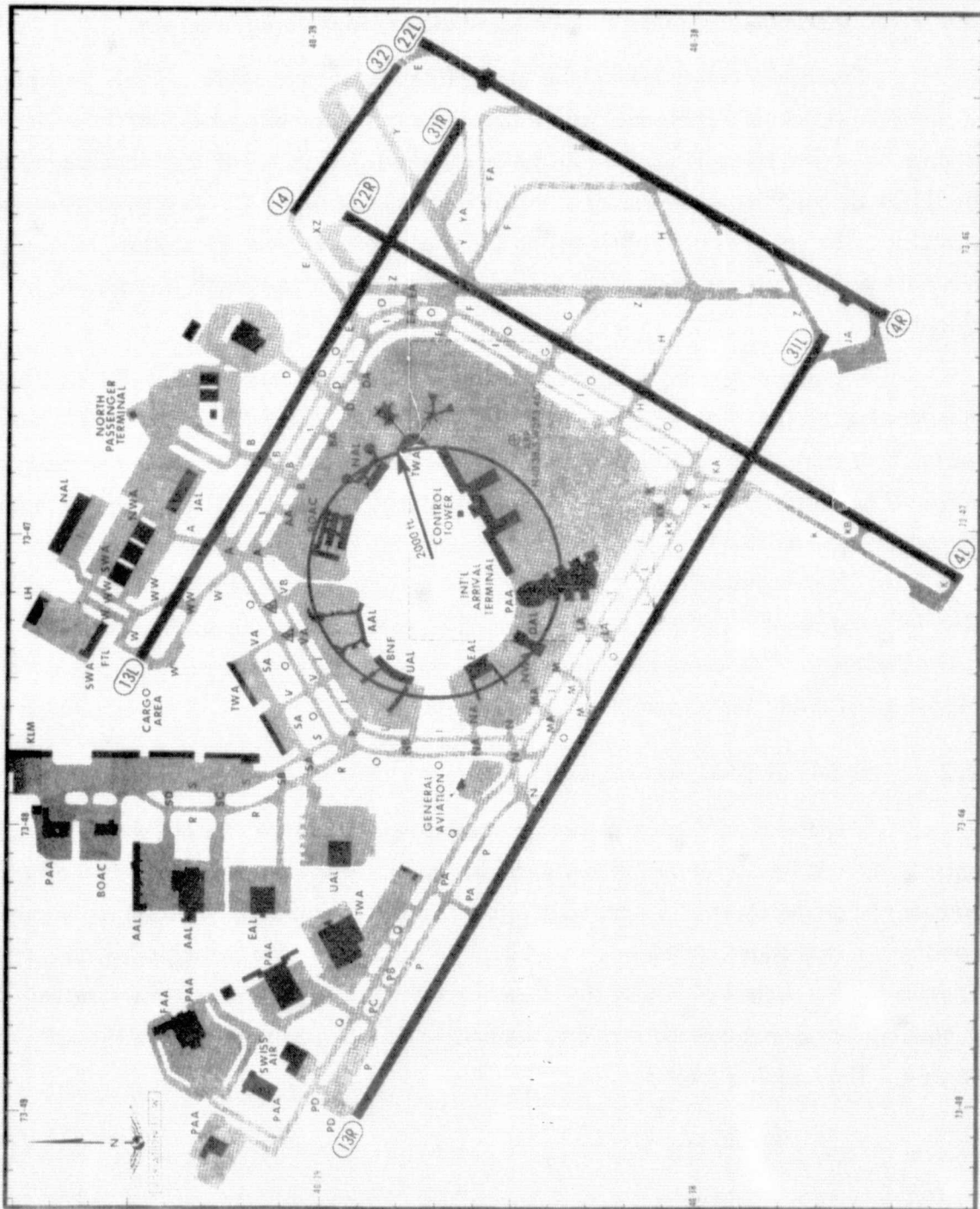


Figure 2. Example Spiral Descent for Kennedy International Airport (JFK).

International Airport. This solution has the advantage of keeping the two traffic flows independent and without mutual interference. It also influences the characteristics of the VTOL approach procedure and the associated guidance requirements.

This spiral technique can be generalized to accommodate arrivals from all directions and could handle multiple helicopters in a "descent tube," as shown in Figure 3. The descent tube would be established in a sector of the airspace not used by CTOL aircraft, with rotorcraft entries occurring above the CTOL approach/departure patterns. The spiral is not restricted to CTOL airports, but can be applied to single or multiple pad V-ports as well, with provisions for a missed approach if required (Figure 4).

The spiral descent retains most of the advantages of a vertical descent, but requires less power, maintains forward airspeed and controllability, and avoids the vortex ring state. The problem with the spiral descent operation is that it presents a difficult guidance and navigation task, particularly in a wind. The steady-state turn introduces an additional integration into the control loop, making it more difficult to stabilize. The maneuvering aircraft may have difficulty in obtaining accurate navigation information at a sufficient data rate. The present study was undertaken to evaluate such problems and to formulate guidance concepts for spiral descents during the planned NASA VALT flight test program.

2.2 BASIC SPIRAL PARAMETERS

The design of the spiral descent in the vertical plane is quite simple, requiring only an appropriate selection of the vertical speed. However, in the horizontal plane, a number of parameters must be properly chosen to satisfy airspace limitations, aircraft constraints, passenger comfort, etc. Figure 5 illustrates the principal spiral parameters in the horizontal plane for the case of no wind. Without wind, the airspeed V is equal to the groundspeed, and the heading angle ψ is perpendicular to the spiral angle θ . The heading rate is

$$\dot{\psi} = \frac{g}{V} \tan \phi \quad (1)$$

where g is the acceleration of gravity.

The bank angle ϕ required to maintain the steady spiral descent is given by

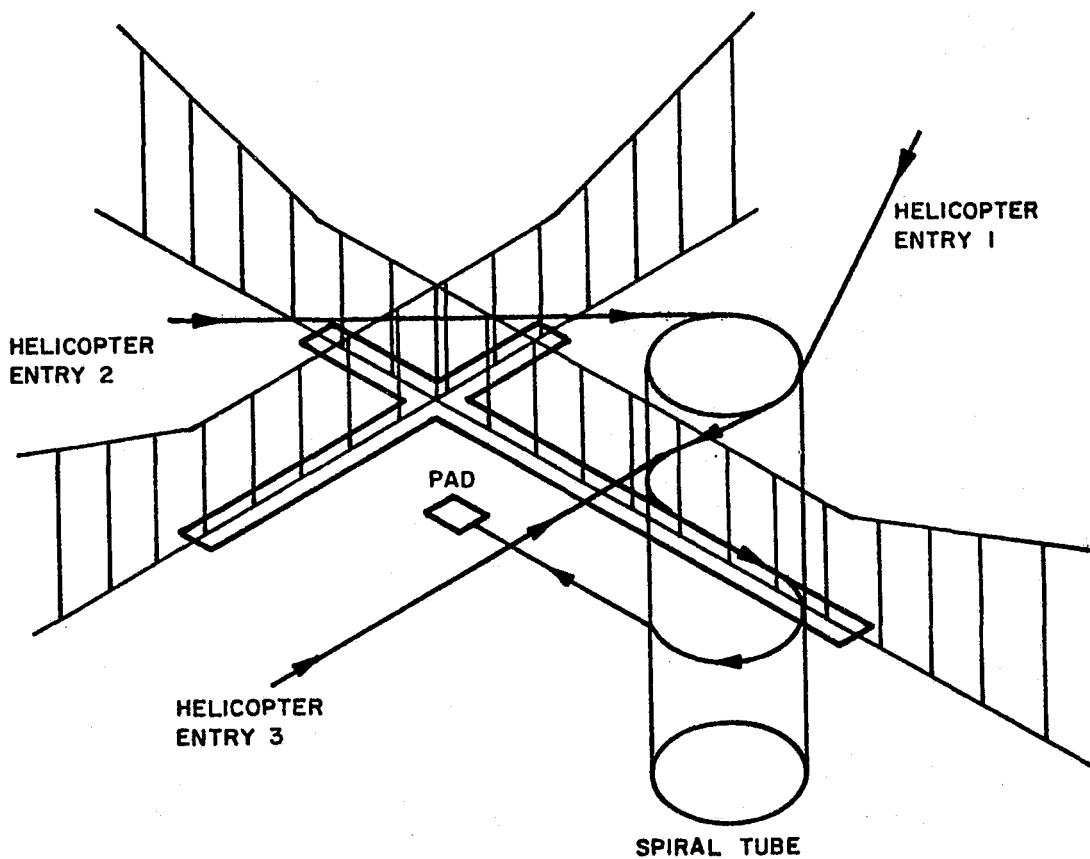


Figure 3. Spiral Descent Approach to CTOL Airport.

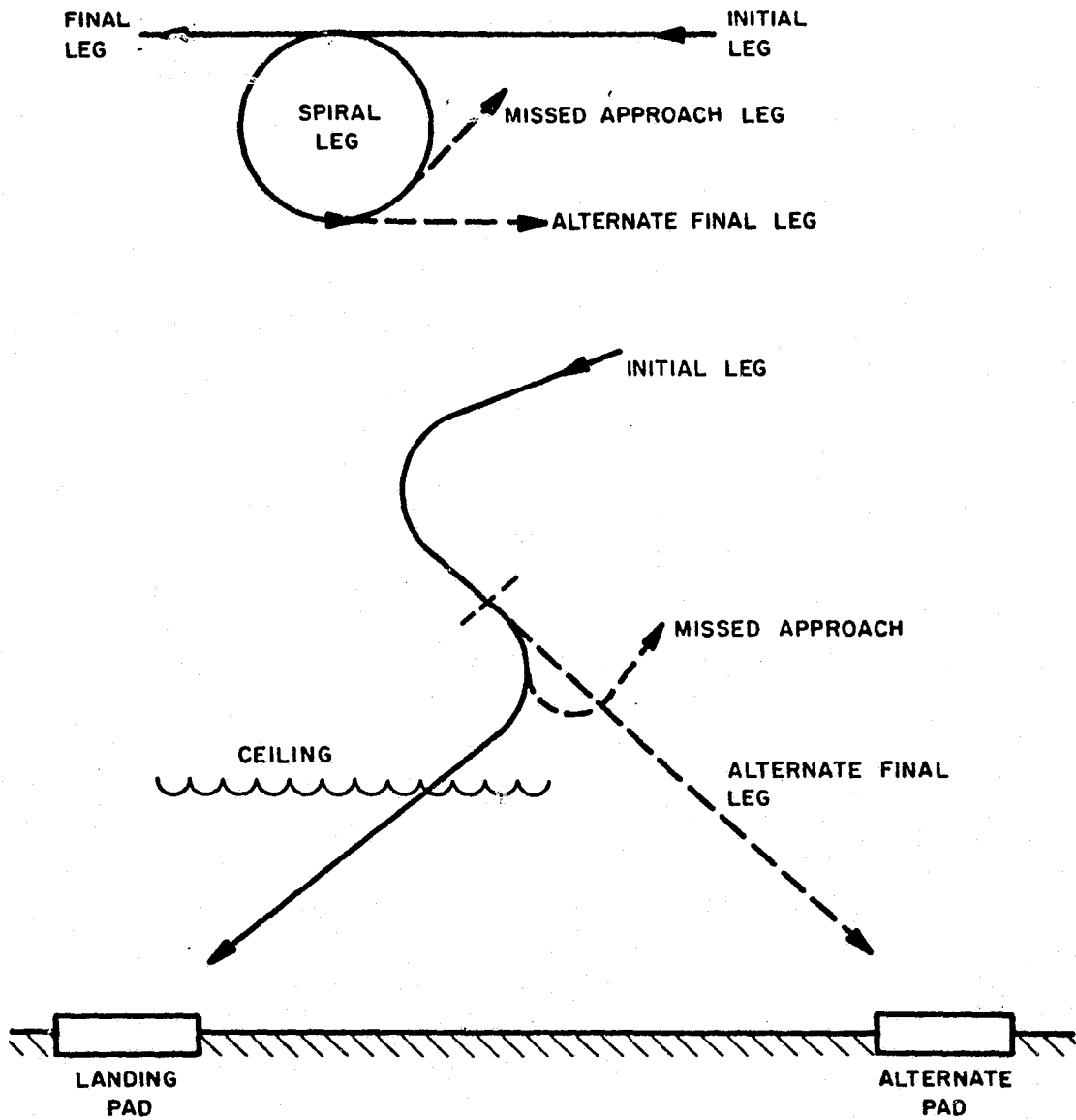


Figure 4. Spiral Descent Approach to Heliport.

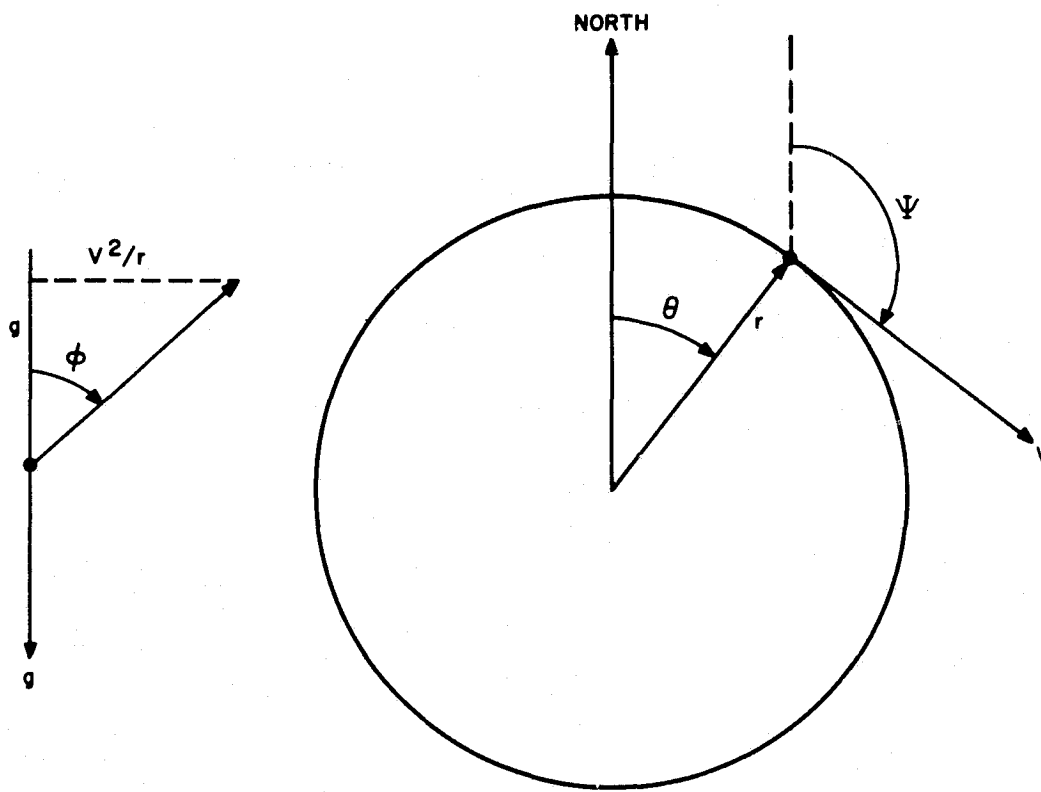


Figure 5. Nominal Spiral Parameters - No Wind.

$$g \tan \phi = V^2/r \quad (2)$$

Thus, from Equations (1) and (2), specifying any two of the four spiral parameters determines the remaining two. For example, a 60 kt spiral with a 2000 ft radius requires a bank angle of 9.05° and a heading rate of $2.9^\circ/\text{sec}$.

The effect of a wind on the spiral descent is to produce a continuous variation in the spiral parameters. The airspeed V and groundspeed V_g now differ, which also results in changing heading rate, bank angle and crab angle (between V and V_g). This is depicted in Figure 6 for a spiral descent which maintains constant airspeed in a steady wind. The magnitude of the crab angle is greatest with a direct crosswind (points 1 and 3), while the bank angle is about the same as the zero-wind case. The highest groundspeed and maximum bank angle, occur downwind (point 2), with the reverse situation at the upwind position (point 4); the crab angle is zero when the

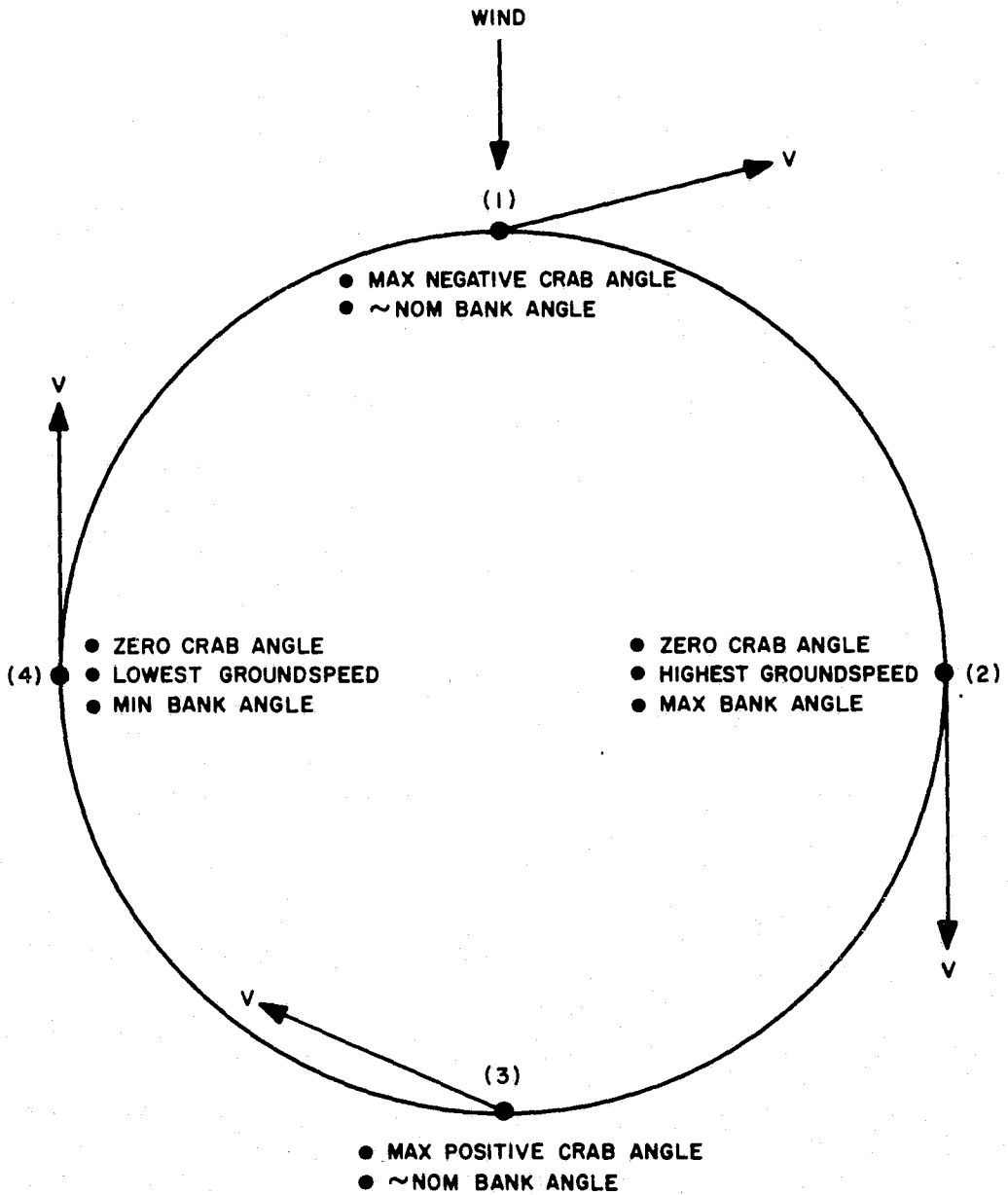


Figure 6. Effect of Wind on Spiral with Constant Airspeed.

aircraft is directly downwind or upwind. If a constant rate of descent is maintained, the changing groundspeed will produce a nonlinear variation in altitude with spiral angle.

The preceding discussion has implied two philosophies in flying the spiral descent in a wind: constant airspeed or constant groundspeed. In the previous analyses of commercial VTOL operations, the groundspeed has been specified to simplify 4-dimensional navigation. However, several factors favor constant airspeed for the spiral approach: the descent airspeed can be chosen for fuel economy; large airspeed variations may take the rotorcraft into unsafe operating regions; and continually-varying longitudinal accelerations would be required to maintain constant groundspeed while spiraling in a steady wind. Some consequences of constant groundspeed versus constant airspeed in a steady wind are summarized in Table 1.

Table 1. Constant Groundspeed Versus Constant Airspeed.

	CONSTANT GROUNDSPEED	CONSTANT AIRSPEED
Acceleration Vector	Constant magnitude (directed to center of spiral)	Variable magnitude (directed perpendicular to airspeed vector)
Longitudinal Acceleration	Variable	Zero
Airspeed	Variable	Constant
Heading Rate	Variable	Variable

Unfortunately, the constant airspeed approach complicates the timing problem of precise inter-aircraft spacing for 4-D guidance. For 4-D guidance at constant airspeed, the wind must be accurately estimated to predict the groundspeed. However, the wind knowledge is also very important for 3-D guidance as well, and a wind estimator will be required in any event. A comparison of important operational procedures for 3-D and 4-D spiral approaches is shown in Table 2.

Table 2. Operational Procedures for 3-D and 4-D Guidance.

<p>Approach Plate Information</p>	<p>Definition of specific spiral approach procedure</p> <ul style="list-style-type: none"> ● Center and radius of spiral tube ● Entry and departure angles ● Altitude versus angle ● Zero-wind time 	
<p>Approach Clearance</p>	<p style="text-align: center;"><u>3-D</u></p> <p>ATC provides wind estimate Clearance assumes constant airspeed during spiral Clearance assumes constant rate of descent based on nominal wind</p>	<p style="text-align: center;"><u>4-D</u></p> <p>ATC provides wind estimate ATC directs time to exit spiral based on constant airspeed and wind estimate Clearance assumes altitude versus time profile based on constant rate of descent and nominal wind</p>
<p>Descent Procedures</p>	<p style="text-align: center;"><u>3-D</u></p> <p>VTOL maintains radius with bank angle Actual wind is estimated to improve nominal control Airspeed is maintained constant Descent rate is adjusted to achieve final altitude at final angle</p>	<p style="text-align: center;"><u>4-D</u></p> <p>VTOL maintains radius with bank angle Actual wind is estimated to improve nominal control Airspeed is adjusted to achieve nominal exit time Descent rate is adjusted to follow altitude versus time profile</p>

SECTION 3 SPIRAL GUIDANCE FORMULATION

3.1 BASIC CONCEPT

The basic concept followed in the spiral descent scheme is that of guiding the rotorcraft to a nominal path which can be prespecified for any specific landing site. The general concept is illustrated in Figure 7 in block diagram form. The navigation system takes measurements of the actual rotorcraft state x , and produces estimates of the state vector \hat{x} , and of the independent variable \hat{t} . The latter is used to calculate nominal values of both the state x^* and the control u^* . The nominal and estimated states are compared, and any errors Δx are fed back through the guidance gain matrix to generate control corrections Δu . These corrections are subtracted from the nominal control to obtain the actual control u . Uncertainties enter the system as wind disturbances on the rotorcraft, navigation system inaccuracies, and approximations used in the nominal calculations in the guidance gains.

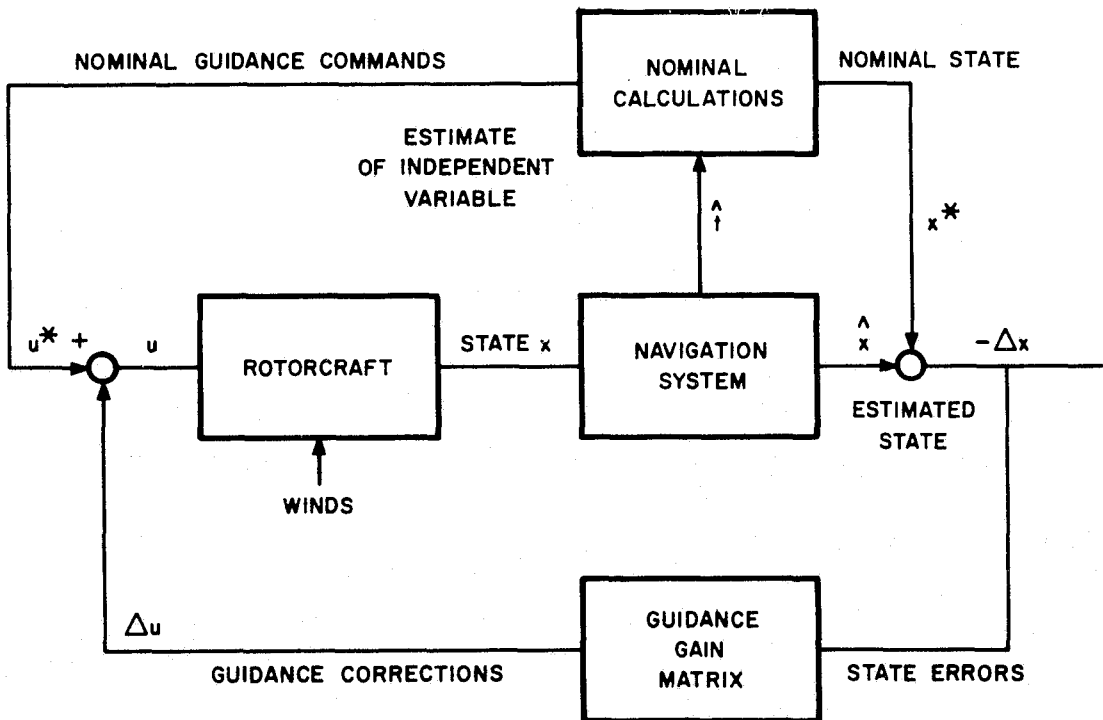


Figure 7. Block Diagram of Spiral Guidance Concept.

3.2 EQUATIONS OF MOTION

The basic dynamics of the spiral descent involve five state variables (Figure 8):

- r = rotorcraft radial distance from nominal spiral center
- θ = rotorcraft azimuth around spiral, clockwise from North
- ψ = heading angle of airspeed vector, clockwise from North
- V = rotorcraft airspeed
- h = rotorcraft altitude

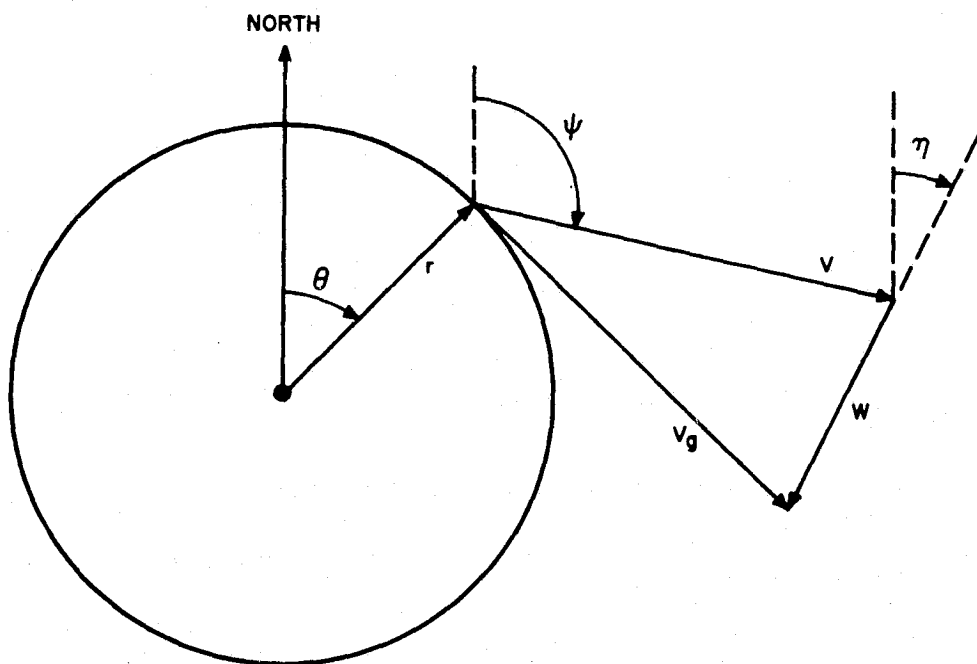


Figure 8. Nomenclature for Spiral Descent.

The basic differential equations describing the actual spiral descent are:

$$\dot{\theta} = \frac{V}{r} \left[\sin(\psi - \theta) - \frac{W}{V} \sin(\eta - \theta) \right] \quad (3)$$

$$\dot{r} = V \left[\cos(\psi - \theta) - \frac{W}{V} \cos(\eta - \theta) \right] \quad (4)$$

$$\dot{\psi} = \frac{g}{V} \tan \phi_c \quad (5)$$

$$\dot{V} = a_c \quad (6)$$

$$\dot{h} = \dot{h}_c \quad (7)$$

where

W = magnitude of wind

η = direction from which wind is blowing

The three control inputs are:

ϕ_c = bank angle command

a_c = longitudinal acceleration command

\dot{h}_c = vertical speed command

3.3 SPIRAL ANGLE AS INDEPENDENT VARIABLE

It will be convenient to replace time t with turn angle θ as the independent variable in Equations (4) - (7). Dividing Equations (4) - (7) by (3) gives:

$$\frac{dr}{d\theta} = \frac{\dot{r}}{\dot{\theta}} = r \frac{\cos(\psi - \theta) - (W/V) \cos(\eta - \theta)}{\sin(\psi - \theta) - (W/V) \sin(\eta - \theta)} \quad (8)$$

$$\frac{d\psi}{d\theta} = \frac{\dot{\psi}}{\dot{\theta}} = \frac{r g}{\sqrt{2}} \frac{\tan \phi_c}{\sin(\psi - \theta) - (W/V) \sin(\eta - \theta)} \quad (9)$$

$$\frac{dV}{d\theta} = \frac{\dot{V}}{\dot{\theta}} = \frac{r a_c \sqrt{V}}{\sin(\psi - \theta) - (W/V) \sin(\eta - \theta)} \quad (10)$$

$$\frac{dh}{d\theta} = \frac{\dot{h}}{\dot{\theta}} = \frac{r h_c \sqrt{V}}{\sin(\psi - \theta) - (W/V) \sin(\eta - \theta)} \quad (11)$$

The fifth state variable becomes time, which is defined by the reciprocal of Equation (3):

$$\frac{dt}{d\theta} = \frac{1}{\dot{\theta}} = \frac{r/V}{\sin(\psi - \theta) - (W/V) \sin(\eta - \theta)} \quad (12)$$

3.4 TIME IN SPIRAL FOR ARBITRARY TURN ANGLE

One problem in specifying the nominal spiral and associated guidance parameters, is determining the nominal time as a function of turn angle, $t^*(\theta)$. The time to turn from θ_o to θ_f is (see Figure 9 for nomenclature):

$$t(\theta_f) = t(\theta_o) + \int_{\theta_o}^{\theta_f} \frac{d\theta}{\dot{\theta}} = \int_{\theta_o}^{\theta_f} \frac{r}{V_g} d\theta \quad (13)$$

where the ground speed V_g is found by the law of cosines:

$$(V_g) = V \left[\sqrt{1 - \left(\frac{W}{V}\right)^2 \cos^2(\eta - \theta)} - \frac{W}{V} \sin(\eta - \theta) \right] \quad (14)$$

For constant spiral radius and airspeed, and defining the angle $\alpha = \theta - \eta + \pi/2$:

$$t(\theta_f) = t(\theta_o) + \frac{r}{V} \int_{\alpha_o}^{\alpha_f} \frac{d\alpha}{\sqrt{1 - (W/V)^2 \sin^2 \alpha - (W/V) \cos \alpha}} \quad (15)$$

$$= \frac{r}{V [1 - (W/V)^2]} \int_{\alpha_o}^{\alpha_f} \left[\sqrt{1 - \left(\frac{W}{V}\right)^2 \sin^2 \alpha} + \frac{W}{V} \cos \alpha \right] d\alpha \quad (15a)$$

$$= \frac{r}{V [1 - (W/V)^2]} \left[E \left(\frac{W}{V}, \alpha \right) + \frac{W}{V} \sin \alpha \right]_{\alpha_o}^{\alpha_f} \quad (15b)$$

where $E \left(\frac{W}{V}, \alpha \right)$ is an elliptic integral of the second kind:

$$E \left(\frac{W}{V}, \alpha \right) = \int_0^{\alpha} \sqrt{1 - \left(\frac{W}{V}\right)^2 \sin^2 \phi} d\phi \quad (16)$$

The elliptic integral requires a series expansion to evaluate (Ref. 2):

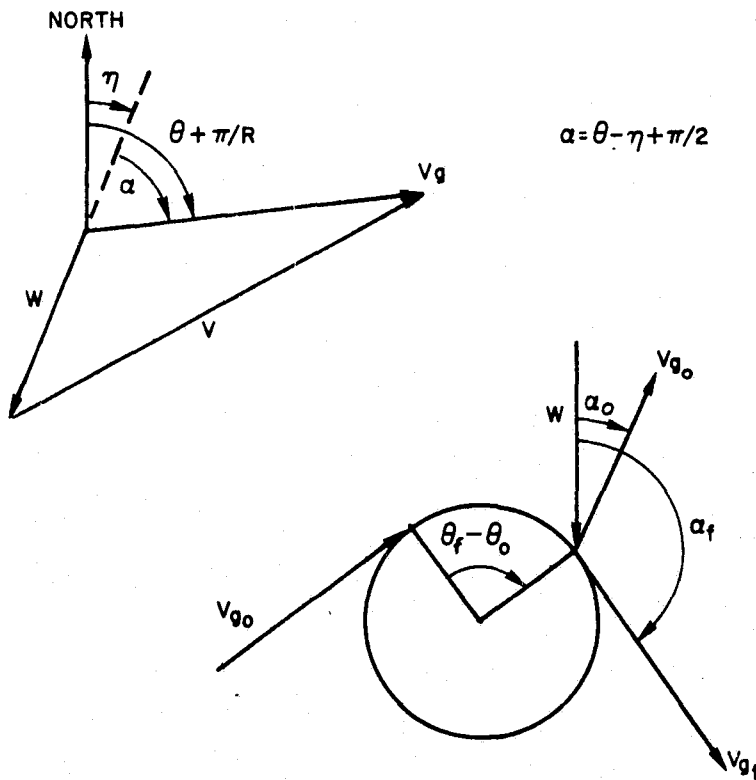


Figure 9 . Nomenclature for Determining $t^*(\theta)$.

$$E\left(\frac{W}{V}, \alpha\right) = \alpha - \frac{1}{2} \left(\frac{W}{V}\right)^2 \int_0^\alpha \sin^2 \phi d\phi - \frac{(W/V)^4}{2 \cdot 4} \int_0^\alpha \sin^4 \phi d\phi \\ \dots - \frac{1 \cdot 3 \cdot 5 \cdot \dots \cdot (2n-3)}{2 \cdot 4 \cdot 6 \cdot \dots \cdot 2n} \left(\frac{W}{V}\right)^{2n} \int_0^\alpha \sin^{2n} \phi d\phi \quad (17)$$

where the following relation can be used:

$$\int_0^\alpha \sin^{2n} \phi d\phi = -\frac{\sin^{2n-1} \alpha \cos \alpha}{2n} + \frac{2n-1}{2n} \int_0^\alpha \sin^{2n-2} \phi d\phi \quad (18)$$

Thus, the elliptic integral can be written as

$$E\left(\frac{W}{V}, \alpha\right) = \alpha - \left(\frac{W}{V}\right)^2 \left(\frac{\alpha}{4} - \frac{1}{4} \sin \alpha \cos \alpha\right) \\ - \left(\frac{W}{V}\right)^4 \left(-\frac{3}{64} \alpha - \frac{3}{64} \sin \alpha \cos \alpha - \frac{1}{32} \sin^3 \alpha \cos \alpha\right) \\ + \text{H.O.T.} \quad (19)$$

For a complete turn, (i.e.), $\theta_f - \theta_0 = 2\pi$

$$E_f = 2\pi \left[1 - \frac{1}{4} \left(\frac{W}{V}\right)^2 - \frac{3}{64} \left(\frac{W}{V}\right)^4 \dots \right] \quad (20)$$

and the time for one complete turn is

$$T = \frac{2\pi r}{V} \cdot \left[1 - \left(\frac{W}{V}\right)^2 \right]^{-1} \left[1 - \frac{1}{4} \left(\frac{W}{V}\right)^2 - \frac{3}{64} \left(\frac{W}{V}\right)^4 \dots \right] \quad (21)$$

Neglecting the $\left(\frac{W}{V}\right)^6$ term in the series expansion of E (assuming $\frac{W}{V} < \frac{1}{2}$) causes an error less than 0.1%; while neglecting the $\left(\frac{W}{V}\right)^4$ term causes an error less than 0.3%. However, neglecting the $\left(\frac{W}{V}\right)^2$ term can cause an error greater than 6%. Thus, it seems reasonable to keep terms out to $\left(\frac{W}{V}\right)^2$ and expect an accuracy of better than 0.3%.

To verify this conclusion, the elliptic integral expansion was calculated for various values of (W/V) and α , using 2, 3 and 25 terms. The results are compared in Table 3. Note that by keeping two terms in the expansion, i.e. $(W/V)^4$ terms, the maximum error is only 0.04% for $W = V/2$, i.e., $\sin^{-1}(W/V) = 30^\circ$.

Table 3. Approximate Solution to Elliptic Integral of the Second Kind.

		<u>Two Terms in Expansion</u>								
θ		$\sin^{-1}(w/V)$								
	0	10	20	30	40	50	60	70	80	90
0	0.0000	0.0000	0.0000	0.0000	0.0000	0.0000	0.0000	0.0000	0.0000	0.0000
10	0.1745	0.1745	0.1744	0.1743	0.1741	0.1740	0.1738	0.1737	0.1736	0.1736
20	0.3490	0.3488	0.3482	0.3473	0.3461	0.3449	0.3438	0.3428	0.3422	0.3420
30	0.5235	0.5229	0.5209	0.5178	0.5140	0.5100	0.5061	0.5029	0.5008	0.5000
40	0.6981	0.6965	0.6920	0.6850	0.6763	0.6668	0.6577	0.6501	0.6451	0.6434
50	0.8726	0.8697	0.8614	0.8483	0.8318	0.8138	0.7964	0.7818	0.7721	0.7688
60	1.0471	1.0425	1.0289	1.0076	0.9805	0.9506	0.9215	0.8970	0.8807	0.8750
70	1.2217	1.2149	1.1949	1.1633	1.1230	1.0781	1.0341	0.9969	0.9720	0.9633
80	1.3962	1.3869	1.3597	1.3164	1.2607	1.1985	1.1371	1.0850	1.0500	1.0376
90	1.5707	1.5588	1.5238	1.4680	1.3959	1.3149	1.2348	1.1666	1.1206	1.1044

		<u>Three Terms in Expansion</u>								
θ		$\sin^{-1}(w/V)$								
	0	10	20	30	40	50	60	70	80	90
0	0.0000	0.0000	0.0000	0.0000	0.0000	0.0000	0.0000	0.0000	0.0000	0.0000
10	0.1745	0.1745	0.1744	0.1743	0.1741	0.1740	0.1738	0.1737	0.1736	0.1736
20	0.3490	0.3488	0.3482	0.3473	0.3461	0.3449	0.3438	0.3428	0.3422	0.3420
30	0.5235	0.5229	0.5209	0.5178	0.5140	0.5099	0.5060	0.5028	0.5007	0.5000
40	0.6981	0.6965	0.6920	0.6850	0.6762	0.6667	0.6575	0.6498	0.6447	0.6429
50	0.8726	0.8697	0.8614	0.8483	0.8317	0.8134	0.7956	0.7805	0.7704	0.7669
60	1.0471	1.0425	1.0289	1.0075	0.9802	0.9496	0.9193	0.8934	0.8759	0.8697
70	1.2217	1.2149	1.1949	1.1631	1.1222	1.0758	1.0294	0.9892	0.9617	0.9520
80	1.3962	1.3869	1.3596	1.3161	1.2593	1.1944	1.1286	1.0712	1.0317	1.0176
90	1.5707	1.5588	1.5238	1.4675	1.3938	1.3087	1.2219	1.1454	1.0926	1.0737

		<u>Twenty-Five Terms in Expansion</u>								
θ		$\sin^{-1}(w/V)$								
	0	10	20	30	40	50	60	70	80	90
0	0.0000	0.0000	0.0000	0.0000	0.0000	0.0000	0.0000	0.0000	0.0000	0.0000
10	0.1745	0.1745	0.1744	0.1743	0.1741	0.1740	0.1738	0.1737	0.1736	0.1736
20	0.3490	0.3488	0.3482	0.3473	0.3461	0.3449	0.3438	0.3428	0.3422	0.3420
30	0.5235	0.5229	0.5209	0.5178	0.5140	0.5099	0.5060	0.5028	0.5007	0.5000
40	0.6981	0.6965	0.6920	0.6850	0.6762	0.6667	0.6574	0.6497	0.6445	0.6427
50	0.8726	0.8697	0.8614	0.8483	0.8317	0.8133	0.7953	0.7800	0.7697	0.7660
60	1.0471	1.0425	1.0289	1.0075	0.9801	0.9492	0.9183	0.8914	0.8727	0.8660
70	1.2217	1.2149	1.1949	1.1631	1.1220	1.0749	1.0266	0.9829	0.9514	0.9397
80	1.3962	1.3869	1.3596	1.3160	1.2589	1.1925	1.1224	1.0564	1.0057	0.9856
90	1.5707	1.5588	1.5237	1.4674	1.3931	1.3055	1.2110	1.1184	1.0421	1.0098

3.5 NOMINAL SPIRAL SPECIFICATION

The guidance concept in Figure 7 requires the specification of the nominal state vector x^* and control vector u^* as functions of the independent variable θ ; i.e.,

$$x^*(\theta) = [r^*(\theta), V^*(\theta), \psi^*(\theta), t^*(\theta), h^*(\theta)]^T \quad (22)$$

$$u^*(\theta) = [\phi_c^*(\theta), a_c^*(\theta), \dot{h}_c^*(\theta)]^T \quad (23)$$

The basic assumptions used for the nominal spiral are

- Constant radius (r^*)
- Constant airspeed (V^*)
- Constant rate of descent (\dot{h}^*)
- Steady wind (η^*, W^*)

For right-hand turns (clockwise from above), the nominal spiral state variables are defined by the following equations:

$$r^* = \text{constant} \quad (24)$$

$$V^* = \text{constant} \quad (25)$$

$$\psi^*(\theta) = \theta + \frac{\pi}{2} - \sin^{-1} \left[\frac{W^*}{V^*} \cos(\theta - \eta^*) \right] \quad (26)$$

$$t^*(\theta) = t^*(\theta_0) + \frac{r^*}{V^*} \left[1 - \left(\frac{W^*}{V^*} \right)^2 \right]^{-1} \left\{ \theta - \theta_0 + \frac{W^*}{V^*} [\cos(\theta - \eta^*) - \cos(\theta_0 - \eta^*)] - \frac{1}{4} \left(\frac{W^*}{V^*} \right)^2 [\theta - \theta_0 + \cos(\theta - \eta^*) \sin(\theta - \eta^*) - \cos(\theta_0 - \eta^*) \sin(\theta_0 - \eta^*)] \right\} \quad (27)$$

$$h^*(\theta) = h^*(\theta_0) + \dot{h}^* [t^*(\theta) - t^*(\theta_0)] \quad (28)$$

where θ_0 is the entry angle into the spiral.

The nominal heading, Equation (26), is obtained geometrically from Figure 8. The nominal time expression uses the expansion of Equation (19), neglecting terms of higher order than $(W/V)^2$ and inserts this into Equation (15b).

The nominal control variables for a right-hand spiral are:

$$\phi^*(\theta) = \tan^{-1} \left\{ \frac{V^{*2}}{r^* g A} \left[A + \frac{W^*}{V^*} \sin(\theta - \eta^*) \right]^2 \right\} \quad (29)$$

where

$$A \triangleq \left[1 - \left(\frac{W^*}{V^*} \right)^2 \cos^2(\theta - \eta^*) \right]^{1/2}$$

$$a^* = 0 \quad (30)$$

$$\dot{h}^* = \frac{h^*(\theta_f) - h^*(\theta_0)}{t^*(\theta_f) - t^*(\theta_0)} = \text{constant} \quad (31)$$

θ_f is the exit angle from the spiral. The nominal bank angle is obtained by differentiating Equation (26) with respect to θ , and substituting into Equation (5).

Right Versus Left Turns

For right turns, $\theta - \theta_0 > 0$, and Equations (26) - (31) above apply. However, for left turns, $\theta - \theta_0 < 0$, and the following sign changes are required in Equations (26), (27) and (29):

$$\psi^*(\theta) = \theta - \frac{\pi}{2} + \sin^{-1} \left[\frac{W^*}{V^*} \cos(\theta - \eta^*) \right] \quad (26')$$

$$t^*(\theta) = t^*(\theta_0) - \frac{r^*}{V^*} \left[1 - \left(\frac{W^*}{V^*} \right)^2 \right]^{-1/2} \left\{ \theta - \theta_0 - \frac{W^*}{V^*} [\cos(\theta - \eta^*) - \cos(\theta_0 - \eta^*)] \right. \\ \left. - \frac{1}{4} \left(\frac{W^*}{V^*} \right)^2 [\theta - \theta_0 + \cos(\theta - \eta^*) \sin(\theta - \eta^*) \right. \\ \left. - \cos(\theta_0 - \eta^*) \sin(\theta_0 - \eta^*)] \right\} \quad (27')$$

$$\phi^*(\theta) = -\tan^{-1} \left\{ \frac{V^{*2}}{r^* g A} \left[A - \frac{W^*}{V^*} \sin(\theta - \eta^*) \right] \right\} \quad (29')$$

3.6 WIND EFFECTS ON NOMINAL SPIRAL

Except for r^* and V^* , all the nominal spiral parameters depend on the nominal wind speed W^* and direction η^* . To illustrate the effects of wind on the nominal spiral, Table 4 compares several constant airspeed turns ($V^* = 60$ kt, $r^* = 2000$ ft) of 360° . The table shows the nominal time, ground speed, heading, heading rate and bank angle as functions of the spiral turn angle for winds from 0 to 30 kt. Notice that in a 30 kt wind ($W/V = 0.5$), the time for the turn is more than 30 seconds greater than the zero-wind turn. The ground speed varies from 30 kt to 90 kt, the wind crab angle ($\psi - \theta$) reaches 30° , and the heading rate exceeds 6.5 deg/sec with a peak bank angle of nearly 20° .

Table 4. Wind Effects on 360° Turns ($V^* = 60$ kt, $R^* = 2000$ ft).

Wind Speed = 0 kt

θ (deg)	t (sec)	V_g (kt)	ψ (deg)	$\dot{\psi}$ (deg/sec)	ϕ (deg)
0.0	0.0	60.0	0.0	2.90	9.05
30.0	10.3	60.0	30.0	2.90	9.05
60.0	20.6	60.0	60.0	2.90	9.05
90.0	31.0	60.0	90.0	2.90	9.05
120.0	41.3	60.0	120.0	2.90	9.05
150.0	51.6	60.0	150.0	2.90	9.05
180.0	62.0	60.0	180.0	2.90	9.05
210.0	72.3	60.0	210.0	2.90	9.05
240.0	82.7	60.0	240.0	2.90	9.05
270.0	93.0	60.0	270.0	2.90	9.05
300.0	103.3	60.0	300.0	2.90	9.05
330.0	113.7	60.0	330.0	2.90	9.05
360.0	124.0	60.0	360.0	2.90	9.05

Wind Speed = 10 kt

θ (deg)	t (sec)	V_g (kt)	ψ (deg)	$\dot{\psi}$ (deg/sec)	ϕ (deg)
0.0	0.0	50.0	0.0	2.01	6.31
30.0	12.3	51.1	25.2	2.11	6.62
60.0	24.1	54.3	51.7	2.40	7.53
90.0	35.0	59.1	80.4	2.86	8.93
120.0	45.1	64.3	111.7	3.37	10.50
150.0	54.4	68.4	145.2	3.78	11.76
180.0	63.3	69.9	180.0	3.94	12.24
210.0	72.2	68.4	214.7	3.78	11.76
240.0	81.6	64.3	248.2	3.37	10.50
270.0	91.6	59.1	279.5	2.86	8.93
300.0	102.6	54.3	308.2	2.40	7.53
330.0	114.4	51.1	334.7	2.11	6.62
360.0	126.7	50.0	360.0	2.01	6.31

Wind Speed = 20 kt

θ (deg)	t (sec)	V_g (kt)	ψ (deg)	$\dot{\psi}$ (deg/sec)	ϕ (deg)
0.0	0.0	40.0	0.0	1.28	4.05
30.0	15.2	41.8	20.4	1.43	4.49
60.0	29.2	47.4	43.2	1.89	5.94
90.0	41.3	56.5	70.5	2.73	8.54
120.0	51.3	67.4	103.2	3.82	11.88
150.0	59.9	76.4	140.4	4.78	14.71
180.0	67.8	79.9	180.0	5.15	15.82
210.0	75.6	76.4	219.5	4.78	14.71
240.0	84.2	67.4	256.7	3.82	11.88
270.0	94.3	56.5	289.4	2.73	8.54
300.0	106.3	47.4	316.7	1.89	5.94
330.0	120.3	41.8	339.5	1.43	4.49
360.0	135.6	40.0	360.0	1.28	4.05

Wind Speed = 30 kt

θ (deg)	t (sec)	V_g (kt)	ψ (deg)	$\dot{\psi}$ (deg/sec)	ϕ (deg)
0.0	0.0	30.0	0.0	0.72	2.28
30.0	20.2	32.1	15.5	0.85	2.70
60.0	37.9	39.0	34.3	1.36	4.29
90.0	51.8	51.9	60.0	2.51	7.86
120.0	62.1	69.0	94.3	4.26	13.19
150.0	70.2	84.0	135.5	5.88	17.91
180.0	77.3	90.0	180.0	6.52	19.73
210.0	84.3	84.0	224.4	5.88	17.91
240.0	92.4	69.0	265.6	4.26	13.19
270.0	102.7	51.9	300.0	2.51	7.86
300.0	116.6	39.0	325.6	1.36	4.29
330.0	134.3	32.1	344.4	0.85	2.70
360.0	154.6	30.0	360.0	0.72	2.28

It is apparent from Table 4 that the nominal spiral is very sensitive to the predicted wind. If the wind speed and/or direction differ from the values used in the nominal calculations, the guidance system performance can suffer considerably. Consequently, a wind estimator will be an essential element in the guidance concept to update the forecast winds and to correct for wind shears during the descent. The estimated wind will then be used to compute the nominal bank angle and heading since they are the primary variables that affect the desired radius. However, the nominal time will be based only on the original wind estimate to maintain proper aircraft spacing. The wind estimator is discussed in Section 5 of the report.

3.7 FEEDBACK GUIDANCE LAWS

As shown in Figure 7, the navigation system estimate of the vehicle state $\hat{x}(\theta)$ is compared with the nominal state $x^*(\theta)$, and any differences are fed back through the guidance gain matrix to generate corrections Δu to the nominal control $u^*(\theta)$; i.e.,

$$u(\theta) = u^*(\theta) + K [\hat{x}(\theta) - x^*(\theta)] \quad (32)$$

Theoretically, K is a 3×5 matrix so that an error in any element of the state will produce a correction in all three control channels. In practice, however, many of the elements of K can be neglected. As a result, the guidance laws of Equation (32) can be written for the individual control channels as follows:

$$\phi_c = \phi^*(\theta) \pm C_r(\hat{r} - r^*) + C_\psi[\hat{\psi} - \psi^*(\theta)] + C_t[\hat{t} - t^*(\theta)] \quad (33)$$

$$a_c = K_v(\hat{V} - V^*) + K_t[\hat{t} - t^*(\theta)] \quad (34)$$

$$\dot{h}_c = \dot{h}^* + K_h[\hat{h} - h^*(\theta)] \quad (35)$$

The choice of upper or lower sign in Equation (33) depends on whether the turn is to the right or the left, respectively.

For passenger comfort and safety, the guidance commands would be limited to reasonable levels. Typical constraints might be

$$|\phi_c| < 30^\circ \quad (36a)$$

$$|a_c| < 0.1 g \quad (36b)$$

$$|\dot{h}_c| < 1000 \text{ ft/min} \quad (36c)$$

The selection of appropriate values for the feedback gains in Equations (33) - (35) is an iterative design process. A linearized analysis, described in Section 4, was used to provide a satisfactory set of guidance gains for preliminary evaluation of the guidance concept.

The gains C_f and K_f are included in Equations (33) and (34) to provide 4-D guidance capability. The guidance system can control time either with airspeed adjustments or by small changes in the radius, since the time varies with both; i.e.

$$t_f - t_o \approx \int_{\theta_0}^{\theta_f} \frac{r}{V} d\theta \quad (37)$$

The change in final time is

$$\delta t_f \approx \left(\frac{\delta r}{V} - \frac{r \delta V}{V^2} \right) \Delta \theta \quad (38)$$

At $V = 60$ kt and $r = 2000$ ft, a 1-knot change in airspeed has the same effect on final time as a 35 ft change in radius. Another consideration is that the airspeed response to commands is approximately linear with time, while the radius change is proportional to the second power of time (through ψ). Thus, time should be controlled only by airspeed adjustment and not by changing the radius.

SECTION 4
PERTURBATION GUIDANCE ANALYSIS

4.1 SIMPLIFIED 3-D GUIDANCE WITHOUT WIND

A simplified analysis was conducted for 3-dimensional guidance during a zero-wind descent, with constant groundspeed ($V = V_g$) and flight path angle. For this simple spiral, the state variables are spiral radius r , spiral azimuth θ , aircraft heading Ψ , and altitude h (Figure 10). The guidance scheme can be simplified by using θ as the independent variable in place of time, and by separating the vertical and horizontal channels.

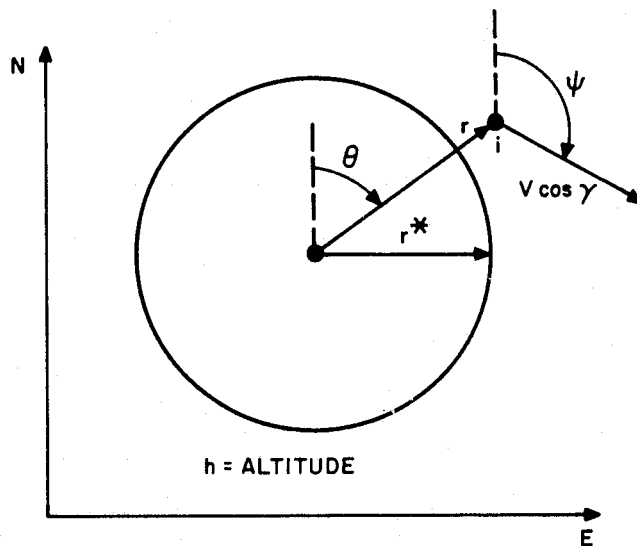


Figure 10. Nomenclature for Spiral Descent Guidance Scheme.

The perturbation equations of motion for a right-hand turn are approximately:

$$\delta \dot{\psi} = \frac{g}{V} \sec^2 \phi^* \delta \phi_c \quad (39)$$

$$\delta \dot{r} = -V \delta \psi \quad (40)$$

$$\delta \ddot{h} = \delta \dot{h}_c \quad (41)$$

where ϕ^* is the nominal rotorcraft bank angle. The control variables are $\delta \phi_c$ and $\delta \dot{h}_c$. Since

$$\dot{\theta} = V/r \approx V/r^* \quad (42)$$

we can use θ as the independent variable. Hence, dividing Equations (39) - (41) by (42), the perturbation equations of motion become:

$$\frac{d(\delta\psi)}{d\theta} = r^* n^2 \delta\phi_c \quad (43)$$

$$\frac{d(\delta r)}{d\theta} = -r^* \delta\psi \quad (44)$$

$$\frac{d(\delta h)}{d\theta} = \frac{r^*}{V} \delta h_c \quad (45)$$

where $n^2 \triangleq g (\sec^2 \phi^*) / V^2$

4.1.1 HORIZONTAL PLANE GUIDANCE

The perturbation state and control vectors for motions in the horizontal plane are:

$$x = \begin{bmatrix} \delta\psi \\ \delta r \end{bmatrix}, u = \delta\phi \quad (46)$$

where x satisfies the linear differential equation

$$\frac{dx}{d\theta} = Fx + Gu \quad (47)$$

where

$$F = \begin{bmatrix} 0 & 0 \\ -r^* & 0 \end{bmatrix}, G = \begin{bmatrix} r^* n^2 \\ 0 \end{bmatrix} \quad (48)$$

Applying the Quadratic Synthesis technique, the optimum linear feedback guidance law is $u = -Cx$, or

$$\delta\phi = -C_\psi \delta\psi - C_r \delta r \quad (49)$$

where the feedback gain matrix is $C = [C_\psi \ C_r] = B^{-1} G^T S$

The B matrix is determined by the maximum allowable bank control, $\delta\phi_m$:

$$B^{-1} = (\delta\phi_m)^2 \quad (50)$$

The steady-state gains are obtained from the solution of the matrix-Ricatti equations:

$$\dot{S} = -SF - F^T S + SGB^{-1} G^T S - A = 0 \quad (51)$$

where the matrix A describes the maximum allowable state perturbations:

$$A = \begin{bmatrix} (\delta\psi_m)^{-2} & 0 \\ 0 & (\delta r_m)^{-2} \end{bmatrix} \quad (52)$$

The guidance gains then become:

$$C_\psi = \sqrt{\left(\frac{\delta\phi_m}{\delta\psi_m}\right)^2 + \frac{2\delta\phi_m}{n^2\delta r_m}} \quad (\text{rad/rad}) \quad (53)$$

$$C_r = \frac{\delta\phi_m}{\delta r_m} \quad (\text{rad/ft}) \quad (54)$$

An alternate approach to selecting the feedback gains is provided by substituting the guidance equation into the perturbation equations of motion to obtain the characteristic equation of the closed-loop system:

$$(\delta r)'' + r^* n^2 C_\psi (\delta r)' + r^{*2} n^2 C_r (\delta r) = 0; \quad (55)$$

where

$$(\delta r)' = \frac{1}{r^*} \frac{d(\delta r)}{d\theta} \quad (56)$$

This is a second-order system whose angular natural frequency and damping ratio are given by

$$\omega_n^2 = r^{*2} n^2 C_r \quad (57)$$

$$\zeta = \frac{r^* n^2 C_\psi}{2\omega_n} \quad (58)$$

A reasonable response can be obtained by specifying the frequency of response in terms of a characteristic angle, θ_c , of the order of 1/4 of the turn, and a damping ratio ζ of approximately 0.7:

$$C_r = (2\pi/\theta_c)^2 / n^2 r^{*2} \quad (59)$$

$$C_\psi = \frac{2(0.7)}{r_n^*} \left(\frac{2\pi}{\theta_c} \right) \quad (60)$$

Thus, any radial error would be corrected with critical damping after a turn angle of approximately θ_c .

4.1.2 VERTICAL PLANE GUIDANCE

This is a scalar problem, with the state and control defined from Equation (45) as follows:

$$x = \delta h; \quad u = \delta \dot{h}_c \quad (61)$$

$$F = 0; \quad G = r^*/V \quad (62)$$

The feedback guidance law is

$$\delta \dot{h}_c = -K_h \delta h \quad (63)$$

where the feedback gain is

$$K_h = (\delta \dot{h}_c)_m^2 \frac{r^*}{V} s \quad (64)$$

The Ricatti equation is a scalar:

$$\dot{s} = s^2 (r^*/V)^2 (\delta \dot{h}_c)_m^2 - \delta h_m^{-2} = 0 \quad (65)$$

Thus the feedback gain is

$$K_h = \frac{(\delta \dot{h}_c)_m}{\delta h_m} \quad (1/\text{sec}) \quad (66)$$

Using the alternate approach, the characteristic equation is

$$(\delta h)^2 + \frac{r^*}{V} K_h (\delta h) = 0 \quad (67)$$

Choose the characteristic response angle here to be θ_c ; i.e.,

$$K_h = V/r^* \theta_c \quad (68)$$

4.1.3 EXAMPLE

As an example of the feedback gains required, assume a descent with the following parameters:

$$r^* = 2000 \text{ ft}$$

$$V^* = 60 \text{ kt} = 101.27 \text{ fps}$$

$$\gamma = -6^\circ$$

$$\dot{\psi} = 3^\circ/\text{sec}$$

Selecting the characteristic angle to be $\theta_c = \pi/2$, give

$$\phi_m = 9.443^\circ$$

$$n^2 = 0.003224 \text{ ft}^{-1}$$

Let

$$\delta \phi_m = 5^\circ \quad (\delta h_c)_m = 200 \text{ fpm}$$

$$\delta r_m = 75 \text{ ft} \quad \delta h_m = 100 \text{ ft}$$

$$\delta \psi_m = 15^\circ$$

These give the guidance gains:

$$C_r = 0.06667 \text{ deg/ft}$$

$$C_\psi = 1.0272 \text{ rad/rad}$$

$$K_h = 0.03333 \text{ ft/sec/ft}$$

Using the alternate approach, the same example gives:

$$C_r = 0.07111 \text{ deg/ft}$$

$$C_\psi = 0.8685 \text{ rad/rad}$$

$$K_h = 0.03224 \text{ ft/sec/ft}$$

Comparison of these results indicates very good agreement for the two approaches.

4.2 4-D GUIDANCE

The perturbation state equations for no wind, linearized about the nominal spiral are:

$$d(\delta x)/d\theta = F \delta x + G \delta u \quad (69)$$

where

$$\delta x = \begin{bmatrix} \delta r \\ \delta V \\ \delta \psi \\ \delta t \\ \delta h \end{bmatrix} \quad F = \begin{bmatrix} 0 & 0 & -r^* & 0 & 0 \\ 0 & 0 & 0 & 0 & 0 \\ 0 & 0 & 0 & 0 & 0 \\ 1/V^* & -r^*/V^{*2} & 0 & 0 & 0 \\ 0 & 0 & 0 & 0 & 0 \end{bmatrix} \quad (70)$$

$$\delta u = \begin{bmatrix} \delta a_c \\ \delta \phi_c \\ \delta \dot{h}_c \end{bmatrix} \quad G = \begin{bmatrix} 0 & 0 & 0 \\ r^*/V^* & 0 & 0 \\ 0 & r^*g/V^{*2} & 0 \\ 0 & 0 & 0 \\ 0 & 0 & r^*/V^* \end{bmatrix}$$

The feedback guidance laws of Equations (33) - (35) are, in vector-matrix form:

$$\delta u = -C \delta x \quad (71)$$

where

$$-C = \begin{bmatrix} 0 & K_V & 0 & K_t & 0 \\ C_r & 0 & C_\psi & C_t & 0 \\ 0 & 0 & 0 & 0 & K_h \end{bmatrix} \quad (72)$$

A block diagram of the horizontal guidance system is shown in Figure 11.

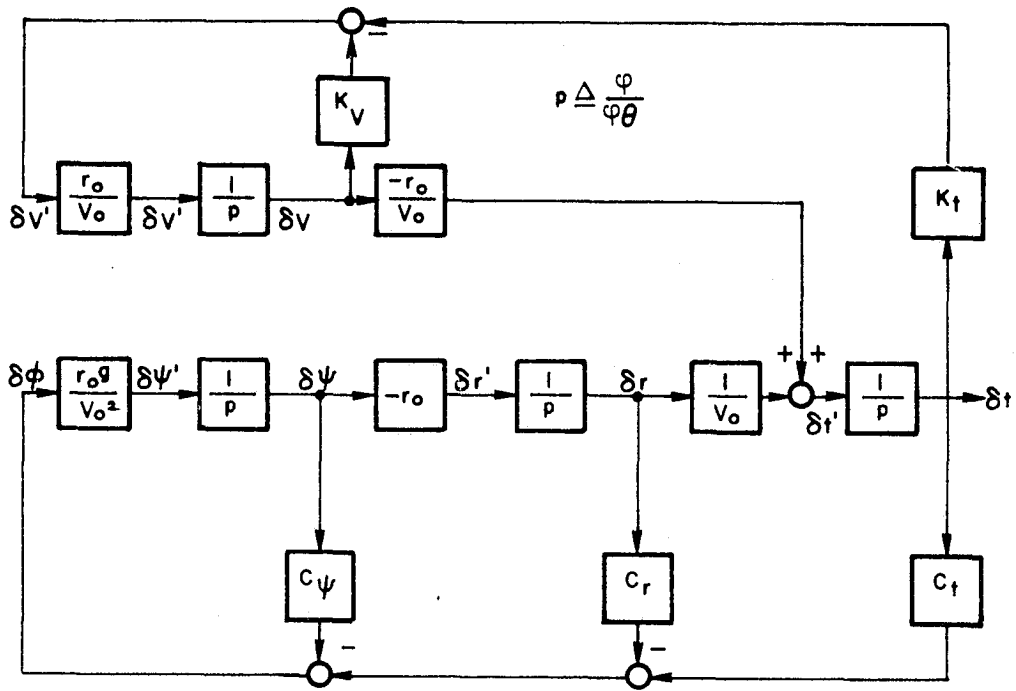


Figure 11. Linearized Block Diagram of Horizontal Guidance System.

The characteristic equation for this system is given by

$$\det (Ip - F + GC) = 0 \quad (73)$$

In expanded form this gives

$$\left[p^4 - \frac{r^*g}{V^{*2}} \left(C_\psi + \frac{V^*}{g} K_V \right) p^3 + \frac{r^{*2}g}{V^{*2}} \left(C_r + \frac{K_V C_\psi}{V^*} + \frac{K_t}{gV^*} \right) p^2 + \frac{gr^{*2}}{V^{*3}} \left(C_t - \frac{r^*}{V^{*2}} K_t C_\psi - r^* C_r K_V \right) p + \frac{gr^{*3}}{V^{*4}} \left(\frac{r^*}{V^*} C_r K_t - K_V C_t \right) \right] p - \frac{r^*}{V^*} K_h = 0 \quad (74)$$

For constant airspeed, $K_V = K_T = \dot{V} = 0$, and the characteristic equation for the horizontal axes becomes

$$p^3 - \left(\frac{r^*g}{V^{*2}} C_\psi \right) p^2 + \left(\frac{r^{*2}g}{V^{*2}} C_r \right) p + \left(\frac{gr^{*2}}{V^{*3}} C_t \right) = 0 \quad (75)$$

For stability, the guidance gains must satisfy the following constraints

$$C_r, C_t > 0, \text{ and } C_\psi < 0, \text{ and } C_t < \frac{r^*g}{V^*} C_\psi C_r$$

Approximate magnitudes of C_ψ and C_r were determined in Section 4.1.3 for $r^* = 2000$ ft and $V^* = 60$ kt:

$$C_\psi = 1 \text{ rad/rad}$$

$$C_r = 0.001 \text{ rad/ft}$$

This requires $C_t < 0.635$ rad/sec. To achieve approximately 0.7 damping, we can select

$$C_t = 0.1 \text{ rad/sec}$$

Now it is convenient to convert back to the time domain: $s \triangleq d/dt = \dot{\theta} d/d\theta = (V^*/r^*) p$. The above gains give

$$s^3 + 0.3177s + 0.03217s + 0.001609 = 0 = (s^2 + 2\zeta\omega_N s + \omega_N^2)(s + 1/\tau) \quad (76)$$

which yields $\omega_N = 0.092$ rad/sec, $\zeta = 0.66$, $\tau = 5.6$ sec.

The performance of the bank guidance loop with no acceleration feedback and perfect navigation was examined by simulation for the first two minutes of a level turn*. Table 5 shows the nominal time histories, while Tables 6 - 8 illustrate the effects of initial errors in r , ψ and V . Note that nominal conditions have been re-established within one half a turn for the first two cases; however, since there is no acceleration feedback, the airspeed error creates steady-state radius and time errors. Tables 9 and 10 present the effects of a 5-knot wind from 90° and 180° ; it is worth noting that even such small winds cause significant radial position errors. Table 11 shows that a 20-knot wind from the north produces very large errors in position and time. However, these errors can be almost eliminated, as shown in Table 12, by including the wind in the nominal calculations.

*Section 8 describes the simulation programs.

Table 5. Nominal Turn With Bank Control Only.

t	θ	ψ	R	ϕ	t*	ψ^*	ϕ^*
0.0	0.0	0.0	2000.0	9.05	0.00	0.0	9.05
5.0	14.5	14.5	2000.0	9.05	5.00	14.5	9.05
10.0	29.0	29.0	2000.0	9.05	10.00	29.0	9.05
15.0	43.5	43.5	2000.0	9.05	15.00	43.5	9.05
20.0	58.0	58.0	2000.0	9.05	20.00	58.0	9.05
25.0	72.5	72.5	2000.0	9.05	25.00	72.5	9.05
30.0	87.0	87.0	2000.0	9.05	30.00	87.0	9.05
35.0	101.5	101.5	2000.0	9.05	35.00	101.5	9.05
40.0	116.0	116.0	2000.0	9.05	40.00	116.0	9.05
45.0	130.5	130.5	2000.0	9.05	45.00	130.5	9.05
50.0	145.0	145.0	2000.0	9.05	50.00	145.0	9.05
55.0	159.5	159.5	2000.0	9.05	55.00	159.5	9.05
60.0	174.0	174.0	2000.0	9.05	60.00	174.0	9.05
65.0	188.5	188.5	2000.0	9.05	65.00	188.5	9.05
70.0	203.0	203.0	2000.0	9.05	70.00	203.0	9.05
75.0	217.5	217.5	2000.0	9.05	75.00	217.5	9.05
80.0	232.0	232.0	2000.0	9.05	80.00	232.0	9.05
85.0	246.5	246.5	2000.0	9.05	85.00	246.5	9.05
90.0	261.1	261.1	2000.0	9.05	90.00	261.1	9.05
95.0	275.6	275.6	2000.0	9.05	95.00	275.6	9.05
100.0	290.1	290.1	2000.0	9.05	100.00	290.1	9.05
105.0	304.6	304.6	2000.0	9.05	105.00	304.6	9.05
110.0	319.1	319.1	2000.0	9.05	110.00	319.1	9.05
115.0	333.6	333.6	2000.0	9.05	115.00	333.6	9.05
120.0	348.1	348.1	2000.0	9.05	120.00	348.1	9.05

$R^* = 2000$ ft
 $V^* = 60$ kt
 $W^* = 0$ kt
 $\eta^* = 0$ deg
 $C_r = 0.001$ rad/sec
 $C_\psi = -1.0$
 $C_t = 0$ rad/sec
 $R_o = 2000$ ft
 $\theta_o = 0$ deg
 $V_o = 60$ kt
 $\psi_o = 0$ deg
 $W = 0$ kt
 $\eta = 0$ deg

Table 6. Effect of Initial Radial Error with Bank Control Only.

t	θ	ψ	R	ϕ	t*	ψ^*	ϕ^*
0.0	0.0	0.0	2200.0	20.51	0.00	0.0	9.05
10.0	26.7	36.3	2052.8	6.89	9.22	26.7	9.05
20.0	55.7	58.4	1940.8	7.46	19.21	55.7	9.05
30.0	85.7	84.5	1932.1	8.83	29.56	85.7	9.05
40.0	115.6	113.9	1960.6	9.36	39.84	115.6	9.05
50.0	144.9	143.9	1985.2	9.34	49.97	144.9	9.05
60.0	174.1	173.7	1997.6	9.20	60.01	174.1	9.05
70.0	203.1	203.0	2001.4	9.10	70.01	203.1	9.05
80.0	232.1	232.1	2001.6	9.05	80.01	232.1	9.05
90.0	261.1	261.1	2000.9	9.04	90.00	261.1	9.05
100.0	290.1	290.1	2000.3	9.04	100.00	290.1	9.05
110.0	319.1	319.1	2000.0	9.05	109.99	319.1	9.05
120.0	348.1	348.1	1999.9	9.05	119.99	348.1	9.05

$R_o = 2200$ ft

Table 7. Effects of Initial Heading Error With Bank Control Only.

t	θ	ψ	R	ϕ	t*	ψ^*	ϕ^*
0.0	0.0	10.0	2000.0	-0.94	0.00	0.0	9.05
10.0	29.4	27.1	1971.2	8.90	10.13	29.4	9.05
20.0	58.5	57.3	2005.9	9.54	20.18	58.5	9.05
30.0	87.3	87.4	2015.1	9.19	30.12	87.3	9.05
40.0	116.1	116.5	2010.9	9.01	40.05	116.1	9.05
50.0	145.0	145.3	2004.9	8.98	50.01	145.0	9.05
60.0	174.0	174.1	2001.3	9.01	59.9	174.0	9.05
70.0	203.0	203.1	1999.9	9.03	69.99	203.0	9.05
80.0	232.0	232.0	1999.6	9.05	79.99	232.0	9.05
90.0	261.0	261.0	1999.7	9.05	89.99	261.0	9.05
100.0	290.1	290.1	1999.8	9.05	99.99	290.1	9.05
110.0	319.1	319.1	1999.9	9.05	110.00	319.1	9.05
120.0	348.1	348.1	2000.0	9.05	120.00	348.1	9.05

$\psi_0 = 10 \text{ deg}$

Table 8. Effects of Airspeed Error With Bank Control Only.

t	θ	ψ	R	ϕ	t*	ψ^*	ϕ^*
0.0	0.0	0.0	2000.0	9.05	0.00	0.0	9.05
10.0	31.2	27.9	2036.1	10.05	10.76	31.2	9.05
20.0	61.5	58.7	2099.2	10.55	21.22	61.5	9.05
30.0	91.2	89.7	2140.6	10.31	31.43	91.2	9.05
40.0	120.4	119.9	2158.7	10.02	41.50	120.4	9.05
50.0	149.4	149.3	2164.6	9.87	51.52	149.4	9.05
60.0	178.5	178.4	2166.1	9.81	61.53	178.5	9.05
70.0	207.5	207.5	2166.5	9.79	71.53	207.5	9.05
80.0	236.5	236.5	2166.5	9.79	81.53	236.5	9.05
90.0	265.5	265.5	2166.6	9.79	91.53	265.5	9.05
100.0	294.5	294.5	2166.6	9.79	101.53	294.5	9.05
110.0	323.5	323.5	2166.6	9.79	111.53	323.5	9.05
120.0	352.5	352.5	2166.6	9.79	121.53	352.5	9.05

$V_0 = 65 \text{ kt}$

Table 9. Effect of 5-Knot Wind With Bank Control Only (90°).

t	θ	ψ	R	ϕ	t*	ψ^*	ϕ^*
0.0	0.0	0.0	2000.0	9.05	0.00	0.0	9.05
10.0	27.9	32.1	2053.7	10.01	9.64	27.9	9.05
20.0	54.7	62.2	2010.1	8.67	18.86	54.7	9.05
30.0	81.7	88.3	1911.6	7.77	28.18	81.7	9.05
40.0	110.2	112.7	1817.6	7.57	37.98	110.2	9.05
50.0	140.4	137.5	1770.7	8.00	48.39	140.4	9.05
60.0	171.8	164.3	1787.7	8.81	59.23	171.8	9.05
70.0	203.6	193.8	1860.7	9.66	70.21	203.6	9.05
80.0	235.1	225.9	1967.3	10.29	81.07	235.1	9.05
90.0	265.8	259.5	2079.8	10.56	91.63	265.8	9.05
100.0	295.2	293.4	2169.6	10.44	101.78	295.2	9.05
110.0	323.4	326.3	2214.5	9.98	111.47	323.4	9.05
120.0	350.3	357.3	2203.8	9.32	120.77	350.3	9.05

W = 5 kt
 $\eta = 90$ deg

Table 10. Effect of 5-Knot Wind With Bank Control Only (180°).

t	θ	ψ	R	ϕ	t*	ψ^*	ϕ^*
0.0	0.0	0.0	2000.0	9.05	0.00	0.0	9.05
10.0	31.0	28.9	2044.5	9.64	10.71	31.0	9.05
20.0	60.5	61.3	2123.3	10.31	20.87	60.5	9.05
30.0	88.2	93.7	2149.0	9.71	30.41	88.2	9.05
40.0	114.7	123.4	2103.7	8.79	39.56	114.7	9.05
50.0	141.1	150.3	2008.7	8.02	48.65	141.1	9.05
60.0	168.3	175.2	1898.0	7.60	58.01	168.3	9.05
70.0	196.9	199.4	1807.2	7.60	67.88	196.9	9.05
80.0	227.1	224.3	1764.4	8.05	78.31	227.1	9.05
90.0	258.6	251.2	1781.3	8.81	89.14	258.6	9.05
100.0	290.4	280.7	1851.6	9.61	100.11	290.4	9.05
110.0	322.0	312.6	1956.3	10.24	110.99	322.0	9.05
120.0	352.7	346.0	2069.2	10.55	121.59	352.7	9.05

W = 5 kt
 $\eta = 180$ deg

Table 11. Effect of 20-Knot Wind With Bank Control Only.

t	θ	ψ	R	ϕ	t*	ψ^*	ϕ^*
0.0	0.0	0.0	2000.0	9.05	0.00	0.0	9.05
10.0	19.7	30.5	1844.8	7.63	6.82	19.7	9.05
20.0	44.0	48.5	1508.3	4.00	15.18	44.0	9.05
30.0	78.4	60.6	1315.4	4.55	27.04	78.4	9.05
40.0	117.9	82.3	1455.8	9.64	40.66	117.9	9.05
50.0	155.2	120.5	1828.1	13.78	53.50	155.2	9.05
60.0	189.3	168.3	2268.9	15.26	65.28	189.3	9.05
70.0	219.6	217.1	2620.8	14.40	75.69	219.6	9.05
80.0	245.1	260.5	2774.5	12.19	84.50	245.1	9.05
90.0	266.2	296.1	2710.9	9.78	91.76	266.2	9.05
100.0	283.7	324.1	2462.9	7.71	97.80	283.7	9.05
110.0	298.9	346.1	2074.1	5.99	103.03	298.9	9.05
120.0	313.5	362.8	1586.7	4.39	108.08	313.5	9.05

W* = 0 kt
W = 20 kt

Table 12. Effect of Including Wind Estimate in Nominal Calculation.

t	θ	ψ	R	ϕ	t*	ψ^*	ϕ^*
0.0	0.0	0.0	2000.0	4.05	0.00	0.0	4.05
10.0	19.4	13.0	1999.9	4.24	9.99	13.0	4.23
20.0	39.6	27.4	1999.5	4.86	19.98	27.3	4.83
30.0	61.5	44.5	1998.6	6.07	29.97	44.4	6.04
40.0	86.2	66.9	1997.6	8.20	39.96	66.8	8.16
50.0	115.3	97.8	1996.9	11.42	49.94	97.8	11.36
60.0	149.8	140.2	1995.9	14.76	59.93	140.1	14.70
70.0	188.0	190.7	1995.1	15.72	69.95	190.7	15.73
80.0	225.3	238.9	1996.2	13.34	80.00	239.0	13.41
90.0	257.7	276.4	2000.5	9.80	90.07	276.8	9.86
100.0	285.0	303.3	2007.0	7.09	100.14	303.7	7.10
110.0	308.3	323.3	2012.6	5.46	110.15	323.5	5.42
120.0	329.3	339.2	2013.7	4.55	120.11	339.1	4.51

W* = 20 kt
W = 20 kt

Turning now to the airspeed control loop, it is apparent from Figure 11 that it decouples from the bank control loop if $C_f = 0$. In this case, the characteristic equation of the acceleration loop, in the time domain, is:

$$s^2 - K_V s + K_f/V^* = 0 \quad (77)$$

Thus the natural frequency is $\omega_n = \sqrt{K_f/V^*}$ with damping $\zeta = -K_V/2\omega_n$. Selecting the gains to provide approximately the same response as the bank loop gives

$$K_V = -0.15 \text{ sec}^{-1}$$

$$K_f = 1.0 \text{ ft/sec}^3$$

Using these acceleration loop gains and the bank loop gains previously defined, the response to an airspeed error is very acceptable, as shown in Table 13. The response to the same error, but with $C_f = 0$ is shown in Table 14; note that the radial position error is smaller than before, while the time error is about the same. The responses to a 20-knot wind for $C_f = 0.1$ and $C_f = 0$ are compared in Tables 15 and 16. On the average, the timing errors are about the same, but the radial error is considerably improved by the decoupled system. However, the radial error still exceeds 300 ft, which would generally not be acceptable.

It is readily apparent from this analysis that the winds are a very important disturbance on the spiral guidance system performance. In order to reduce the sensitivity to wind effects, it will be necessary to include the wind estimates in the nominal path calculations, and perhaps increase the guidance gains.

Table 13. Effects of Airspeed Error With Coupled Bank & Throttle Control.

t	θ	ψ	R	V	ϕ	α	t*	ψ^*	ϕ^*
0.0	0.0	0.0	2000.0	50.00	9.05	1.500	0.00	0.00	9.05
10.0	27.0	29.6	1959.4	59.65	8.09	0.461	9.30	27.00	9.05
20.0	57.2	55.9	1947.2	61.38	8.87	-0.048	19.73	57.24	9.05
30.0	87.2	85.2	1982.2	60.38	9.57	-0.103	30.07	87.25	9.05
40.0	116.3	115.7	2005.6	59.74	9.36	-0.019	40.09	116.33	9.05
50.0	145.1	145.3	2006.7	59.79	9.05	0.021	50.01	145.10	9.05
60.0	174.0	174.2	2001.0	59.99	8.97	0.013	59.97	174.00	9.05

$K_V = 0.15 \text{ sec}^{-1}$
 $K_t = 1.0 \text{ ft/sec}^3$
 $C_t = 0.1 \text{ sec}^{-1}$
 $V_o = 50 \text{ kt}$

Table 14. Effects of Airspeed Error With Uncoupled Bank & Throttle Control.

t	θ	ψ	R	V	ϕ	α	t*	ψ^*	ϕ^*
0.0	0.0	0.0	2000.0	50.00	9.05	1.500	0.00	0.00	9.05
10.0	26.9	26.8	1985.6	59.68	8.32	0.474	9.27	26.92	9.05
20.0	56.5	55.7	1998.1	61.82	9.77	0.017	19.50	56.59	9.05
30.0	86.3	86.2	2007.2	61.39	9.61	-0.073	29.77	86.37	9.05
40.0	115.7	115.9	2006.4	60.71	9.26	-0.054	39.91	115.78	9.05
50.0	144.9	145.1	2003.4	60.30	9.10	-0.027	49.96	144.96	9.05
60.0	174.0	174.1	2001.5	60.11	9.06	-0.011	59.99	174.03	9.05

$C_t = 0.0 \text{ sec}^{-1}$
 $V_o = 50 \text{ kt}$

Table 15. Effects of Wind With Coupled Bank & Throttle Control.

t	θ	ψ	R	V	ϕ	α	t^*	ψ^*	ϕ^*
0.0	0.0	0.0	2000.0	60.00	9.05	0.000	0.00	0.00	9.05
10.0	20.8	29.6	1846.4	65.72	7.62	0.817	7.17	20.80	9.05
20.0	50.3	45.5	1576.4	70.70	4.66	-0.047	17.37	50.39	9.05
30.0	87.1	62.8	1568.9	65.49	8.47	-0.847	30.03	87.14	9.05
40.0	122.0	93.2	1725.9	57.00	10.23	-0.786	42.08	122.09	9.05
50.0	155.1	129.8	1923.9	50.10	10.09	-0.567	53.46	155.10	9.05
60.0	185.5	170.6	2154.3	45.90	10.13	-0.235	63.96	185.57	9.05
70.0	212.7	213.5	2365.6	45.51	10.05	0.187	73.35	212.79	9.05
80.0	236.8	254.2	2479.1	49.42	9.70	0.606	81.65	236.88	9.05
90.0	258.7	288.3	2431.2	57.10	8.81	0.913	89.19	258.75	9.05
100.0	280.4	313.6	2214.7	66.75	7.20	0.958	96.67	280.45	9.05
110.0	305.5	331.0	1920.8	74.82	5.80	0.553	105.31	305.52	9.05
120.0	336.0	346.4	1729.8	77.13	7.07	-0.103	115.83	336.05	9.05

$C_t = 0.1 \text{ sec}^{-1}$
 $W = 20 \text{ kt}$

Table 16. Effects of Wind With Uncoupled Bank & Throttle Control.

t	θ	ψ	R	V	ϕ	α	t^*	ψ^*	ϕ^*
0.0	0.0	0.0	2000.0	60.00	9.05	0.000	0.00	0.00	9.05
10.0	20.7	19.9	1924.7	65.72	5.53	0.829	7.14	20.74	9.05
20.0	47.6	38.7	1837.7	72.08	8.63	0.313	16.41	47.61	9.05
30.0	80.6	66.0	1793.3	71.62	11.79	-0.435	27.79	80.62	9.05
40.0	117.8	101.4	1781.7	64.27	12.96	-1.018	40.63	117.89	9.05
50.0	156.1	142.9	1818.4	52.84	11.79	-1.182	53.80	156.10	9.05
60.0	190.5	185.6	1913.6	42.56	9.08	-0.759	65.69	190.58	9.05
70.0	218.9	224.0	2055.2	38.48	7.10	-0.004	75.45	218.90	9.05
80.0	242.3	256.5	2202.3	41.71	6.42	0.641	83.54	242.37	9.05
90.0	263.5	283.3	2297.0	50.05	6.24	0.992	90.84	263.54	9.05
100.0	284.5	305.0	2309.0	60.49	6.24	1.055	98.09	284.57	9.05
110.0	307.1	323.9	2255.4	70.42	6.79	0.891	105.85	307.10	9.05
120.0	331.9	342.8	2171.9	78.00	7.99	0.598	114.43	331.97	9.05

$C_t = 0.0 \text{ sec}^{-1}$
 $W = 20 \text{ kt}$

4.3 GUIDANCE GAINS

The linearized model of the horizontal guidance law in Figure 11 allows the analyst to apply all the standard techniques of linear control theory to select an appropriate set of guidance gains. However, the following cautions should be noted:

- The actual guidance law places a limit on the magnitude of the commanded bank angle.
- The preceding analysis has neglected any attitude dynamics in the rotorcraft's response to bank angle commands.
- The actual system may operate outside the range where the linear model is valid.

To avoid potential problems, the linear model is used to select the guidance gains and to predict system performance; and the prediction is then verified using the non-linear model in a trial and error fashion. Improved gains were selected using this technique together with a determination of the effect of a finite bank angle rate.

The analysis led to selection of the following guidance gains:

$$C_r = 0.005 \text{ rad/ft}$$

$$C_\psi = -1.77 \text{ rad/rad}$$

$$C_f = 0 \text{ rad/sec}$$

The value of C_f is based on results presented in Section 3.7; C_f has a relatively minor effect on the 4-D guidance performance, and tends to destabilize the 3-D response. The guidance gains C_r and C_ψ were selected iteratively from combinations that provide a natural damping of 70%. Figure 12 compares the radius error, heading error, and bank histories in response to a 100 ft initial radius error for four sets of gains. The error responses of the first three cases are very similar, while case four is extremely slow in settling out. Case 3 has a much less violent bank history, and was therefore selected as the best compromise.

In Figure 12 the actual bank angle begins at the maximum allowable value (30°) for cases 1 - 3 in response to the initial condition error on r . To determine the effect of a finite bank angle rate, the guidance law was modified to generate a bank rate command proportional to the error between desired and actual angle, viz

$$\dot{\phi} = K_\phi (\phi_c - \phi) \quad (78)$$

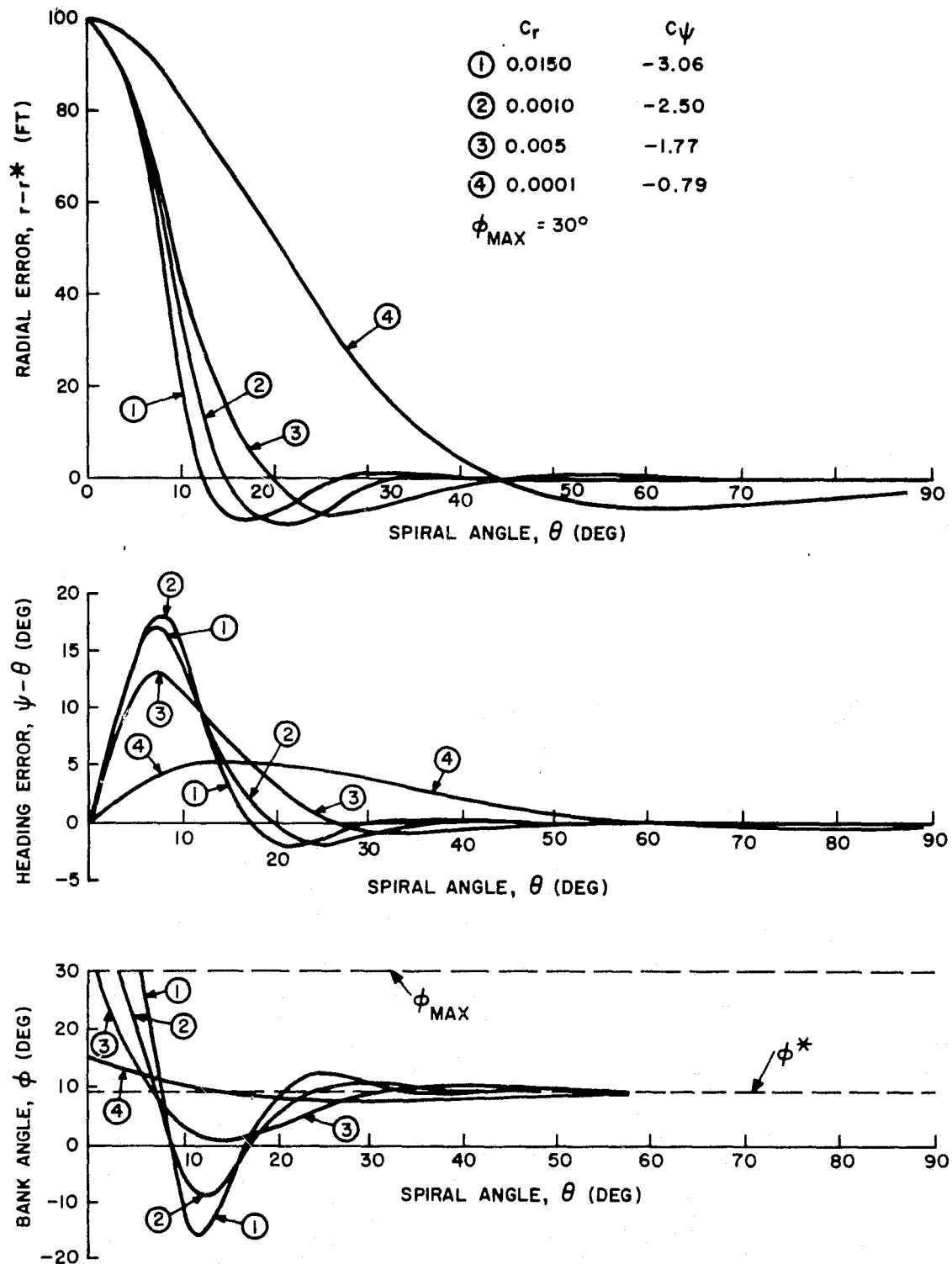


Figure 12. Spiral Guidance Response for Various Sets of Gains.

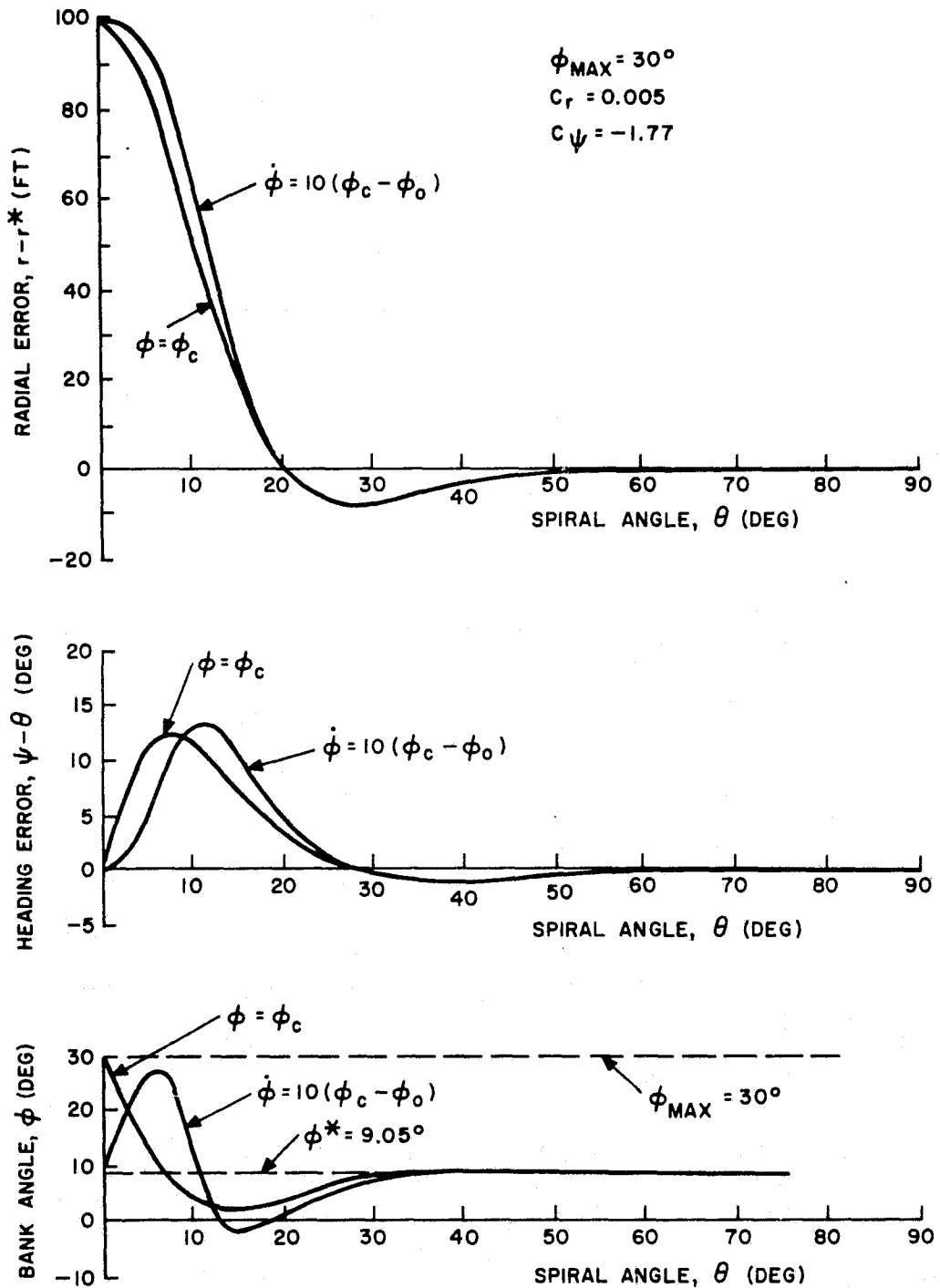


Figure 13. Effect of Finite Bank Rate.

The results for $K_{\dot{\phi}} = 10 \text{ sec}^{-1}$ are compared in Figure 13 with the infinite bank rate results of Figure 12. The finite bank rate has little effect on the radial error history, and produces only a small delay in the heading response. For lower values of $K_{\dot{\phi}}$ the response lags more, but is practically the same within 40° of turn angle for $K_{\dot{\phi}} = 1.0 \text{ sec}^{-1}$.

4.4 ERROR SENSITIVITY

Figure 11 is valuable for determining the sensitivity and dynamic response of the system to measurement errors. Disturbances can be entered at the points labelled $\delta\phi$, $\delta\Psi$, δr , δV , and δt to correspond, respectively, to errors in the measurement of bank angle, heading angle, radial position, airspeed and time. Since the steady-state input to all the integrators has to be zero, the position error sensitivity to heading error, for example, is given by

$$\left. \frac{\delta r}{\delta \Psi} \right|_{\text{steady state}} = \frac{C_{\Psi}}{C_r} \cong 6 \text{ ft/deg} \quad (79)$$

for

$$C_r \cong .3 \text{ deg/ft}$$

$$C_{\Psi} \cong 1.8 \text{ deg/deg}$$

$$\frac{1}{\omega_n} \cong 2.5 \text{ sec} \quad \frac{1}{\omega_p} \cong 7.5 \text{ deg} \quad \xi = .7 \quad (80)$$

Similarly, the steady-state sensitivity of position error to bank angle error is given by

$$\frac{\delta r}{\delta \phi} = \frac{1}{C_r} \cong 3.5 \text{ ft/deg.} \quad (81)$$

SECTION 5 WIND ESTIMATION

The previous section has demonstrated the need for a reliable estimate of the winds in order to achieve the required guidance accuracy during the spiral descent. This section presents two approaches to providing this capability.

5.1 KALMAN WIND ESTIMATOR FORMULATION

The first approach is an extension of the wind estimator in the Kalman filter developed for the Straw-Man navigation system (Reference 1). The nomenclature for the Kalman wind estimator for spiral approaches is shown in Figure 14.

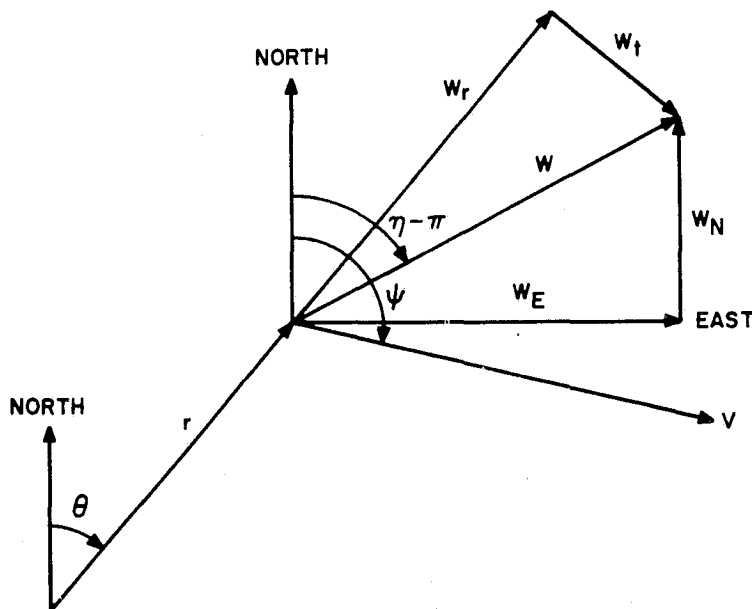


Figure 14. Nomenclature for Wind Analysis.

The North and East wind components are

$$W_N = -W \cos \eta \quad (82a)$$

$$W_E = -W \sin \eta \quad (82b)$$

The tangential and radial components are:

$$W_t = -W \sin (\eta - \theta) = -W_N \sin \theta + W_E \cos \theta \quad (83a)$$

$$W_r = -W \cos (\eta - \theta) = W_N \cos \theta + W_E \sin \theta \quad (83b)$$

The state equations (8) - (12), in terms of the North and East wind components, are

$$\frac{dr}{d\theta} = r \frac{V \cos (\psi - \theta) + W_N \cos \theta + W_E \sin \theta}{V \sin (\psi - \theta) - W_N \sin \theta + W_E \cos \theta} \quad (84)$$

$$\frac{d\psi}{d\theta} = \frac{rg}{V} \frac{\tan \phi_c}{V \sin (\psi - \theta) - W_N \sin \theta + W_E \cos \theta} \quad (85)$$

$$\frac{dV}{d\theta} = \frac{ra_c}{V \sin (\psi - \theta) - W_N \sin \theta + W_E \cos \theta} \quad (86)$$

$$\frac{dh}{d\theta} = \frac{rh_c}{V \sin (\psi - \theta) - W_N \sin \theta + W_E \cos \theta} \quad (87)$$

$$\frac{dt}{d\theta} = \frac{r}{V \sin (\psi - \theta) - W_N \sin \theta + W_E \cos \theta} \quad (88)$$

These must be augmented by the equations for the wind component models. For example, if these are assumed to be exponentially-correlated random processes (i.e., first-order colored noises), the appropriate equations are

$$\frac{dW_N}{d\theta} = -\frac{W_N}{\theta_c} + q_N \quad (89a)$$

$$\frac{dW_E}{d\theta} = -\frac{W_E}{\theta_c} + q_E \quad (89b)$$

where θ_c is the characteristic angle of the processes, and q_N and q_E are driving white noises.

The optimum estimator for the wind is formulated as follows. The linearized state equations with the guidance loop closed are:

$$\frac{dx}{d\theta} = Fx + q \quad (90)$$

The perturbation state vector is

$$x = [\delta r, \delta \psi, \delta V, \delta h, \delta t, \delta W_N, \delta W_E]^T \quad (91)$$

where δW_N = North component of wind error

δW_E = East component of wind error

The driving noise vector is

$$q = [0, 0, 0, 0, 0, q_N, q_E]^T \quad (92)$$

The linearized closed-loop system matrix is approximately

$$F = \begin{bmatrix} 0 & -r & 0 & 0 & 0 & r \cos \theta/V & +r \sin \theta/V \\ rgC_r/V^2 & rgC_\psi/V^2 & 0 & rgC_r/V^2 & 0 & +rg \tan \phi \sin \theta/V^3 & -rg \tan \phi \cos \theta/V^3 \\ 0 & 0 & rK_r/V & rK_\psi/V & 0 & 0 & 0 \\ 0 & 0 & 0 & 0 & rK_h/V & 0 & 0 \\ 1/V & 0 & -r/V^2 & 0 & 0 & +r \sin \theta/V^2 & -r \cos \theta/V^2 \\ 0 & 0 & 0 & 0 & 0 & -1/\theta_c & 0 \\ 0 & 0 & 0 & 0 & 0 & 0 & -1/\theta_c \end{bmatrix} \quad (93)$$

The linearized measurement vector is given by

$$m = Hx + r \quad (94)$$

where r is the vector of measurement noises, and H is the measurement geometry matrix.

For example, if direct measurements are made of δr , δV , $\delta \psi$, δt and δh , then

$$H = \begin{bmatrix} 1 & 0 & 0 & 0 & 0 & 0 & 0 \\ 0 & 1 & 0 & 0 & 0 & 0 & 0 \\ 0 & 0 & 1 & 0 & 0 & 0 & 0 \\ & & & 1 & 0 & 0 & 0 \\ & & & & 1 & 0 & 0 \\ & & & & & 0 & 0 \\ 0 & 0 & 0 & 0 & 0 & 0 & 0 \end{bmatrix} \quad (95)$$

The estimate of the state \hat{x} is propagated by

$$\dot{\hat{x}} = F\hat{x} + PH^T R^{-1} (m - H\hat{x}) \quad (96)$$

where R is the power spectral density of r. The error covariance matrix P propagates as follows:

$$\dot{P} = FP + PF^T + Q - PH^T R^{-1} HP \quad (97)$$

where Q, the power spectral density of q, defines the wind strengths.

Further development and analysis of the Kalman wind estimator were discontinued in favor of the simplified wind estimator described subsequently.

5.2 SIMPLIFIED WIND ESTIMATOR

One simplified wind estimator can be formulated by reasoning that the lateral errors δr and $\delta \psi$ are due primarily to the radial wind component, while the longitudinal errors δV and δt are due primarily to the tangential wind component:

$$\begin{bmatrix} \delta \dot{\hat{W}}_N \\ \delta \dot{\hat{W}}_E \end{bmatrix} = \begin{bmatrix} \sin \theta & \cos \theta \\ -\cos \theta & \sin \theta \end{bmatrix} \begin{bmatrix} K_1 \delta r + K_2 \delta \psi \\ K_3 \delta V + K_4 \delta t \end{bmatrix} \quad (98)$$

The net effect of this estimator is to provide an additional integration to null the "quasi steady-state" error due to an unknown wind. However, the proper gains are difficult to pick by trial and error, so it may still be easier to use the optimum Kalman formulation.

Another simplified wind estimator is obtained by using the off-nominal values of bank angle and heading angle to estimate the tangential and radial wind components. The changes in the north and east components are transformed from the tangential and radial components by the spiral angle θ .

$$\begin{bmatrix} \delta \hat{W}_N \\ \delta \hat{W}_E \end{bmatrix} = \begin{bmatrix} -\sin \theta & \cos \theta \\ \cos \theta & \sin \theta \end{bmatrix} \begin{bmatrix} \delta \hat{W}_t \\ \delta \hat{W}_r \end{bmatrix} \quad (99)$$

If the rotorcraft is close to the nominal spiral, a tangential wind requires a change in bank angle, while a radial wind requires a change in heading into the wind. Thus, the bank and heading perturbations give an indication of the unknown wind:

$$\frac{\delta \hat{W}_t}{\delta \theta} = \frac{1}{\theta_c} \left(\frac{\partial W_t}{\partial \phi} \right) \delta \phi \quad (100)$$

$$\frac{\delta \hat{W}_r}{\delta \theta} = \frac{1}{\theta_c} \left(\frac{\partial W_r}{\partial \psi} \right) \delta \psi \quad (101)$$

where θ_c is a "characteristic turn angle" over which the wind estimate is averaged, and the estimator "gains" are given by

$$\frac{\partial W_t}{\partial \phi} = \frac{r^*g}{2V^*} \quad \text{"bank sensitivity to tail wind"} \quad (102)$$

$$\frac{\partial W_r}{\partial \psi} = V^* \quad \text{"crab sensitivity to crosswind"} \quad (103)$$

Example

$$r^* = 2000 \text{ ft}$$

$$V^* = 60 \text{ kt}$$

For a characteristic time of the estimator of about 30 sec, let $\theta_c = 90^\circ$. The estimator gains are

$$\frac{r^*g}{2V^*} \approx 320 \frac{\text{ft/sec}}{\text{rad}} \approx 3 \text{ kt/deg} \quad (104a)$$

$$V^* \approx 100 \frac{\text{ft/sec}}{\text{rad}} \approx 1 \text{ kt/deg} \quad (104b)$$

The performance of the simplified estimator is shown in Figures 15, 16 and 17 for an unknown steady wind of 20 kts from four directions, using the above gains and the same nominal spiral as used previously. The wind speed estimate is within 62% of the actual after a 90° turn in all cases, and the direction estimate is even better. The maximum radial error is less than 90 ft for initial cross winds, and less than 50 ft for an initial head or tail wind.

From these results, the simplified estimator seems to provide an effective means of reducing the effects of unknown winds on the spiral guidance scheme.

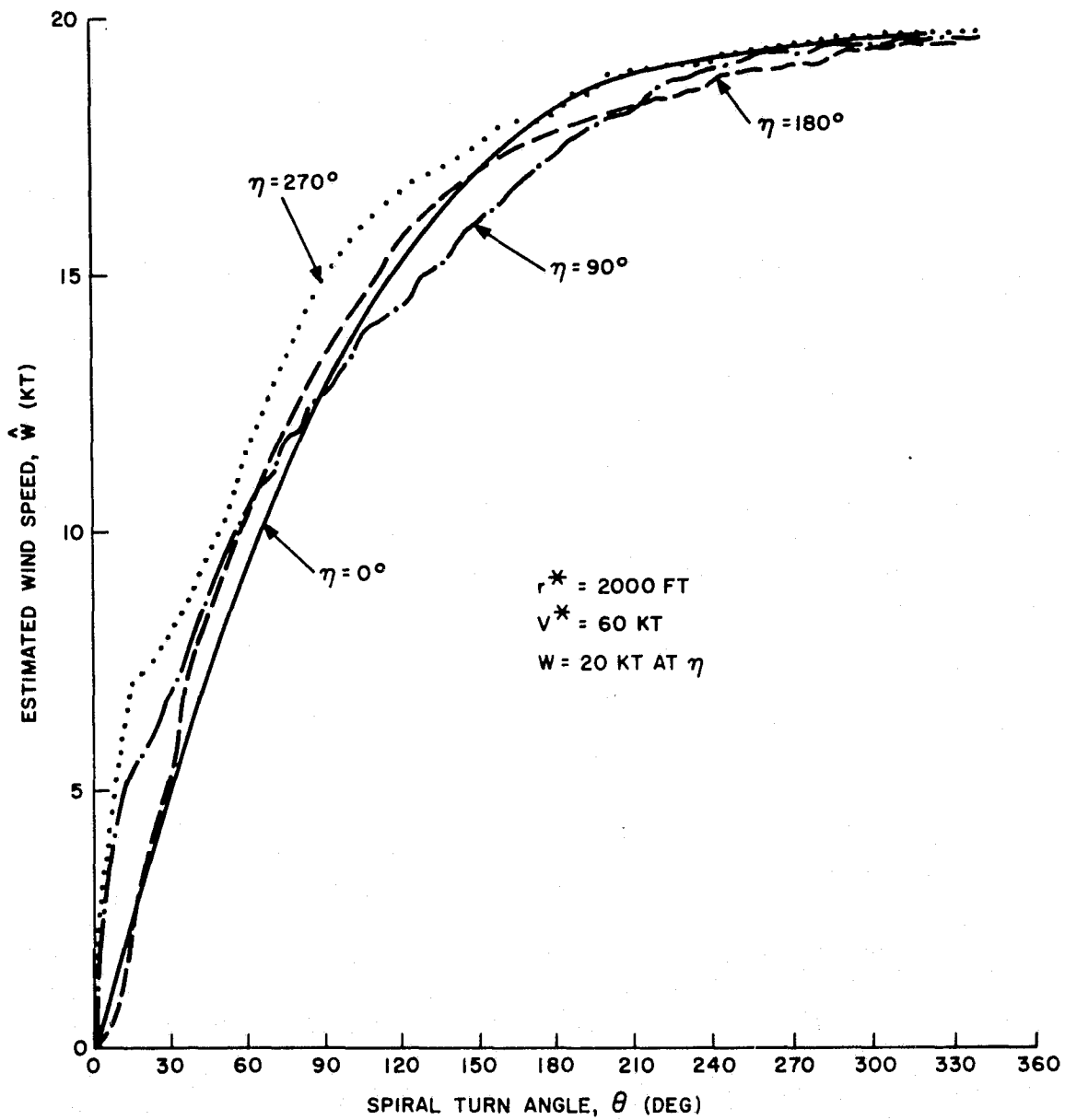


Figure 15. Estimated Wind Speed With Simplified Estimator.

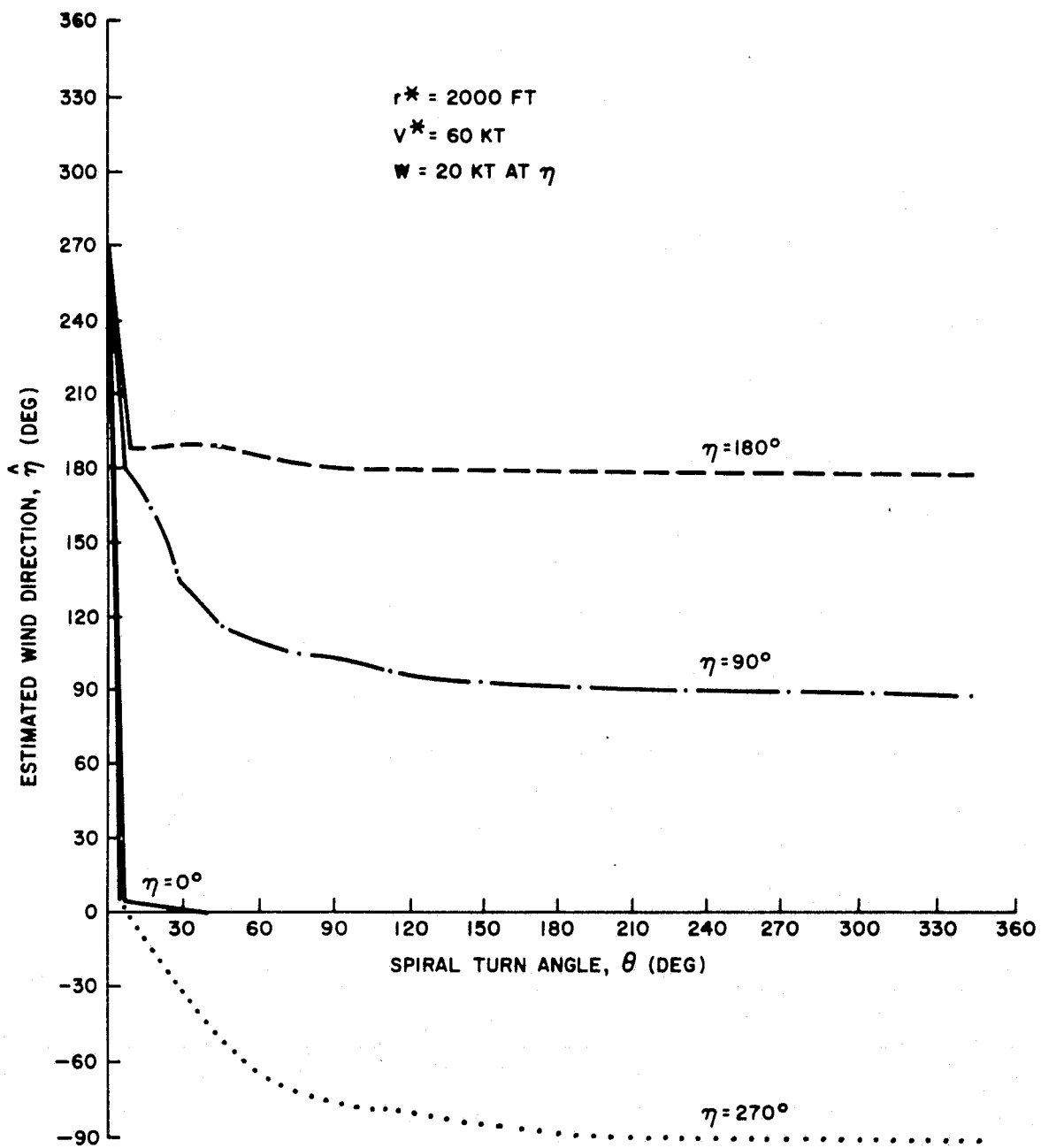


Figure 16. Estimated Wind Direction With Simplified Estimator.

- 54 -

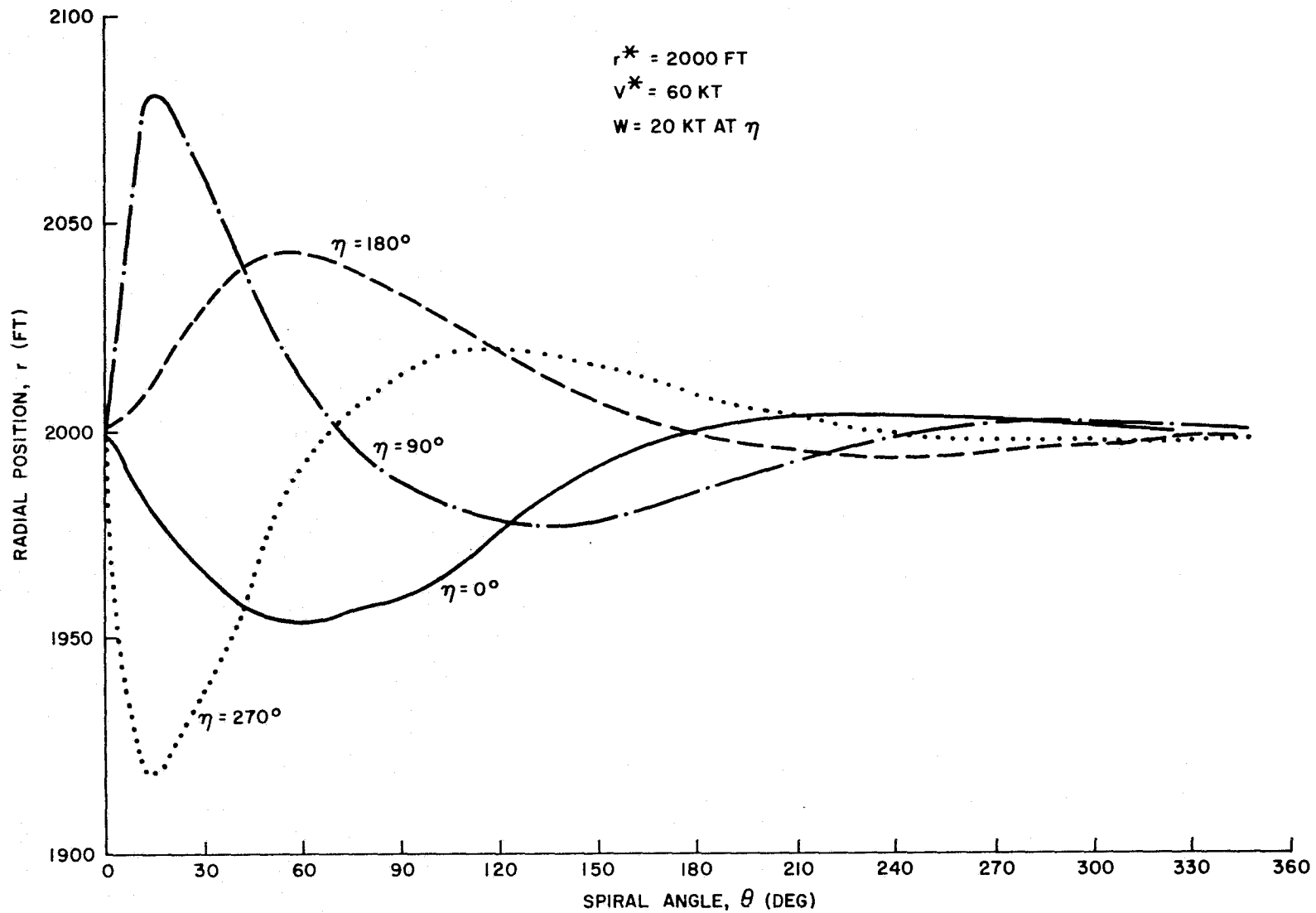


Figure 17. Radial Position Accuracy With Simplified Wind Estimator.

5.3 WIND ESTIMATOR DYNAMICS

Because knowledge of the wind is crucial to the performance of the guidance law, it is important to consider the dynamics of the wind estimator. The effect of the wind estimator is to produce variations in ϕ^* and ψ^* to eliminate radial errors:

$$p\psi^* = \frac{1}{\theta_c} (\hat{\psi} - \psi^*) , \quad \psi_0^* = 0 \quad (105a)$$

$$p\phi^* = \frac{1}{\theta_c} (\phi_c - \phi^*) , \quad \phi_0^* = \text{constant} \quad (105b)$$

where $p = d/d\theta$. Substituting (105a) and (105b) into (33) with $C_\psi =$, solving for ϕ gives

$$\phi_c = C_r \left(1 + \frac{1}{\theta_c p} \right) \delta r + C_\psi \psi \quad (106)$$

where $\delta r = \hat{r} - r^*$.

The result of the wind estimator is to produce an effective integral-plus-bypass term in the feedback of δr . This is exactly the technique used in mechanizing ILS couplers for conventional aircraft.

The linear signal flow diagram in the "angle domain" is shown in Figure 18. The characteristic equation of this system is third order:

$$p^3 - C_\psi \frac{r^* g}{V^{*2}} p^2 + \frac{r^{*2} g}{V^{*2}} C_r p + C_r \frac{r^{*2} g}{V^{*2}} \frac{1}{\theta_c} = 0 \quad (107)$$

For stability, the characteristic angle of the estimator must satisfy

$$\theta_c > - \frac{V^{*2}}{r^* g C_\psi} \quad (108)$$

The sensitivity of the estimator to a crosswind is

$$\delta r \cong \frac{-C_\psi}{C_r} \frac{W_r}{V^*} \quad (109)$$

For $C_r = 0.005$, $C_\psi = -1.77$, $V^* = 60$ kt, this gives $\delta r \cong 6$ ft/kt of unknown crosswind.

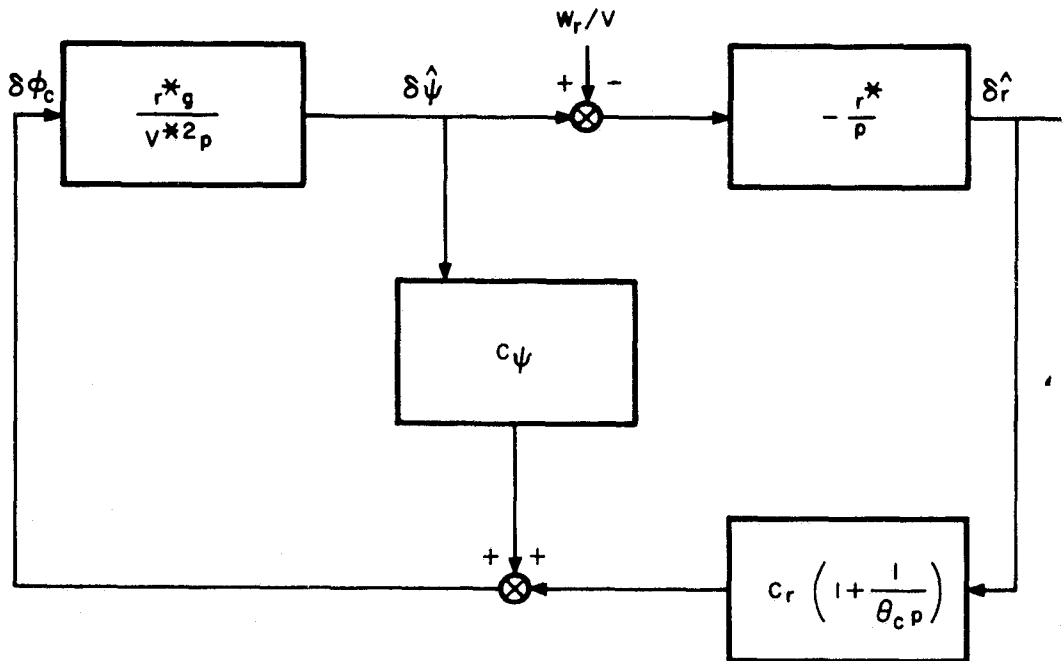


Figure 18. Linear Signal Flow Diagram for Wind Estimator.

The wind estimator will lag in a steady shear wind by approximately the characteristic angle θ_c . The maximum error due to a shear is about

$$\hat{w} \approx \theta_c \dot{h} \frac{V^*}{r^*} (dW/dh) \delta r \quad (110)$$

Conventional automatic landing systems are normally certificated on the basis of $dW/dh = 8$ knots/30 meters ≈ 0.08 kt/ft. With $\theta_c = 30^\circ$ and $\dot{h} = 500$ ft/min, this produces a maximum radial error in a shear of 38 ft. Figure 19 illustrates the performance of the wind estimator during a 300° spiral descent of 1000 ft in a steady shear of 0.01 kt/ft. As expected, the estimated wind lags the true wind, with a peak error of about 3 kts.

For straight flight during a transition segment (see Section 7), the preceding analysis is modified as follows:

$$\phi_c = C_y \hat{y} + C_\psi (\hat{\psi} - \psi^*) \quad (111)$$

$$\psi^* = \frac{1}{\theta_c p} (\hat{\psi} - \psi^*) = \frac{\hat{\psi}}{1 + \theta_c p} \quad (112)$$

† This is not maintained over altitude changes of more than a couple hundred of feet.

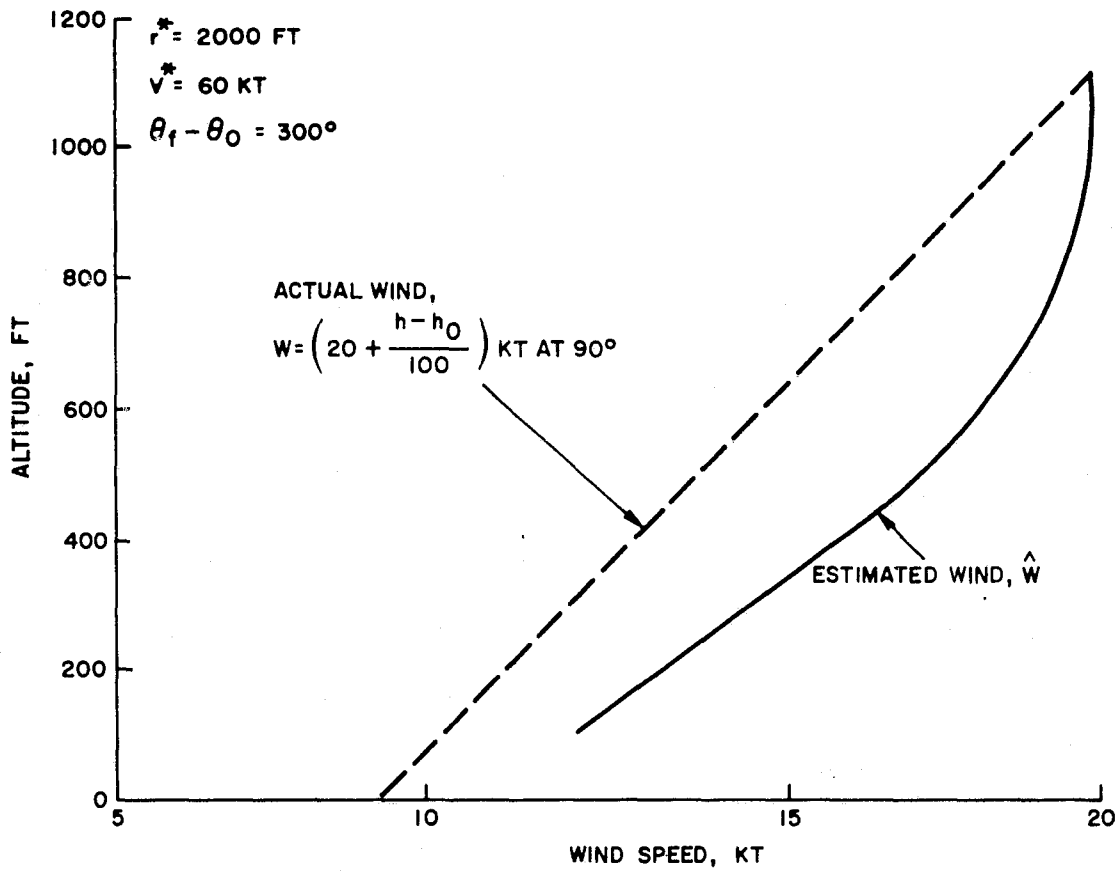


Figure 19. Wind Estimator in a Steady Shear.

Therefore,

$$\phi_c = C_y y + C_\psi \frac{\theta_c p}{1 + \theta_c p} \hat{\psi} \quad (113)$$

The linearized block diagram is shown in Figure 20.

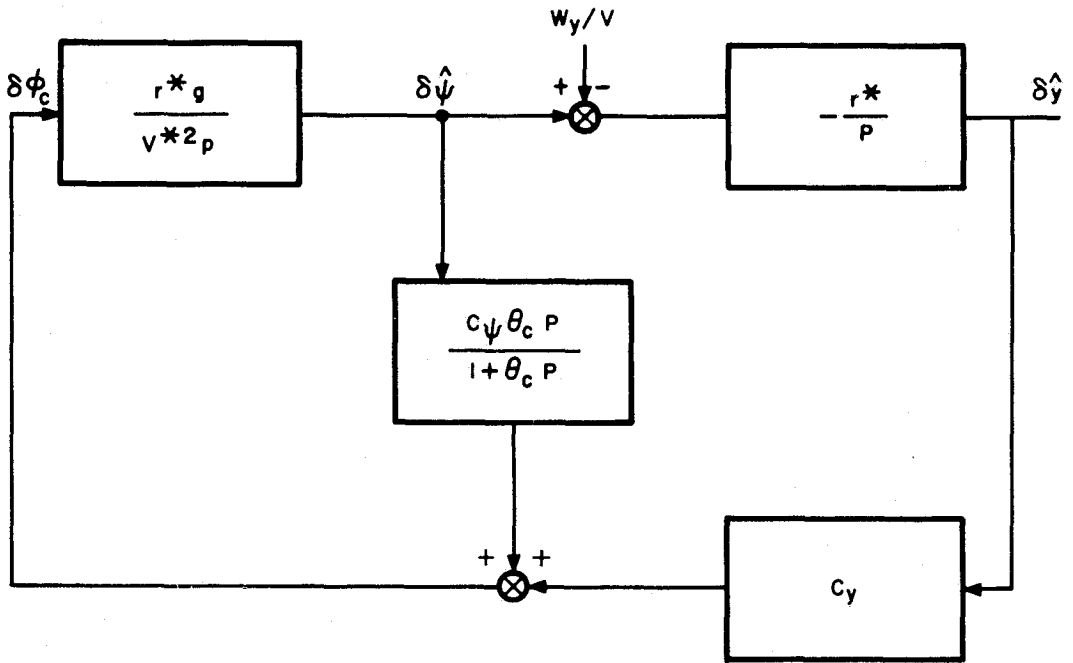


Figure 20. Linear Signal Flow Diagram for Wind Estimator During Transition Segment.

SECTION 6 PHASE PLANE ANALYSIS

In this section the nonlinear response of the guidance laws are interpreted in the phase plane. The problem of capture when spiral guidance is initiated a long way from equilibrium conditions leads to a modification in the guidance algorithm.

6.1 THE PHASE PLANE

The phase plane is a plot of heading error, $\hat{\psi} - \psi^*$, vs radial position error, $\hat{r} - r^*$. Since the lateral guidance variable, ϕ_c , is determined as a nonlinear function of these two parameters, it is possible to plot lines of constant bank in the phase plane as shown in Figure 21. It is also possible to plot trajectories of the nonlinear response of the system as shown in Figure 22.

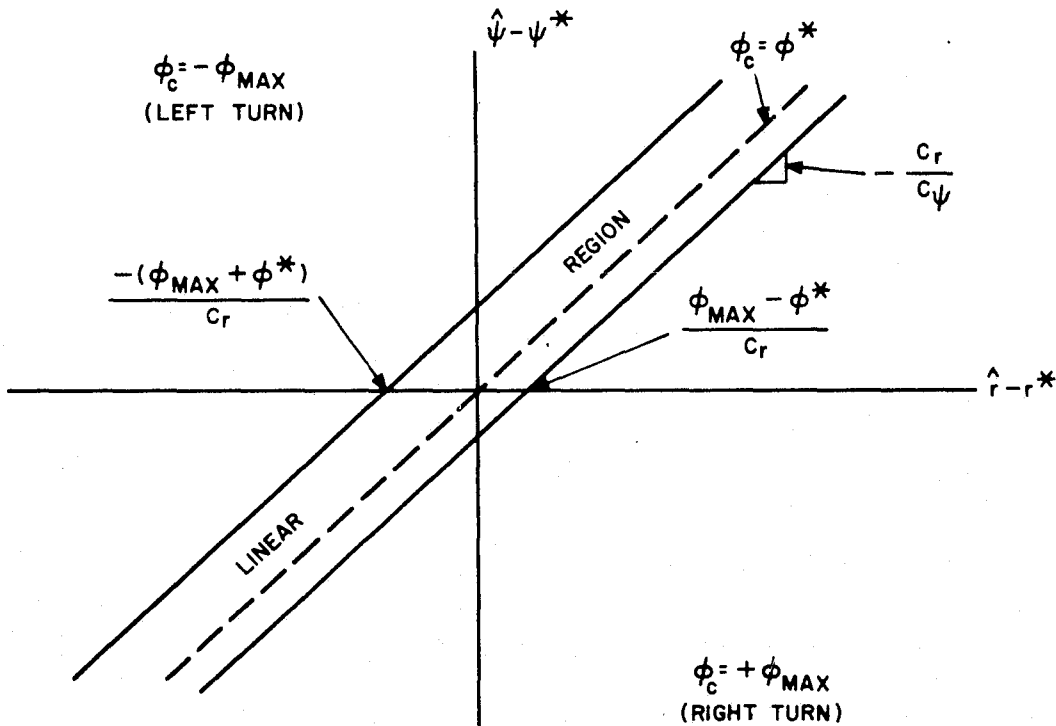


Figure 21. Phase-Plane Plot of Guidance Law.

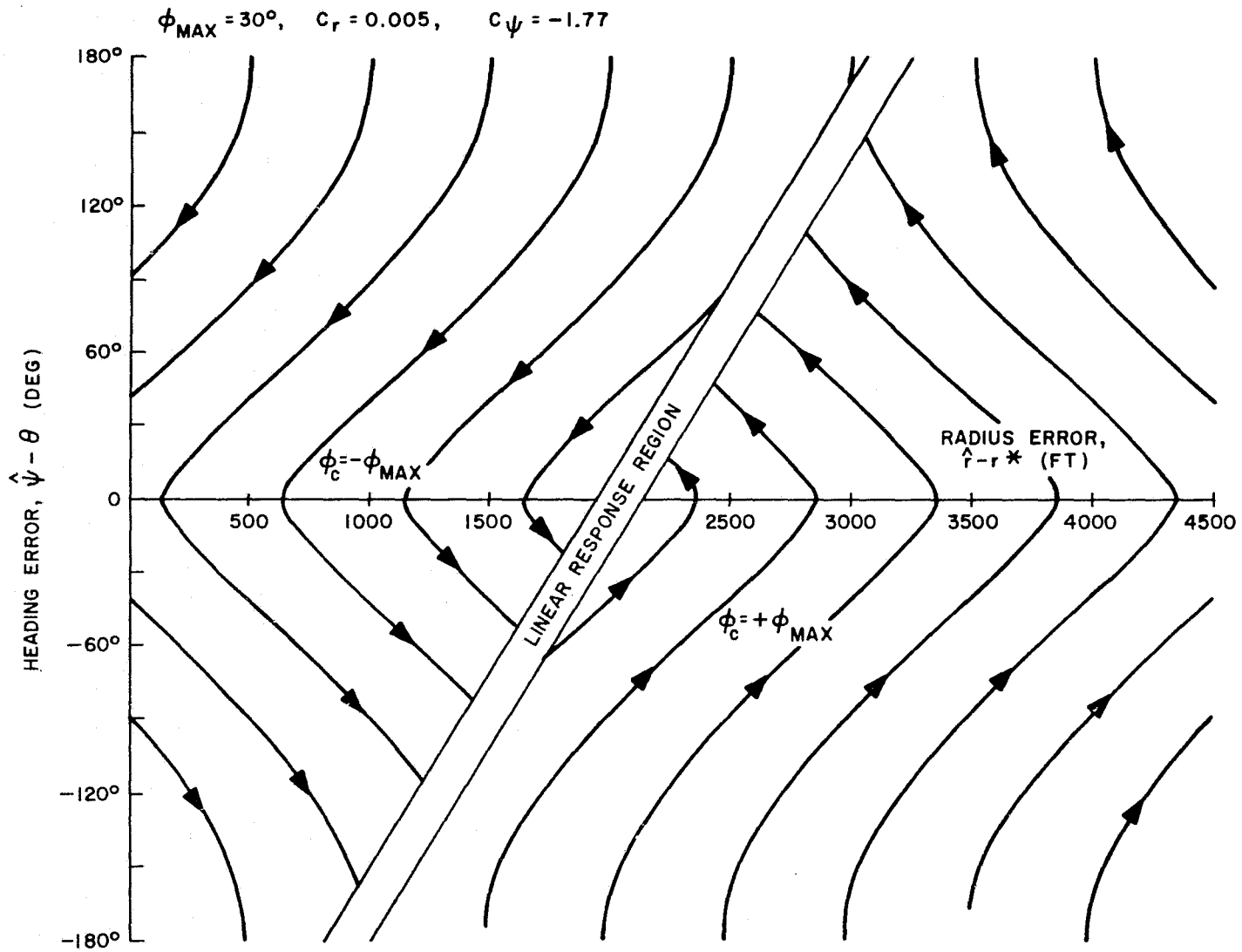


Figure 22. Phase-Plane Performance of Horizontal Spiral Guidance Law.

Some examples of horizontal system performance for large initial errors are shown in Figure 23. In examples A and B, large initial heading and radial errors, respectively, are eventually corrected and the rotorcraft trajectory settles into the desired spiral in an equilibrium condition. In example C, the extremely large initial radial error prevents the rotorcraft from leaving the maximum right-turn bank command, and consequently it fails to capture the equilibrium spiral condition.

6.2 GUARANTEED SPIRAL CAPTURE

For initial spiral offsets greater than 1200 - 1500 ft, the spiral guidance laws will command a continuous maximum bank angle (left or right) and result in a circular flight which never intercepts the desired spiral. Although such large deviations should not normally occur, the guidance law must still guarantee capture in the event they do exist.

6.2.1 RIGHT HAND TURNS

To ensure spiral capture, the guidance law can be modified to restrict the heading angle error, $\hat{\psi} - \psi^*$. The modified phase plane is shown in Figure 24 for driving $|\hat{\psi} - \psi^*| \leq \Delta\psi_{\max}$. The modified bank guidance algorithm becomes

$$\phi_c = \begin{cases} C_\psi (\hat{\psi} - \psi^* - \Delta\psi_{\max}) & , \hat{r} > r_1 \\ \phi^* + C_r (\hat{r} - r^*) + C_\psi (\hat{\psi} - \psi^*) & , r_2 < \hat{r} < r_1 \\ C_\psi (\hat{\psi} - \psi^* + \Delta\psi_{\max}) & , \hat{r} < r_2 \end{cases} \quad (114)$$

where

$$r_1 = r^* - \frac{C_\psi \Delta\psi_{\max} + \phi^*}{C_r} \quad (115)$$

$$r_2 = r^* + \frac{C_\psi \Delta\psi_{\max} - \phi^*}{C_r} \quad (116)$$

and $\Delta\psi_{\max}$ is the largest value of $|\hat{\psi} - \psi^*|$ for $\phi_c = 0$.

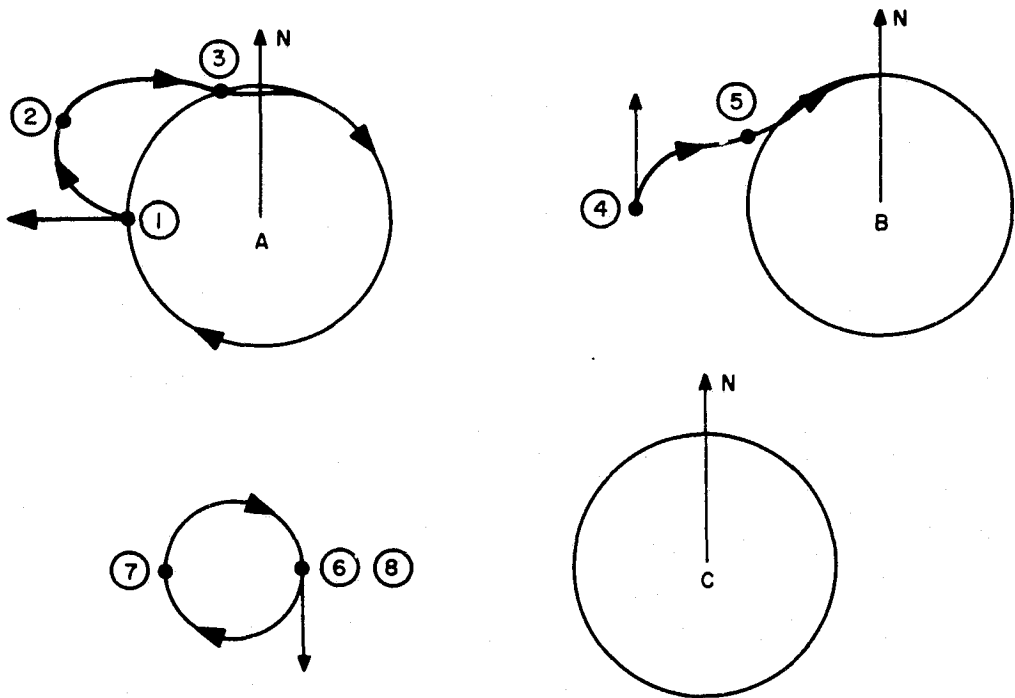
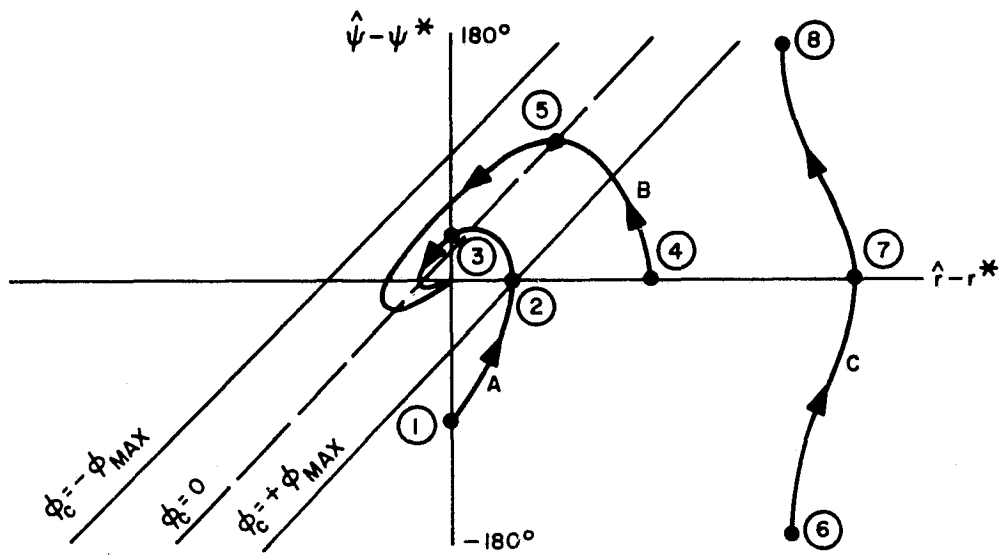


Figure 23 . Phase-Plane Examples .

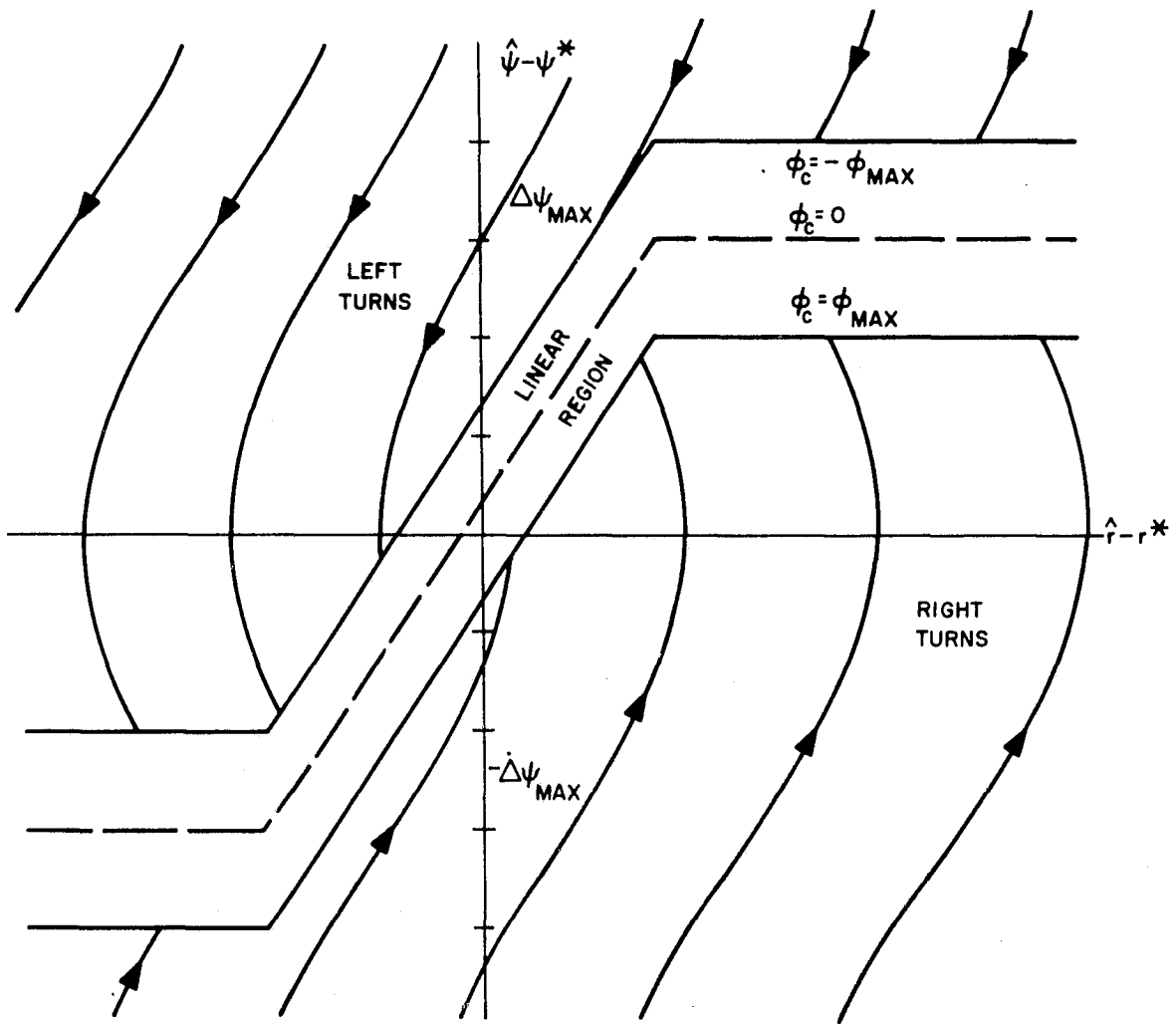


Figure 24. Modified Guidance Law.

Figure 25 shows two examples of the modified guidance law performance with a large initial error for $\Delta\psi_{max} = 60^\circ$ and 90° . The capture region in Figure 25 is only shown for $\Delta\psi_{max} = \pm 60^\circ$. There is a different capture zone for the case of $\Delta\psi_{max} = \pm 90^\circ$. The 60° case has a large initial heading error overshoot of $\Delta\psi_{max}$, but relatively smaller final overshoots of the nominal heading and radius. The initial heading overshoot for the case of $\Delta\psi_{max} = \pm 90^\circ$ is smaller. If the capture region were shown it would be evident that the initial overshoot does not exceed the linear region. The final overshoots are larger in the case of $\Delta\psi_{max} = \pm 90^\circ$. Consequently, 60° seems to provide a good compromise solution.

6.2.2 LEFT-HAND TURNS

For left-handed spirals, the phase plane is effectively "flipped" around the $\hat{\psi} - \psi^*$ axis. The modified bank guidance law is

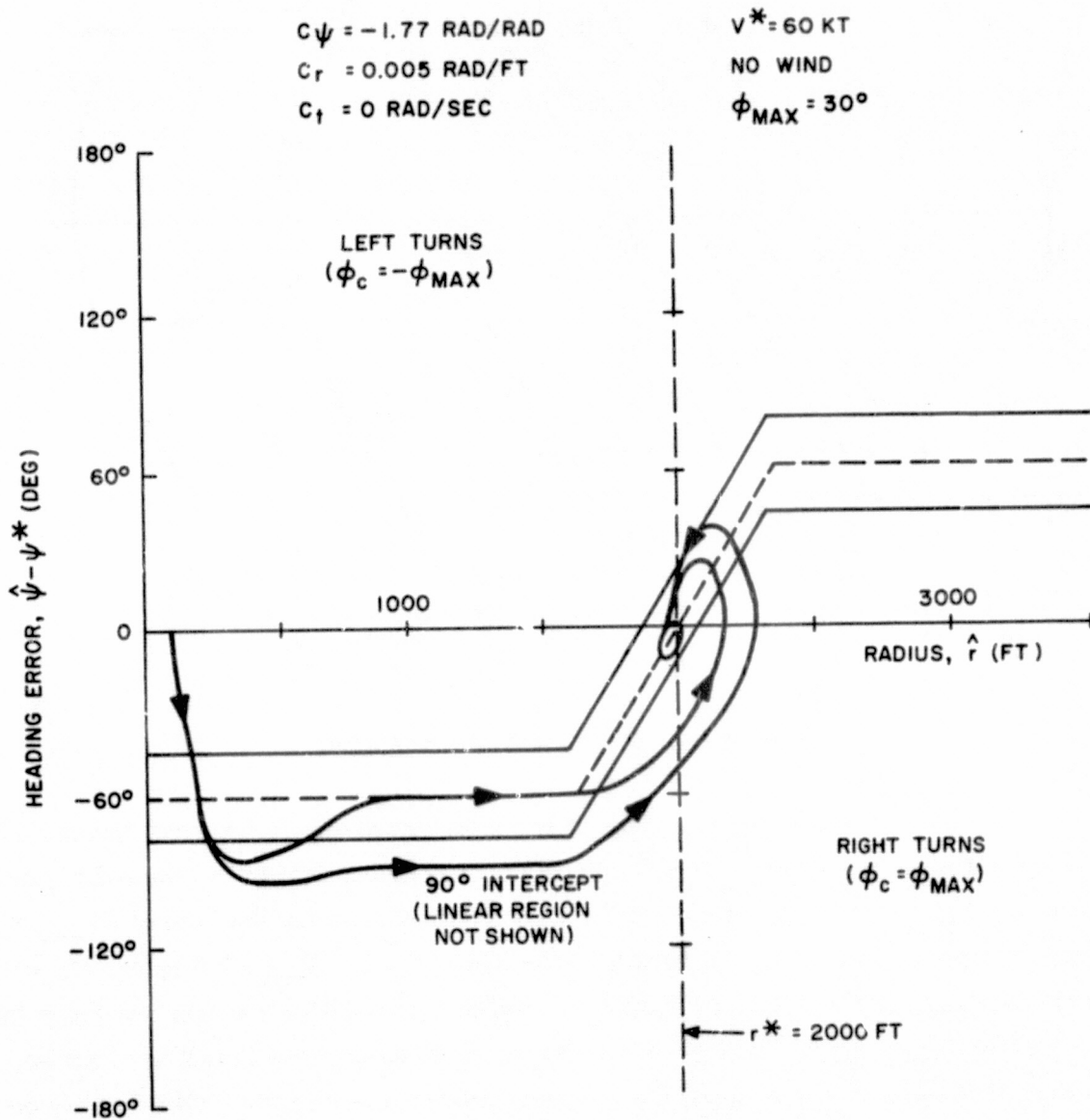


Figure 25. Example of Modified Guidance Law for $\Delta\psi_{\text{max}} = 60^\circ$ and 90° .

$$\phi_c = \begin{cases} C_\psi (\hat{\psi} - \psi^* + \Delta\psi_{\max}) & , \hat{r} > r_1 \\ \phi^* - C_r(\hat{r} - r^*) + C_\psi(\hat{\psi} - \psi^*) & , r_2 < \hat{r} < r_1 \\ C_\psi (\hat{\psi} - \psi^* - \Delta\psi_{\max}) & , \hat{r} < r_2 \end{cases} \quad (114')$$

where

$$r_1 = r^* - \frac{C_\psi \Delta\psi_{\max} - \phi^*}{C_r} \quad (115')$$

$$r_2 = r^* + \frac{C_\psi \Delta\psi_{\max} + \phi^*}{C_r} \quad (116')$$

SECTION 7 SPIRAL TRANSITION SEGMENTS

The transitions between the spiral and straight flight are critical phases which must be accomplished smoothly. In general, the nominal transition paths will consist of straight line segments tangent to the spiral arcs. On the circular arcs, the independent variable is the spiral angle (θ) measured around the center of the arc. Along the transition segments, the independent variable is the along-track distance (x) measured in the direction of the nominal ground track (Figure 26).

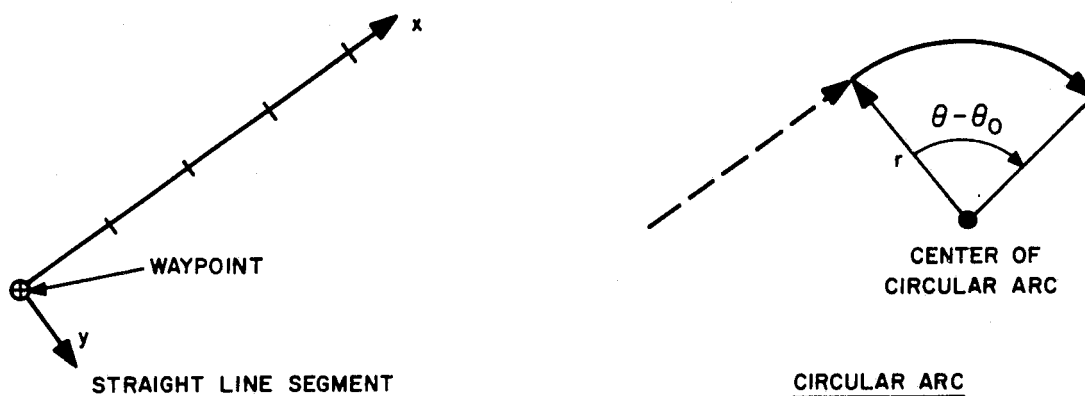


Figure 26. Independent Variables for Straight Segments and Circular Arcs.

7.1 NOMINAL PATH FOR ENTRY TRANSITION TO SPIRAL

7.1.1 RIGHT-HAND SPIRAL ENTRY

A constant groundspeed, constant-altitude transition is assumed, which is tangent to the descent spiral. Slightly more general equations are developed for the simulation described in Section 8 for the straight segments. There, groundspeed is assumed to vary linearly with time during periods of constant acceleration rather than remaining constant as is assumed in this section. An x-y coordinate frame is defined with its origin at the spiral center and with the x-axis parallel to, and in the same direction as, the transition path (Figure 27). The guidance logic switches at $\theta = \theta_0$:

$$\theta < \theta_0 \text{ — guide to straight transition segment}$$

$$\theta \geq \theta_0 \text{ — engage spiral guidance logic} \tag{117}$$

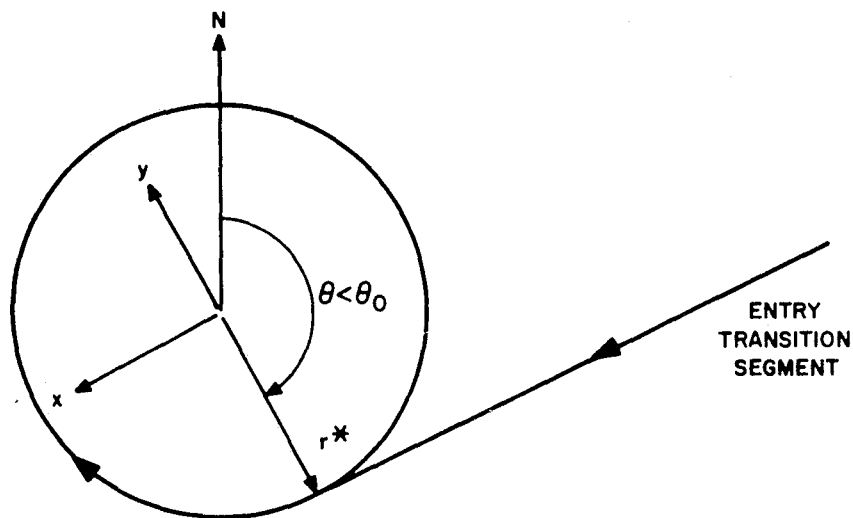


Figure 27. Entry Transition to Right-Hand Spiral.

For a constant groundspeed transition, the nominal path is defined as follows:

$$V^* = \text{const.} = [V_g^{*2} + W^{*2} + 2V_g^* W^* \sin(\eta^* - \theta_0)]^{1/2} \quad (118)$$

$$\psi^* = \text{const.} = \theta_0 + \frac{\pi}{2} - \sin^{-1} [(W^*/V_g^*) \cos(\eta^* - \theta_0)] \quad (119)$$

$$y^* = \text{const.} = -r^* \quad (120)$$

$$t^* = t^*(x) = t^*(\theta_0) - x/V_g^* \quad (\text{Note, } x \leq 0) \quad (121)$$

$$\phi^* = 0 \quad (122)$$

$$\dot{h}^* = 0 \quad (123)$$

$$h^* = \text{const.} = h^*(\theta_0) \quad (124)$$

Equation (118) can be solved for V_g^* in terms of V^* :

$$V_g^* = [V^{*2} + W^{*2} - 2V^*W^* \cos(\eta^* - \psi^*)]^{1/2} \quad (125)$$

7.1.2 LEFT-HAND SPIRAL ENTRY

The x-y axes are defined in the same way as for a right-hand spiral, and the logic is also switched at $\theta = \theta_0$ (Figure 28):

$$\begin{aligned} \theta > \theta_0 & \text{ — guide to straight transition segment} \\ \theta \leq \theta_0 & \text{ — engage spiral guidance logic} \end{aligned} \quad (117')$$

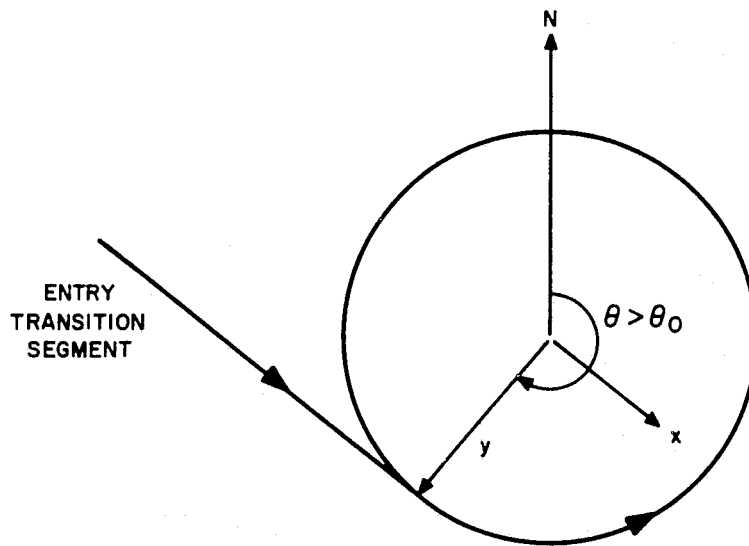


Figure 28. Entry Transition to Left-Hand Spiral.

For a constant-speed transition, Equations (118), (119) and (120) are modified as follows:

$$V^* = \text{const.} = [V_g^{*2} + W^{*2} - 2V_g^*W^* \sin(\eta^* - \theta_0)] \quad (118')$$

$$\psi^* = \text{const.} = \theta_0 - \frac{\pi}{2} + \sin^{-1} [(W^*/V^*) \cos(\eta^* - \theta_0)] \quad (119')$$

$$y^* = \text{const.} = r^* \quad (120')$$

7.2 NOMINAL PATH FOR EXIT TRANSITION FROM SPIRAL

7.2.1 RIGHT-HAND SPIRAL EXIT

This is essentially the same as the transition onto the spiral, with a constant deceleration to hover. As shown in Figure 29, a set of x-y coordinates is defined, centered at the nominal spiral axis with x parallel to the final approach transition segment. The guidance logic switches at $\theta = \theta_f$:

$\theta \leq \theta_f$ — guide to spiral path

$\theta > \theta_f$ — guide to straight transition segment

(126)

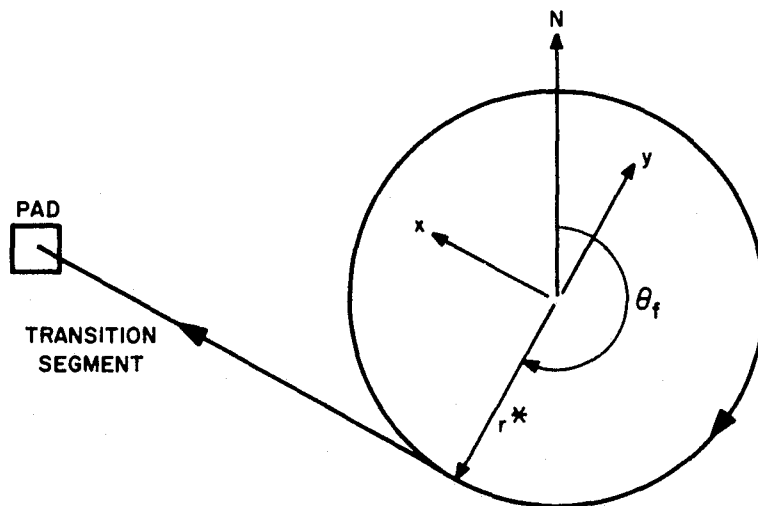


Figure 29. Exit Transition From Spiral.

For this transition, the nominal airspeed and heading will not be constant. For a constant deceleration, the nominal path equations are:

$$t^*(x) = t_f^* - [t_f^* - t^*(\theta_f)] \sqrt{1 - x/x_f} \quad (127)$$

where $x_f = V_g^*(\theta_f) \frac{t_f^* - t^*(\theta_c)}{2}$

$$V_g^*(x) = V_g^*(\theta_f) \left[1 - \frac{t^*(x) - t^*(\theta_c)}{t_f^* - t^*(\theta_f)} \right] \quad (128)$$

where $V_g^*(\theta_f) = [V^{*2} + W^{*2} - 2V^*W^* \cos(\eta^* - \psi^*)]^{1/2} \Big|_{\theta = \theta_f}$

$$V^*(x) = [V_g^*(x)^2 + W^{*2} + 2V_g^*(x)W^* \sin(\eta^* - \theta_f)]^{1/2} \quad (129)$$

$$\psi^*(x) = \theta_f + \tan^{-1} \left[\frac{V_g^*(x)/W^* + \sin(\eta^* - \theta_f)}{\cos(\eta^* - \theta_f)} \right] \quad (130)$$

$$\phi^*(x) = -\tan^{-1} \left\{ \frac{W^*V_g^*(\theta_f) \cos(\eta^* - \theta_f)}{gV^*(x)[t_f^* - t^*(\theta_f)]} \right\} \quad (131)$$

$$y^* = -r^* = \text{const.} \quad (132)$$

$$\alpha^* = \frac{-V_g^*(\theta_f)}{V^*(x)[t_f^* - t^*(\theta_f)]} [V_g^*(x) + W^* \sin(\eta^* - \theta_f)] \quad (133)$$

$$\dot{h}^* = \frac{h_f^* - h^*(\theta_f)}{t_f^* - t^*(\theta_f)} = \text{const.} \quad (134)$$

$$h^*(x) = h_f^* + \dot{h}^* [t^*(x) - t_f^*] \quad (135)$$

7.2.2 LEFT-HAND SPIRAL EXIT

The only differences between the left and right-hand spiral exits are the sign of $\dot{\theta}$, and 180° in the ground track angle at θ_f . The guidance logic switches at θ_f :

$\theta \geq \theta_f$ — guide to nominal spiral

$\theta < \theta_f$ — guide to straight transition segment (136)

The modifications in the above equations are:

$$V^*(x) = [V_g^*(x)^2 + W^{*2} - 2V_g^*(x)W^* \sin(\eta^* - \theta_f)]^{1/2} \quad (137)$$

$$\psi^*(x) = \theta_f - \tan^{-1} \left[\frac{\sin(\eta^* - \theta_f) - V_g^*(x)/W}{\cos(\eta^* - \theta_f)} \right] \quad (138)$$

$$\phi^*(x) = \tan^{-1} \left\{ \frac{W^*V_g^*(\theta_f) \cos(\eta^* - \theta_f)}{gV^*(x)[t_f^* - t^*(\theta_f)]} \right\} \quad (139)$$

$$y^* = r^* = \text{const.} \quad (140)$$

$$a^* = \frac{-V_g^*(\theta_f)}{V^*(x)[t_f - t^*(\theta_f)]} [V_g^*(x) - W^* \sin(\eta^* - \theta_f)] \quad (141)$$

7.3 TRANSITION SEGMENT GUIDANCE LAW

For the circular arc, the proposed guidance law is given by Equations (33), (34) and (35). For consistency, a similar guidance law is proposed for the straight segments:

$$\phi_c = \phi^*(\hat{x}) + C_y [\hat{y} - y^*] + C_\psi [\hat{\psi} - \psi^*(\hat{x})] \quad (142)$$

$$a_c = a^*(\hat{x}) + K_v [\hat{V} - V^*(\hat{x})] + K_t [\hat{t} - t^*(\hat{x})] \quad (143)$$

$$\dot{h}_c = \dot{h}^*(\hat{x}) + K_h [\hat{h} - h^*(\hat{x})] \quad (144)$$

Note that, unlike Equation (3-32), the longitudinal acceleration command in Equation (143) contains a nominal term in addition to the feedback terms.

Outside the linear bank command region ($\phi_c = \pm \phi_{\max}$), the guidance logic must be modified to ensure capture of the transition segment. For large offset errors ($\hat{y} - y^*$), the logic is adjusted to provide a 60° intercept of the nominal path ($\hat{\psi} - \psi^*$); as shown in the phase plane of Figure 30. The change in the guidance algorithm from that of Equation (142) is:

$$\phi_c = \begin{cases} C_\psi [\hat{\psi} - \hat{\psi}^*(x) - \pi/3] & \hat{y} < y_1 \\ \phi^*(\hat{x}) + C_y [\hat{y} - y^*] + C_\psi [\hat{\psi} - \psi^*(\hat{x})] & y_1 \leq \hat{y} \leq y_2 \\ C_\psi [\hat{\psi} - \psi^*(\hat{x}) + \pi/3] & \hat{y} > y_2 \end{cases} \quad (145)$$

$$\text{where } y_1 = y^* - \frac{\pi}{3} \frac{C_\psi}{C_y}$$

$$y_2 = y^* + \frac{\pi}{3} \frac{C_\psi}{C_y}$$

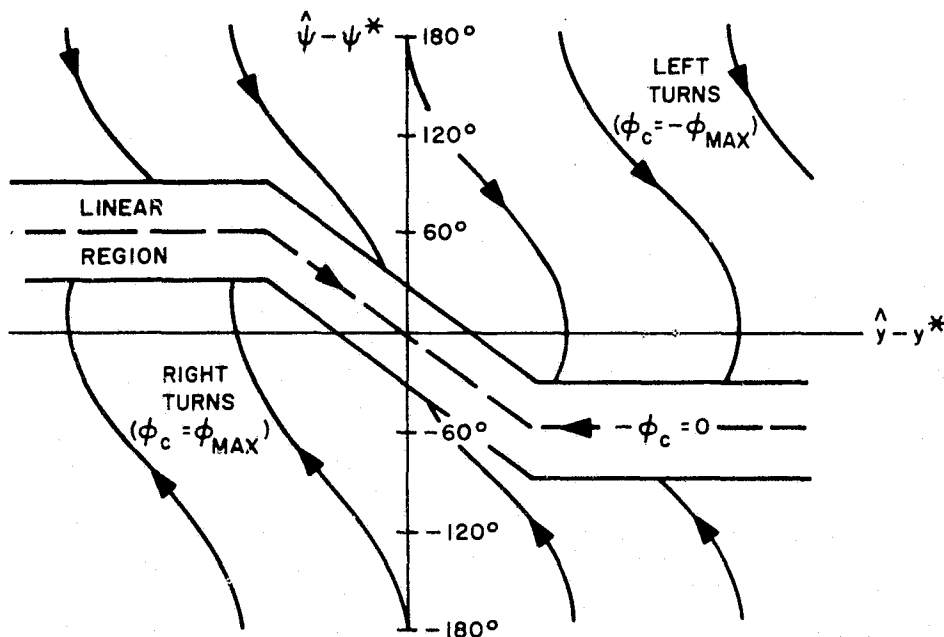


Figure 30. Modified Transition Segment Guidance in Phase Plane.

For the entry transition the linear region is symmetric about the origin since $\phi^* = 0$. This is nearly true in the exit transition as well since the nominal bank angle will be very small. The slope of the trajectories in the phase plane is

$$\frac{dy}{d\psi} = \frac{\dot{y}}{\dot{\psi}} = \frac{V^{*2} \sin(\hat{\psi} - \psi^*)}{g \tan \phi_c} \quad (146)$$

Outside the linear region, $\phi_c = \pm \phi_{\max}$, the paths are given by

$$(\hat{y} - y^*) = \mp \frac{V^{*2} \cos(\hat{\psi} - \psi^*)}{g \tan \phi_{\max}} + (\hat{y} - y^*) \big|_{\hat{\psi} - \psi^* = 90^\circ} \quad (147)$$

7.4 HOVER AND TOUCHDOWN PHASE

The final phase of the approach and landing is not unique to the spiral descent. A hover mode must be engaged when the rotorcraft is over the pad. Using a pad-centered frame (Figure 31),

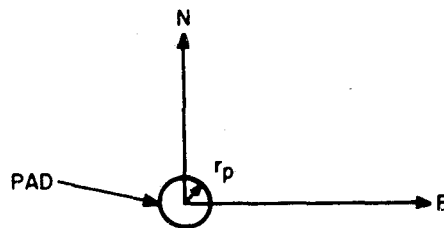


Figure 31. Pad-centered Frame for Hover and Touchdown.

the hover mode is engaged when the rotorcraft is within a desired radius r_h of the hover point; i.e., when

$$[N^2 + E^2]^{1/2} < r_h \approx r_p \quad (148)$$

where r_p is the radius of the pad. The nominal conditions are

$$\psi^* = \eta^* \quad (149)$$

$$V^* = W^* \quad (150)$$

$$h^* = h_{\text{hover}}^* \quad (151)$$

$$\dot{h}^* = 0 \quad (152)$$

$$\phi^* = 0 \quad (153)$$

$$\alpha^* = 0 \quad (154)$$

After a short hover (~5 sec), a slow vertical descent to the pad is performed

$$\dot{h}^* = \dot{h}_{\text{TD}}^* = \text{const.} \quad (155)$$

SECTION 8 SIMULATION

Two digital simulation programs have been developed for the analysis and evaluation of the spiral guidance concept. The first, containing a simple model of the vehicle dynamics and no navigation errors, was used in an interactive mode to verify the algorithms and to investigate guidance gain adjustments. The second is a modification of the VALT simulation program described in Reference 1.

8.1 INTERACTIVE SIMULATION

A relatively simple simulation, written in BASIC, was developed for ASI's inhouse minicomputer to provide preliminary verification of the guidance concept. This interactive simulation was particularly valuable for allowing the analysts to conveniently adjust the guidance algorithms, parameters and gains, and thereby gain additional insight and understanding of the system.

This simulation numerically integrates the nonlinear equations of motion for the point-mass rotorcraft model, Equations (3) through (7); the finite bank angle rate command of Equation (78); and the following simplified wind estimator equations, from Equations (100) and (101):

$$\delta \dot{W}_t = \frac{\dot{\theta}}{\theta_c} \left(\frac{\partial W_t}{\partial \phi} \right) \delta \phi \quad (156)$$

$$\delta \dot{W}_r = \frac{\dot{\theta}}{\theta_c} \left(\frac{\partial W_t}{\partial \psi} \right) \delta \psi \quad (157)$$

The following limits are observed in the simulation:

$$|\phi_c| \leq \phi_{\max} \approx 30^\circ \quad (158)$$

$$|\dot{\phi}| \leq \dot{\phi}_{\max} \approx 10^\circ/\text{sec} \quad (159)$$

$$|\dot{h}_c| \leq \dot{h}_{\max} \approx 1000 \text{ ft/min} \quad (160)$$

The nominal path variables are calculated as functions of θ using Equations (24) through (31). The guidance commands are generated using the laws of Equations (34) and (35), with the modified bank command of Equation (117).

Since the simplified wind estimator is based on the premise of small perturbations in ψ and ϕ from their nominal values, the wind estimates are not updated if the rotorcraft is outside an elliptical region in the center of the phase-plane:

$$\left[\frac{\hat{\psi} - \psi^*}{\Delta \psi} \right]^2 + \left[\frac{\hat{r} - r^*}{\Delta r} \right]^2 \leq 1 \quad (161)$$

where $\Delta \psi \approx 90^\circ$ and $\Delta r \approx 200$ ft. The estimator is also deactivated whenever the system is outside the linear bank command region of the phase plane.

The interactive simulation can also be used to analyze the spiral transition segments discussed in Section 7. Thus, it was used to verify the algorithms for left and right spirals, for entry and exit transitions, for nominal time, for wind estimation, for guaranteed capture of the nominal, etc., as well as to select a set of satisfactory guidance gains. The resulting guidance algorithms were then implemented in the Program VALT simulation.

8.2 PROGRAM VALT SIMULATION

The second simulation is a modification of Program VALT (VTOL Automatic Landing Technology) which was developed under a previous investigation (Ref. 1) to analyze the rotorcraft navigation system performance and to conduct subsystem sensitivity studies. The program is written in Fortran IV for operation on the LaRC CDC 6400/6600 computer system. Figure 32 presents a general flow diagram of VALT to illustrate the overall organization and logical operation of the simulation.

In essence, VALT is actually a double simulation. First, it integrates the equations of motion which describe the response of the rotorcraft and flight control system to the guidance system commands, and it simulates the actual noisy output of the various navigation sensors. This part of VALT is a nonlinear, stochastic process which is intended to provide a reasonably accurate representation of the "real world." The second part of VALT simulates the operations of the onboard navigation and guidance systems. This portion also models the rotorcraft motions and navigation measurements, but here the models are much simpler, and are linearized about a desired nominal flight path. The models used in this part of the program are purposely kept as simple as possible to minimize the onboard computation requirements.

The principal outputs of the simulation are time histories of the rotorcraft position and velocity, and two sets of error histories. The estimator errors are the differences between the estimated and actual position/velocity, and thus indicate the navigation systems' performance. The second set of errors show the rotorcraft's actual deviations from the nominal position/velocity profiles; these illustrate the overall

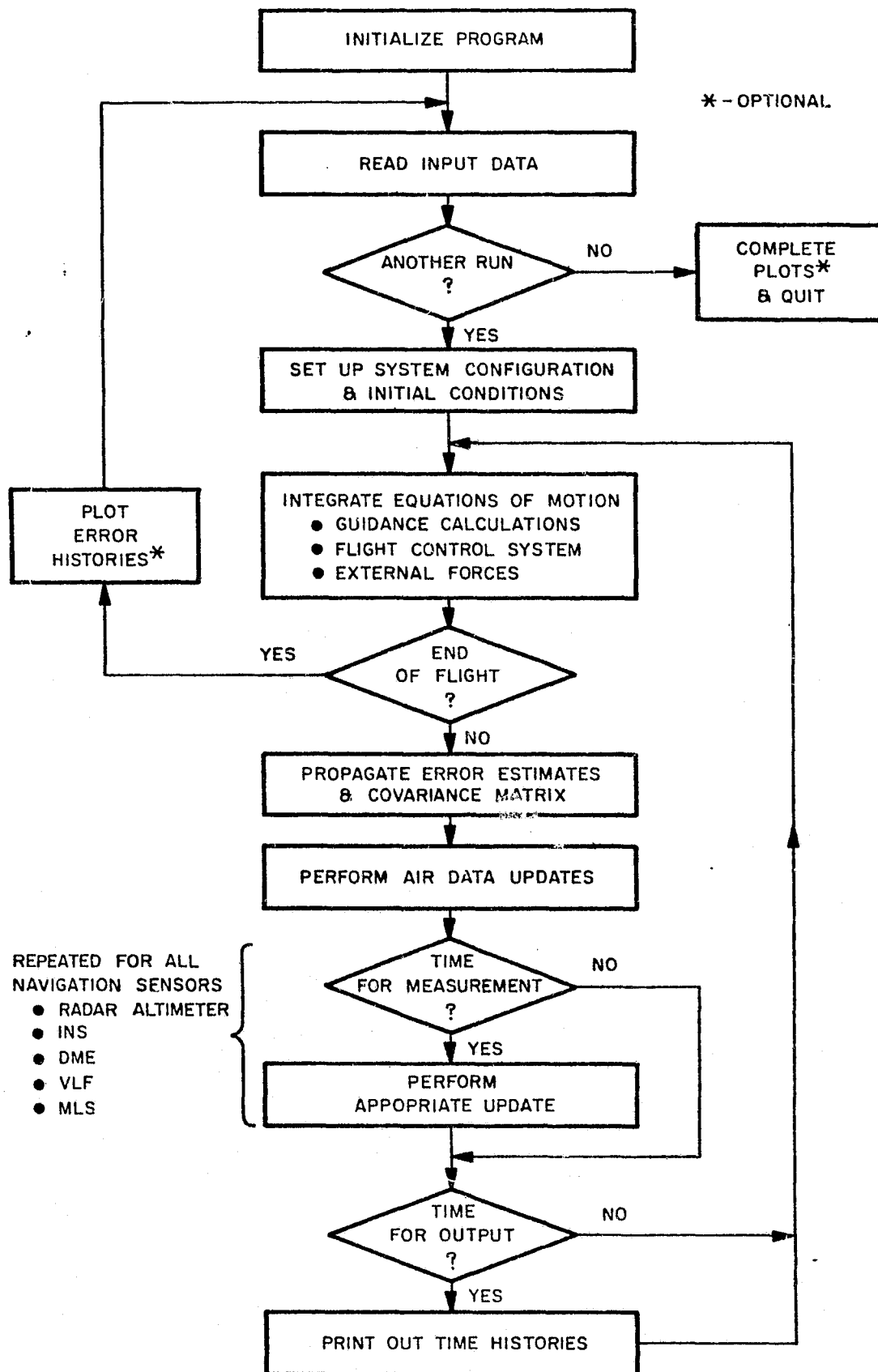


Figure 32. Overall Flow Diagram of Program VALT.

performance of the entire system, including the navigation, guidance scheme, flight control system, rotorcraft capability, and wind effects.

Program VALT was modified for the present investigation by appending to the existing guidance algorithms the option of a spiral entry transition, spiral descent and exit transition. This required the addition of the nominal path calculations, the wind estimator and the new guidance commands. The spiral guidance calculations are divided into three segments, as shown in Figure 33.

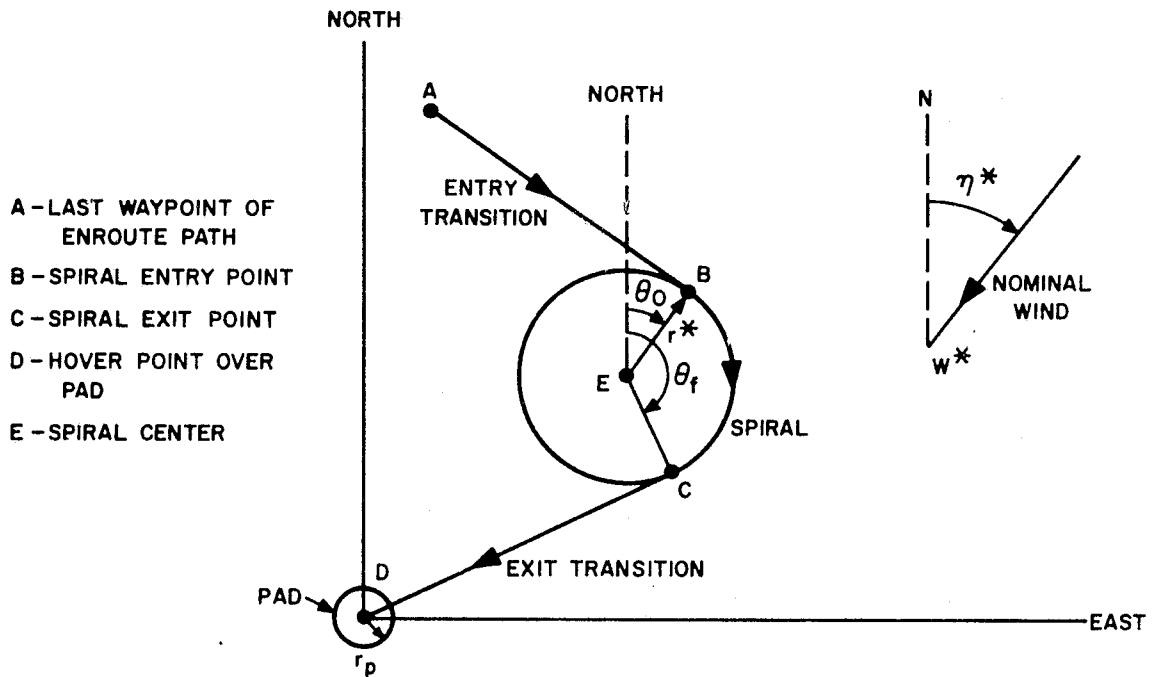


Figure 33. Segments of Nominal Spiral.

- Segment A-B: Entry Transition
- Segment B-C: Spiral Descent
- Segment C-D: Exit Transition

A rectangular reference frame in the horizontal plane, centered at the pad is used (x,y). Figure 34 presents an overall flow diagram of the spiral guidance algorithm. Details of the guidance calculations are summarized in the following subsections.

8.2.1 INITIALIZATION CALCULATIONS

The initialization phase is executed once at the beginning of the flight to calculate a number of parameters at the points indicated in Figure 33:

- Point A is the last waypoint of the enroute path. The given navigation coordinates are its latitude, longitude, altitude, time, groundspeed and ground track:

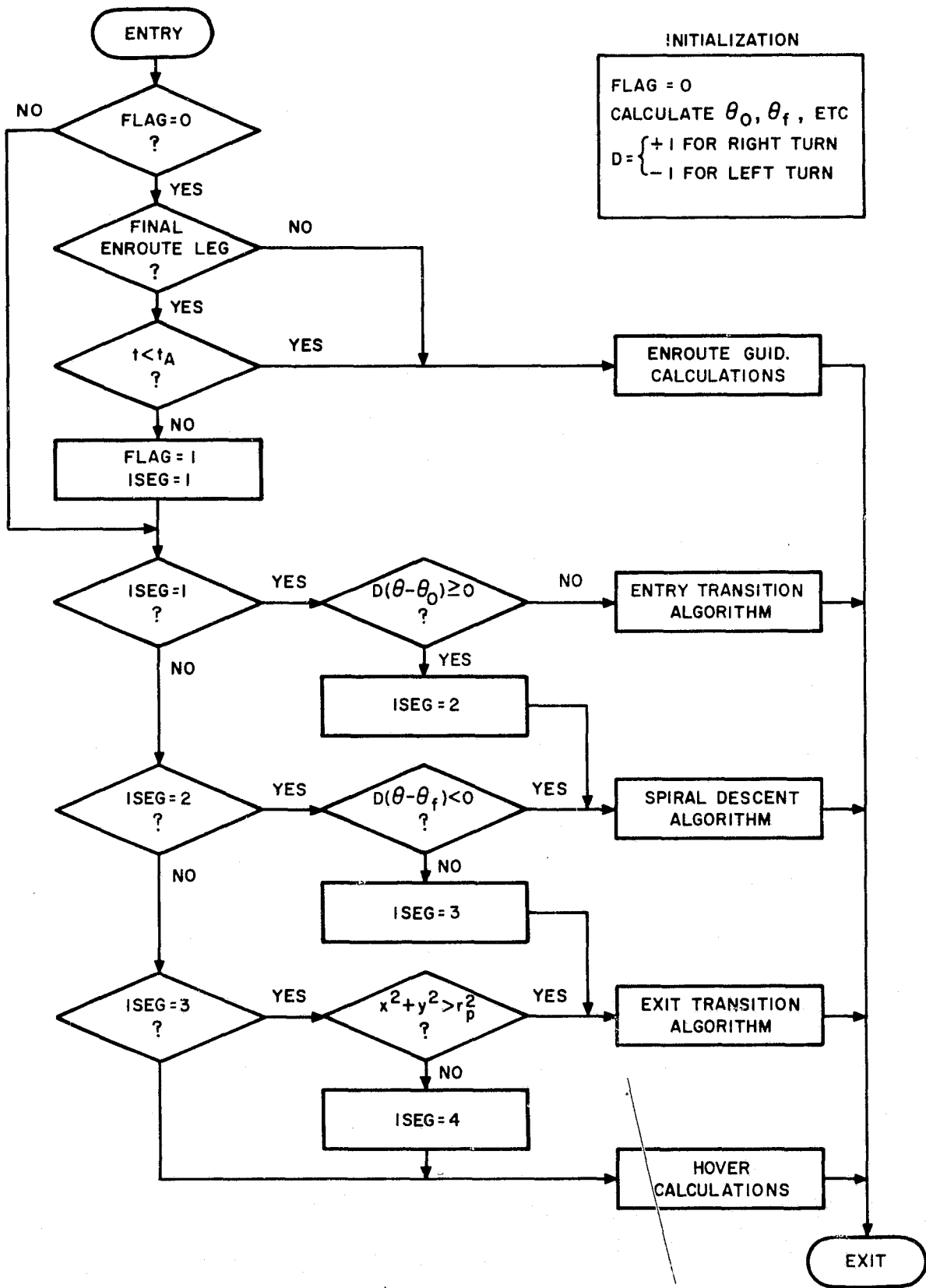


Figure 34. Overall Flow Diagram of Spiral Guidance Algorithm.

$$L_A, \ell_A, h_A, t_A, V_{gA}, x_A \quad (162)$$

The guidance coordinates are:

$$x_A = (\ell_A - \ell_D)r_e \cos L_D \quad (163a)$$

$$y_A = (L_A - L_D)r_e \quad (163b)$$

where r_e is the earth's radius.

• Point B is the spiral entry point: The initial spiral angle is*:

$$\theta_0 = \tan^{-1} \left[\frac{x_A - x_E}{y_A - y_E} \right] \pm \cos^{-1} \left[\frac{r^*}{\sqrt{(x_E - x_A)^2 + (y_E - y_A)^2}} \right] \quad (164)$$

where $\theta_0 \geq 0$ for right turns and $\theta_0 \leq$ for left turns. The guidance coordinates, assuming a constant deceleration along segment A-B, are:

$$x_B = x_E + r^* \sin \theta_0 \quad (165)$$

$$y_B = y_E + r^* \cos \theta_0 \quad (166)$$

$$h_B = h_A \quad (167)$$

$$t_B = t_A + 2\sqrt{(x_B - x_A)^2 + (y_B - y_A)^2} / (V_{gA} + V_{gB}) \quad (168)$$

where

$$V_{gB} = [V^{*2} - W^{*2} \cos^2(\theta_0 - \eta^*)]^{1/2} \pm W^* \sin(\theta_0 - \eta^*) \quad (169)$$

• Point C is the spiral exit point. The exit spiral angle is:

$$\theta_f = \tan^{-1} \left[\frac{-x_E}{-y_E} \right] \mp \cos^{-1} \left[\frac{r^*}{\sqrt{x_E^2 + y_E^2}} \right] \quad (170)$$

where $\theta_f > \theta_0$ for right turns and $\theta_f < \theta_0$ for left turns. The guidance coordinates are:

$$x_C = x_E + r^* \sin \theta_f \quad (171)$$

* Upper algebraic sign is used for right turns; lower sign for left turns.

$$y_C = y_E + r^* \cos \theta_f \quad (172)$$

$$h_C = h_B + \dot{h}_B (t_C - t_B) \quad (173)$$

$$t_C = t_B + \frac{r^*}{V^*} \left[1 - \left(\frac{W^*}{V^*} \right)^2 \right]^{-1} \left\{ \theta_f - \theta_0 + \left(\frac{W^*}{V^*} \right) [\cos(\theta_f - \eta^*) - \cos(\theta_0 - \eta^*)] \right. \\ \left. - \frac{1}{4} \left(\frac{W^*}{V^*} \right)^2 [\theta_f - \theta_0 + \cos(\theta_f - \eta^*) \sin(\theta_f - \eta^*) - \cos(\theta_0 - \eta^*) \sin(\theta_0 - \eta^*)] \right\} \quad (174)$$

The nominal rate of descent is assumed constant from point B to point D, i.e.,

$$\dot{h}_B = (h_B - h_D) / (t_B - t_D) \quad (175)$$

If $|\dot{h}_B| > \dot{h}_{\max}$, the spiral is increased by one turn ($\theta_f = \theta_f \pm 2\pi$), and Eqns. (170) to (176) are recomputed.

- Point D is the hover point over the pad. The given navigation coordinates are:

$$L_D, \ell_D, h_D, V_{gD} = 0$$

The guidance coordinates, assuming a constant deceleration from C, are:

$$x_D = y_D = 0 \quad (176)$$

$$t_D = t_C + \frac{2\sqrt{x_C^2 + y_C^2}}{V_{gC}} \quad (177)$$

$$V_{gC} = [V^{*2} - W^{*2} \cos^2(\theta_f - \eta^*)]^{1/2} \pm W^* \sin(\theta_f - \eta^*) \quad (178)$$

- Point E is the spiral center relative to the pad, with guidance coordinates:

$$x_E, y_E$$

8.2.2 CALCULATING NOMINAL PARAMETERS

The spiral guidance algorithm must compute the nominal path variables based on the estimated position \hat{x} , \hat{y} , \hat{h} .

- Entry Transition Segment (A) - (B). The estimated position relative to the spiral center is:

$$\Delta x = \hat{x} - x_E \quad (179)$$

$$\Delta y = \hat{y} - y_E \quad (180)$$

It is convenient to use a rotated coordinate system with \tilde{x} parallel to the entry transition segment and origin at the spiral center (Figure 35):

$$\tilde{x} = \pm (\Delta x \cos \theta_0 - \Delta y \sin \theta_0) \quad (181)$$

$$\tilde{y} = \mp (\Delta x \sin \theta_0 + \Delta y \cos \theta_0) \quad (182)$$

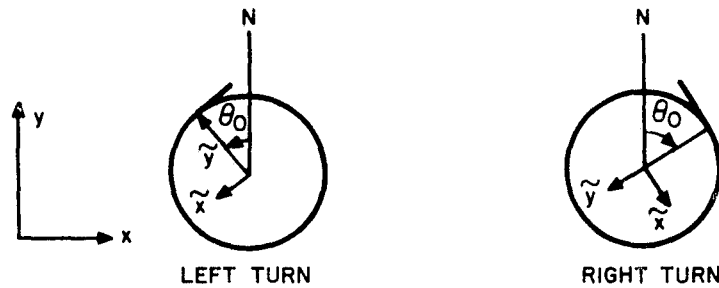


Figure 35. Rotated Coordinate Frame for Spiral Entry.

If $\tilde{x} \geq 0$, the guidance logic switches to the spiral mode [Segment (B) - (C)]. The nominal guidance parameters are calculated along the entry transition as functions of \tilde{x} :

$$t^*(\tilde{x}) = \begin{cases} t_B \mp \frac{t_B - t_A}{V_{gB} - V_{gA}} \left[\sqrt{V_{gB}^2 - \frac{\tilde{x}}{\tilde{x}_A} (V_{gB}^2 - V_{gA}^2)} - V_{gB} \right], & V_{gB} \neq V_{gA} \\ t_B + \frac{\tilde{x}}{V_{gA}}, & V_{gB} = V_{gA} \end{cases} \quad (183)$$

$$\text{where } \tilde{x}_A = -\sqrt{(x_B - x_A)^2 + (y_B - y_A)^2} \quad (184)$$

$$y^* = \mp r^* \quad (185)$$

$$V^*(\tilde{x}) = [V_g^*(\tilde{x})^2 + \hat{W}^2 \mp 2V_g^*(\tilde{x}) \hat{W} \sin(\theta_0 - \hat{\eta})]^{1/2} \quad (186)$$

$$\text{where } V_g^*(\tilde{x}) = V_{gB} - \frac{(V_{gB} - V_{gA})}{(t_B - t_A)} [t_B - t^*(\tilde{x})] \quad (187)$$

$$\psi^*(\tilde{x}) = \tan^{-1} \left\{ \frac{\pm \cos \theta_0 + [\hat{W}/V_g^*(\tilde{x})] \sin \hat{\eta}}{\mp \sin \theta_0 + [\hat{W}/V_g^*(\tilde{x})] \cos \hat{\eta}} \right\} \quad (188)$$

$$\phi^*(\tilde{x}) = -\tan^{-1} \left\{ \mp \frac{\hat{W} \cos(\theta_0 - \hat{\eta})}{gV^*(\tilde{x})} \frac{(V_{g_B} - V_{g_A})}{(t_B - t_A)} \right\} \quad (189)$$

$$\alpha^*(\tilde{x}) = \mp \left(\frac{V_{g_B} - V_{g_A}}{t_B - t_A} \right) \sin[\theta_0 - \psi^*(\tilde{x})] \quad (190)$$

$$\dot{h}^* = 0 \quad (191)$$

$$h^* = h_A = h_B \quad (192)$$

● Spiral Descent Segment (B) - (C)

During the spiral phase, the nominal guidance parameters are determined as functions of the estimated angle around the spiral, $\hat{\theta}$. If $\hat{\theta} \geq \theta_f$, the guidance logic switches to the exit transition phase. The nominal parameters during the spiral are:

$$r^* = \text{const.} \quad (193)$$

$$V^* = \text{const.} \quad (194)$$

$$t^*(\hat{\theta}) = t_B \pm \frac{r^*}{V^*} \left[1 - \left(\frac{W^*}{V^*} \right)^2 \right]^{-1} \left\{ \hat{\theta} - \theta_0 \pm \left(\frac{W^*}{V^*} \right) [\cos(\hat{\theta} - \eta^*) - \cos(\theta_0 - \eta^*)] - \frac{1}{4} \left(\frac{W^*}{V^*} \right)^2 [\hat{\theta} - \theta_0 + \cos(\hat{\theta} - \eta^*) \sin(\hat{\theta} - \eta^*) - \cos(\theta_0 - \eta^*) \sin(\theta_0 - \eta^*)] \right\} \quad (195)$$

$$\phi^*(\hat{\theta}) = \pm \tan^{-1} \left\{ \frac{V^{*2}}{r^* g_A} \left[A \pm \frac{\hat{W}}{V^*} \sin(\hat{\theta} - \hat{\eta}) \right]^2 \right\} \quad (196)$$

where

$$A \triangleq \left[1 - \left(\frac{\hat{W}}{V^*} \right)^2 \cos^2(\hat{\theta} - \hat{\eta}) \right]^{1/2}$$

$$a^* = 0 \tag{197}$$

$$\psi^*(\hat{\theta}) = \hat{\theta} \pm \left\{ \frac{\pi}{2} - \sin^{-1} \left[\frac{\hat{W}}{V^*} \cos(\hat{\theta} - \hat{\eta}) \right] \right\} \tag{198}$$

$$\dot{h}^* = \frac{h_C - h_B}{t_C - t_B} = \text{const.} \tag{199}$$

$$h^*(\hat{\theta}) = h_B + \dot{h}^* [t^*(\hat{\theta}) - t_B] \tag{200}$$

● Spiral Exit Segment (C) - (D)

A rotated coordinate system, centered at the pad is used for the exit segment

(Figure 36):

$$\tilde{x} = \pm (\hat{x} \cos \theta_f - \hat{y} \sin \theta_f) \tag{201}$$

$$\tilde{y} = \mp (\hat{x} \sin \theta_f + \hat{y} \cos \theta_f) \tag{202}$$

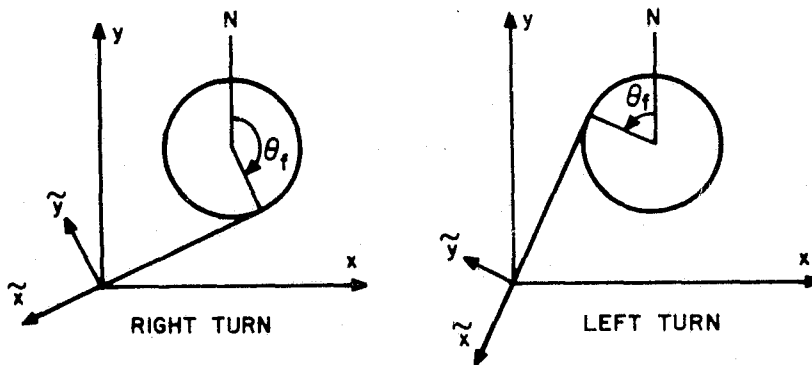


Figure 36. Rotated Coordinate Frame for Spiral Exit.

If $\sqrt{\tilde{x}^2 + \tilde{y}^2} < r_p$, the guidance logic switches to the hover mode. Otherwise the nominal parameters on the exit transition are:

$$t^*(\tilde{x}) = t_D + (t_C - t_D) \sqrt{\tilde{x}/\tilde{x}_C} \quad (203)$$

where $\tilde{x}_C = -\sqrt{x_C^2 + y_C^2}$ (204)

$$y^* = 0 \quad (205)$$

$$V^*(\tilde{x}) = [V_g^*(\tilde{x})^2 + \hat{W}^2 \mp 2V_g(\tilde{x})\hat{W} \sin(\theta_f - \hat{\eta})]^{1/2} \quad (206)$$

where $V_g^*(\tilde{x}) = V_{gC} \left[\frac{t_D - t^*(\tilde{x})}{t_D - t_C} \right]$ (207)

$$\psi^*(\tilde{x}) = \tan^{-1} \left\{ \frac{\pm V_g^*(\tilde{x}) \cos \theta_f + \hat{W} \sin \hat{\eta}}{\mp V_g^*(\tilde{x}) \sin \theta_f + \hat{W} \cos \hat{\eta}} \right\} \quad (208)$$

$$\phi^*(\tilde{x}) = -\tan^{-1} \left\{ \pm \frac{\hat{W} V_{gC} \cos(\theta_f - \hat{\eta})}{g V^*(\tilde{x}) (t_D - t_C)} \right\} \quad (209)$$

$$\alpha^*(\tilde{x}) = \pm \frac{V_{gC} \sin[\theta_f - \psi^*(\tilde{x})]}{t_D - t_C} \quad (210)$$

$$h^* = h_D + \dot{h}^* [t^*(\tilde{x}) - t_D] \quad (211)$$

$$\dot{h}^* = \frac{h_D - h_C}{t_D - t_C} = \text{const.} \quad (212)$$

- Hover Mode

Hover guidance is not unique to the spiral approach, and can be analyzed separately. For the present study, the simulation terminates at the completion of the spiral exit transition.

8.2.3 WIND ESTIMATES

The simplified wind estimator described in Section 5 is engaged during Segment (B) - (C), when the aircraft is close to the nominal path: i.e.,

$$\left(\frac{\hat{\psi} - \psi^*}{\Delta\psi}\right)^2 + \left(\frac{\hat{r} - r^*}{\Delta r}\right)^2 < 1 \quad (213)$$

which defines an ellipse about the nominal path in the phase plane. The wind estimator is also deactivated whenever $|\phi_C| \geq \phi_{\max}$.

When the wind estimator is active, changes in the radial and tangential wind components are estimated over an increment in $\hat{\theta}$:

$$\frac{\delta \hat{W}_r}{\delta \theta} = \frac{V^*}{\theta_C} (\hat{\psi} - \psi^*) \quad (214)$$

$$\frac{\delta \hat{W}_t}{\delta \theta} = \pm \frac{r^* g}{2V^* \theta_C} (\hat{\phi} - \phi^*) \quad (215)$$

These are converted into navigation coordinates:

$$\frac{\delta \hat{W}_N}{\delta \theta} = \cos \hat{\theta} \frac{\delta \hat{W}_r}{\delta \theta} - \sin \hat{\theta} \frac{\delta \hat{W}_t}{\delta \theta} \quad (216)$$

$$\frac{\delta \hat{W}_E}{\delta \theta} = \sin \hat{\theta} \frac{\delta \hat{W}_r}{\delta \theta} + \cos \hat{\theta} \frac{\delta \hat{W}_t}{\delta \theta} \quad (217)$$

The North and East wind estimates are then updated:

$$\hat{W}_N(\hat{\theta} + \delta\theta) = \hat{W}_N(\hat{\theta}) + \left(\frac{\delta \hat{W}_N}{\delta\theta} \right) \delta\theta \quad (218)$$

$$\hat{W}_E(\hat{\theta} + \delta\theta) = \hat{W}_E(\hat{\theta}) + \left(\frac{\delta \hat{W}_E}{\delta\theta} \right) \delta\theta \quad (219)$$

The estimated magnitude and direction of the wind are obtained from:

$$\hat{W} = \sqrt{\hat{W}_N^2 + \hat{W}_E^2} \quad (220)$$

$$\hat{\eta} = \tan^{-1} \left(\frac{-\hat{W}_E}{-\hat{W}_N} \right) \quad (221)$$

8.2.4 GUIDANCE LAWS

The spiral guidance commands are summarized below for the three flight segments:

- Spiral Transition Segments (A) - (B) and (C) - (D)

$$\phi_c = \begin{cases} C_\psi [\hat{\psi} - \psi^*(\tilde{x}) - \Delta\psi_{\max}] & , \tilde{y} < (y^* - \Delta y) \\ \phi^*(\tilde{x}) + C_y [\tilde{y} - y^*] + C_\psi [\hat{\psi} - \psi^*(\tilde{x})], & (y^* - \Delta y) \leq \tilde{y} \leq (y^* + \Delta y) \\ C_\psi [\hat{\psi} - \psi^*(\tilde{x}) + \Delta\psi_{\max}] & , \tilde{y} > (y^* + \Delta y) \end{cases} \quad (222)$$

$$a_c = a^*(\tilde{x}) + K_V [\hat{V} - V^*(\tilde{x})] + K_f [\hat{t} - t^*(\tilde{x})] \quad (223)$$

$$\dot{h}_c = \dot{h}^* + K_h [\hat{h} - h^*(\tilde{x})] \quad (224)$$

where $\Delta y = \Delta\psi_{\max} C_\psi / C_y \quad (225)$

- Spiral Descent Segment (B) - (C)

$$\phi_c = \begin{cases} C_\psi [\hat{\psi} - \psi^*(\hat{\theta}) \mp \Delta\psi_{\max}] & , \hat{r} > r_1 \\ \phi^*(\hat{\theta}) \pm C_r(\hat{r} - r^*) + C_\psi [\hat{\psi} - \psi^*(\hat{\theta})] & , r_1 \geq \hat{r} \geq r_2 \\ C_\psi [\hat{\psi} - \psi^*(\hat{\theta}) \pm \Delta\psi_{\max}] & , \hat{r} < r_2 \end{cases} \quad (226)$$

$$a_c = K_V[\hat{V} - V^*] + K_t[\hat{t} - t^*(\hat{\theta})] \quad (227)$$

$$\dot{h}_c = \dot{h}^* + K_h[\hat{h} - h^*(\hat{\theta})] \quad (228)$$

where

$$r_1 = r^* - \frac{C_\psi \Delta\psi_{\max} \pm \phi^*(\hat{\theta})}{C_r} \quad (229)$$

$$r_2 = r^* + \frac{C_\psi \Delta\psi_{\max} \mp \phi^*(\hat{\theta})}{C_r} \quad (230)$$

- Guidance Command Limits

$$|\phi_c| \leq \phi_{\max} \approx 30^\circ \quad (231)$$

$$|a_c| \leq a_{\max} \approx 2 \text{ kt/sec} \quad (232)$$

$$|\dot{h}_c| \leq \dot{h}_{\max} \approx 1000 \text{ ft/min} \quad (233)$$

- Guidance Gains

Suggested values for the feedback guidance gains are summarized in Table 17.

8.2.5 MEASUREMENTS

The guidance system inputs required for the previous calculations are assumed to come from the navigation system and other onboard equipment.

Table 17. Recommended Values
for Guidance Gains.

C_r	0.005 rad/ft
C_ψ	-1.77 rad/rad
C_t	0 rad/sec
K_v	-0.15 sec ⁻¹
K_t	1.0 ft/sec ³
K_h	0.033 ft/sec/ft

● Position

Position estimates are obtained from the navigation system outputs of \hat{L} , $\hat{\ell}$, \hat{h} :

$$\hat{x} = (\hat{\ell} - \ell_D) r_e \cos L_D \quad (234)$$

$$\hat{y} = (\hat{L} - L_D) r_e \quad (235)$$

$$\hat{r} = \sqrt{(\hat{x} - x_E)^2 + (\hat{y} - y_E)^2} \quad (236)$$

$$\hat{\theta} = \tan^{-1} [(\hat{x} - x_E)/(\hat{y} - y_E)] \quad (237)$$

● Airspeed and Heading

Airspeed and heading estimates are obtained from the navigation systems inertial velocity estimates (\hat{V}_N , \hat{V}_E , \hat{V}_D) and the wind estimator:

$$\hat{V} = \sqrt{(\hat{V}_N - \hat{W}_N)^2 + (\hat{V}_E - \hat{W}_E)^2 + \hat{V}_D^2} \quad (238)$$

$$\hat{\psi} = \tan^{-1} \left[\frac{\hat{V}_E - \hat{W}_E}{\hat{V}_N - \hat{W}_N} \right] \quad (239)$$

- Attitude

Attitude estimates are obtained in the simulation from the lateral acceleration:

$$\hat{\phi} = \tan^{-1} \left[\frac{F_N \cos \hat{\psi} + F_E \sin \hat{\psi}}{mg} \right] \quad (240)$$

where F_N and F_E are the North and East components of total force.

- Time

Time estimates are provided by a clock with a bias Δt_B :

$$\hat{t} = t + \Delta t_B \quad (241)$$

where the time bias is selected from a zero-mean, Gaussian distribution with a standard deviation $\sigma_{t_B} \approx 2 \text{ sec.}$

8.3 SPIRAL APPROACH EXAMPLE

To check out the spiral guidance algorithms in Program VALT, and to evaluate their performance, a realistic example has been chosen for the New York City Kennedy International Airport (JFK). Figure 37 shows two example spiral approaches to an existing helipod (point D) at JFK. The entry transition (A - B) overflies the helipod at 1100 ft; a 270° descending spiral is made to the right (B - C) or left (B - C'); and a short exit transition (C - D or C' - D) completes the maneuver to hover (D).

C.12

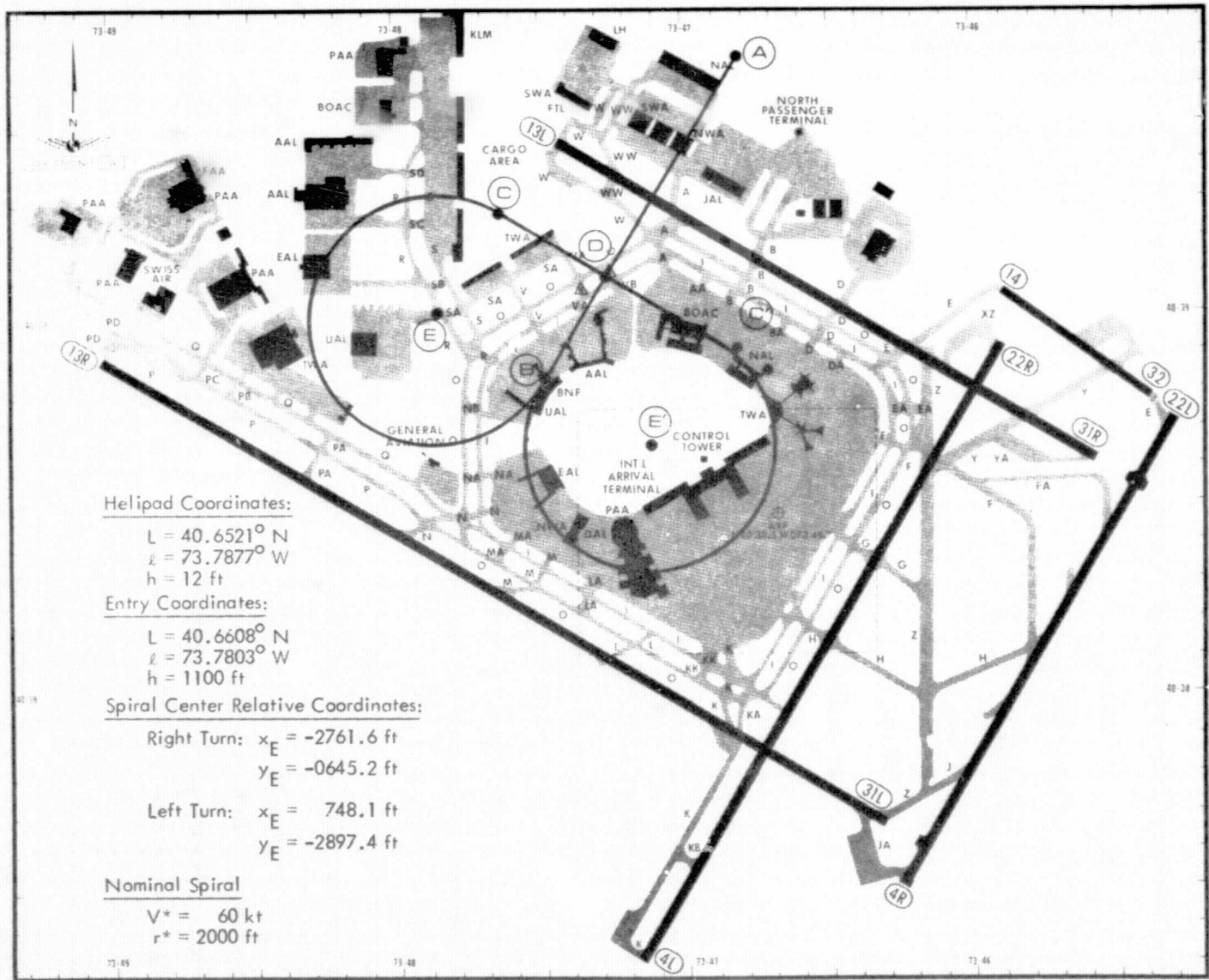


Figure 37. Example Spiral Approaches to Kennedy International Airport (JFK).

The VALT simulation with the spiral guidance system has been used to determine the effect of a variety of initial condition errors, wind errors, guidance parameter variations and navigation system errors for the example approach to JFK. The nominal initial conditions for the runs are:

$$L_o = 40.7053 \text{ N}$$

$$l_o = 73.7803 \text{ W}$$

$$h_o = 1100 \text{ ft}$$

$$V_{go} = 120 \text{ kt}$$

$$x_o = 180 \text{ deg}$$

$$\psi_o = 186.6 \text{ deg}$$

$$W = 15 \text{ kt}$$

$$\eta = 90 \text{ deg}$$

These correspond to a point 2.67 nm north of point A, the beginning of the entry transition segment.

Without navigation measurement errors, the spiral guidance system follows the nominal path almost perfectly. The maximum horizontal error is about 150 ft and occurs four seconds after the entry transition segment logic is engaged. It is corrected within 12 seconds to less than five feet, and remains negligible throughout the descent. This is merely a turn-on transient effect which is the result of a discontinuity in the nominal ground track when switching from the enroute guidance mode to the spiral guidance algorithm. The position and velocity error histories are depicted in Figures 38 and 39.

The remaining VALT runs investigated various errors and system parameter variations. These are summarized in Tables 18 & 19. Typical results are depicted in Figures 40 through 48. In general, large initial condition errors can introduce significant errors due to nonlinear effects.

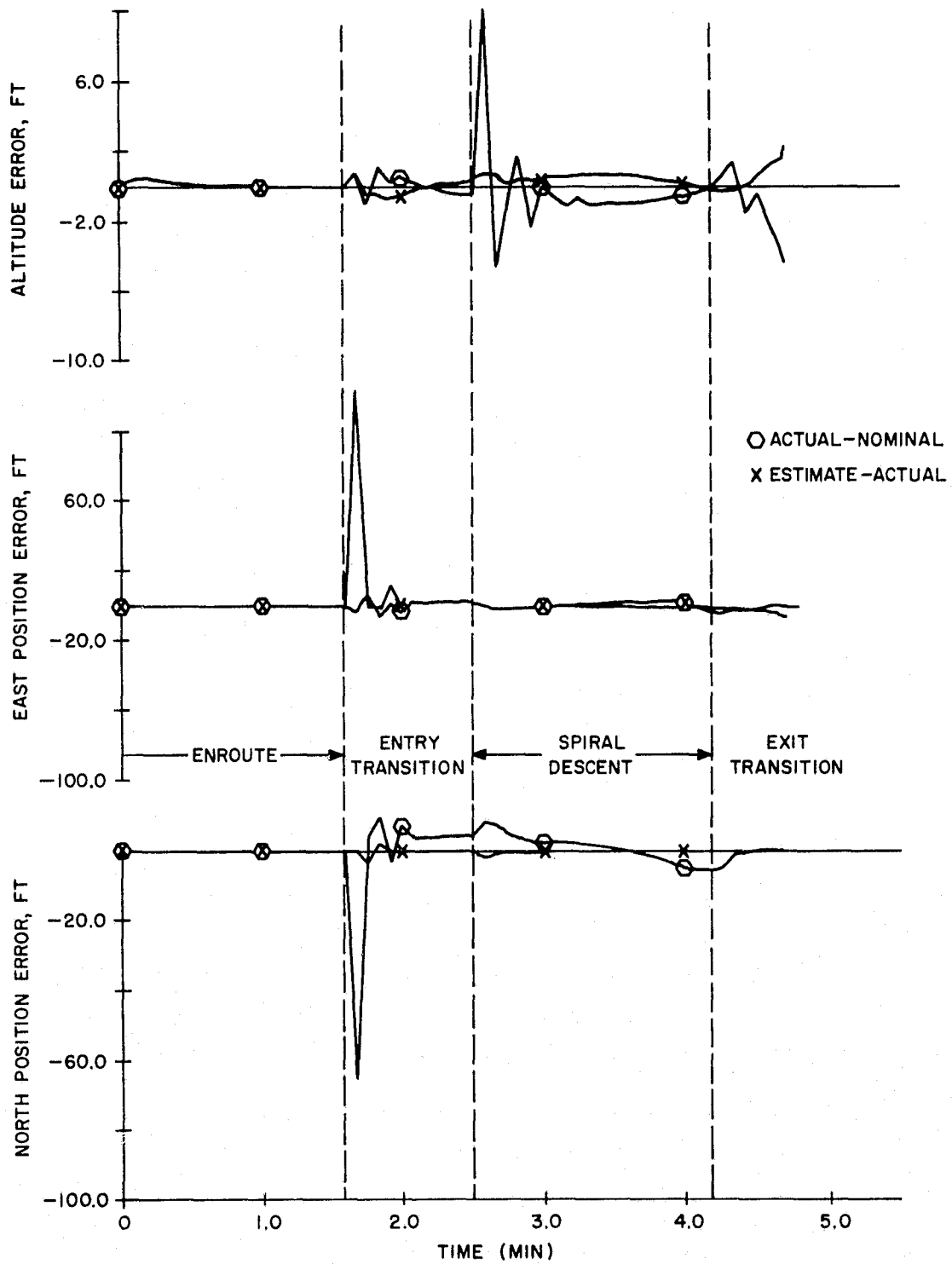


Figure 38. Nominal Spiral Approach to JFK - Position Error Histories

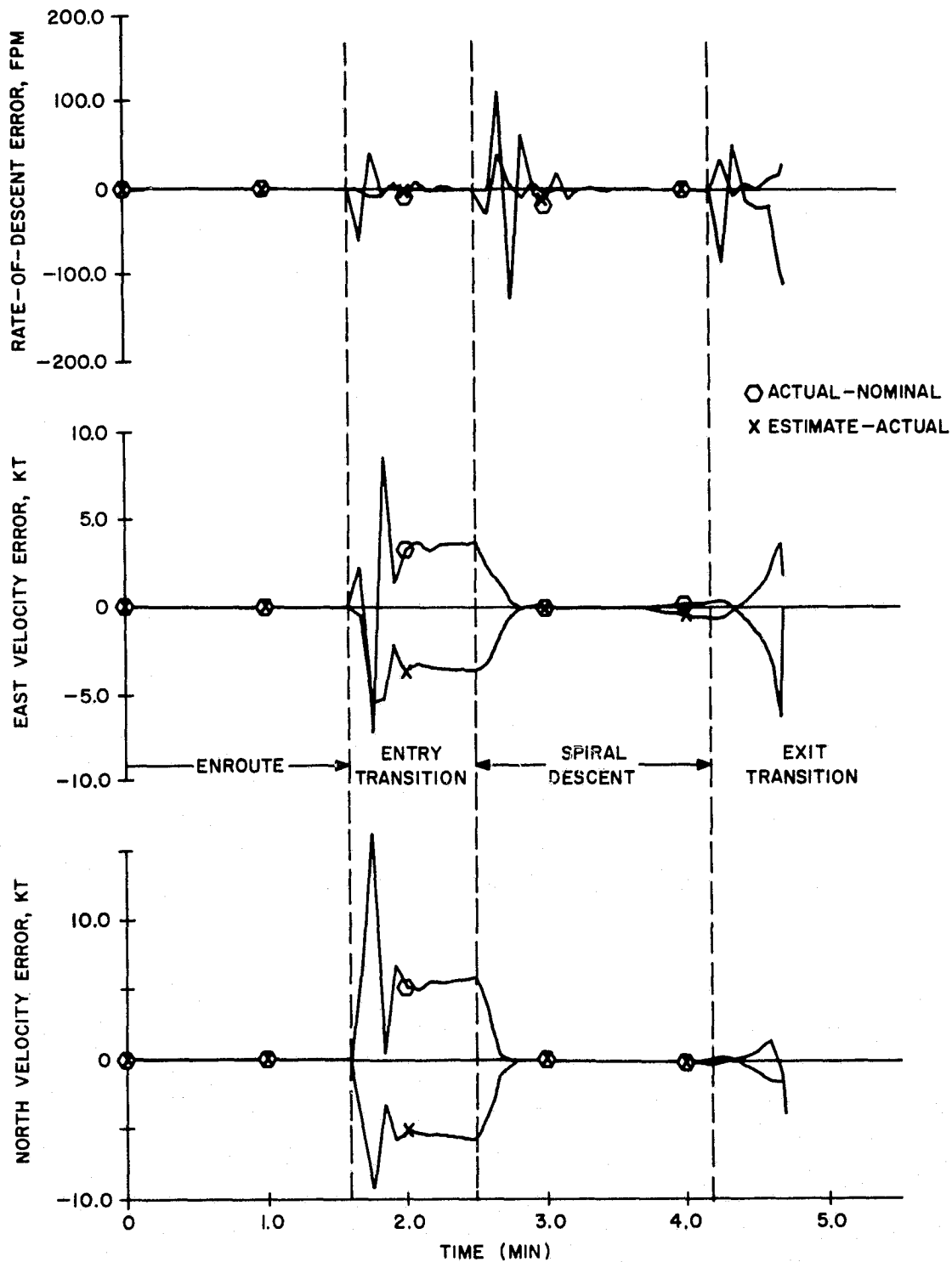


Figure 39. Nominal Spiral Approach to JFK - Velocity Error Histories.

Table 18. Spiral Guidance Parametric Analyses.

INITIAL CONDITION ERRORS	
Cross-track	± 1 nm
Along-track	± 1 nm
Groundspeed	± 20 kt
Groundtrack	± 30 deg
Altitude	± 300 ft
WIND ERRORS	
Wind speed (constant)	± 15 kt
Wind direction (constant)	± 90 deg
Wind speed (shear)	± 1.36 kt/100 ft
Wind direction (shear)	± 8.18 deg/100 ft
GUIDANCE PARAMETERS	
Radial error gain (C_r)	0.001, 0.010 rad/ft
Heading error gain (C_ψ)	-1.0, -3.0 rad/rad
Airspeed error gain (K_r)	-0.10, -0.30 sec ⁻¹
Altitude error gain (K_h)	0.5, 2.0 sec ⁻¹
Characteristic angle (θ_c)	45°, 180°
Nominal wind speed (W^*)	± 15 kt
Nominal wind direction (η^*)	± 90 deg

Table 19. Results of Parametric Analyses.

Run No.	Description	Final Position Error, Ft	RMS Position Error, Ft	Final Altitude Error, Ft	RMS Altitude Error, Ft
1001	Nominal Spiral Approach, 3-D	1.02	19.3	0.34	1.41
1002	Initial Crosstrack Error, 1 nm East	1.02	1667.7	0.34	1.40
1003	Initial Crosstrack Error, 1 nm West	1.05	1681.7	0.36	1.46
1004	Initial Along-Track Error, 1 nm North	1.02	1866.2	0.34	1.37
1005	Initial Along-Track Error, 1 nm South	1.03	2003.1	0.35	1.45
1006	Initial Groundspeed Error, +20 Kt	1.05	66.7	0.36	1.47
1007	Initial Groundspeed Error, -20 Kt	1.05	52.1	0.35	1.43
1008	Initial Altitude Error, +300 Ft	1.02	19.3	0.34	48.36
1009	Initial Altitude Error, -300 Ft	1.02	19.3	0.34	48.38
1010	Initial Track Error, +30 Deg	1.03	139.3	0.35	1.40
1011	Initial Track Error, -30 Deg	1.06	140.1	0.36	1.39
1012	Wind Speed, +15 Kt	1.06	19.4	0.34	1.77
1013	Wind Speed, -15 Kt	0.43	18.8	0.46	1.64
1014	Wind Direction, +90 Deg	0.99	19.1	0.27	1.63
1015	Wind Direction, -90 Deg	12.54	19.7	0.71	1.77
1016	Wind Speed Shear, +15 Kt	0.96	19.1	0.30	1.44
1017	Wind Speed Shear, -15 Kt	0.09	19.4	0.52	1.43
1018	Wind Direction Shear, +90 Deg	1.00	19.3	0.33	1.42
1019	Wind Direction Shear, -90 Deg	2.33	19.3	0.25	1.43
1020	Guidance Parameter, $C_r = 0.001$	0.34	31.9	0.04	1.42
1021	Guidance Parameter, $C_r = 0.010$	0.06	18.9	0.04	1.42
1022	Guidance Parameter, $C_\psi = -1.0$	0.06	19.8	0.04	1.42
1023	Guidance Parameter, $C_\psi = -3.0$	0.16	20.4	0.04	1.42
1024	Guidance Parameter, $K_v = -0.1$	0.11	19.7	0.04	1.39
1025	Guidance Parameter, $K_v = -0.3$	0.19	18.5	0.07	1.42
1026	Guidance Parameter, $K_h = 0.5$	0.11	19.3	0.06	1.98
1027	Guidance Parameter, $K_h = 2.0$	0.11	19.3	0.03	1.15
1028	Guidance Parameter, $\theta_c = 45$ Deg	0.12	19.3	0.04	1.42
1029	Guidance Parameter, $\theta_c = 180$ Deg	0.11	19.3	0.04	1.42
1030	Guidance Parameter, $W^* = 30$ Kt	0.34	19.1	0.32	1.15
1031	Guidance Parameter, $W^* = 0$ Kt	2.49	20.0	1.73	1.95
1032	Guidance Parameter, $\eta^* = 180$ Deg	2.06	20.2	0.27	2.35
1033	Guidance Parameter, $\eta^* = 0$ Deg	32.02	21.1	5.90	1.90

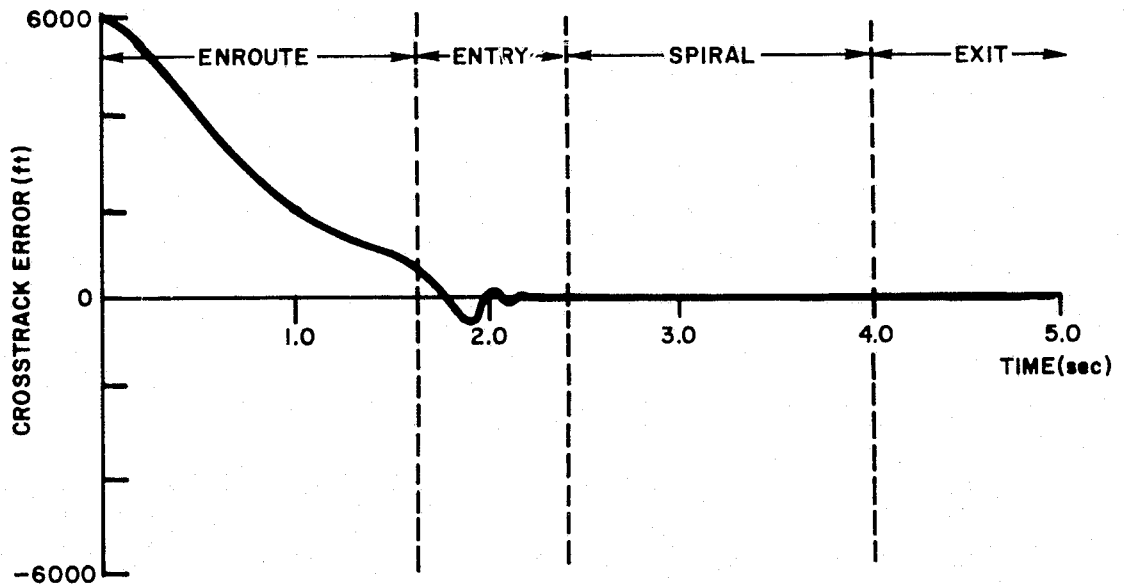
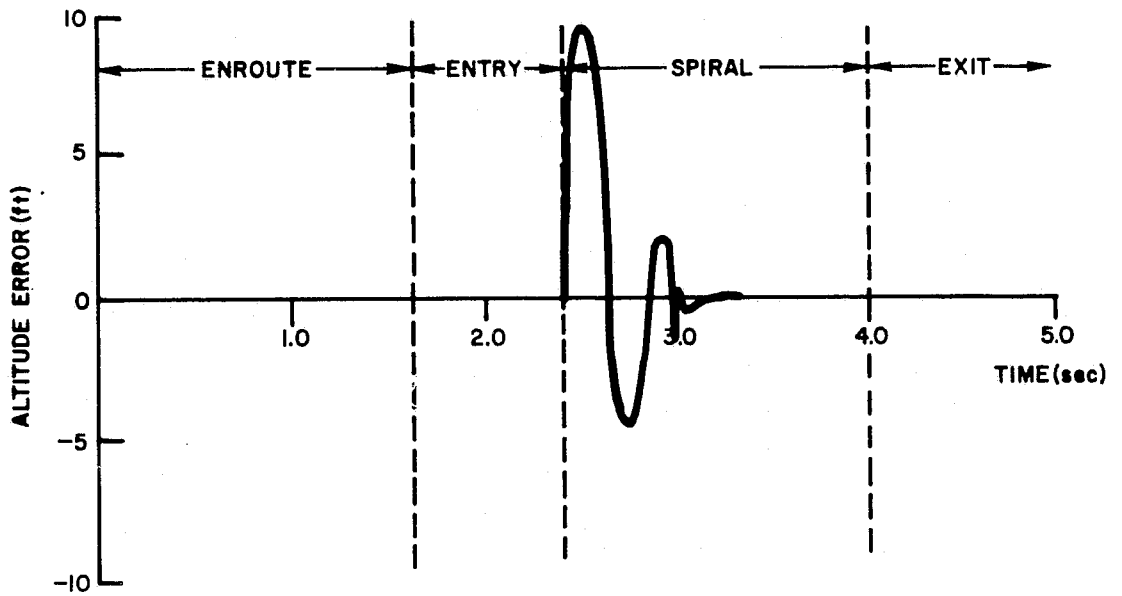


Figure 40. Initial Crosstrack Error of 1 nm.

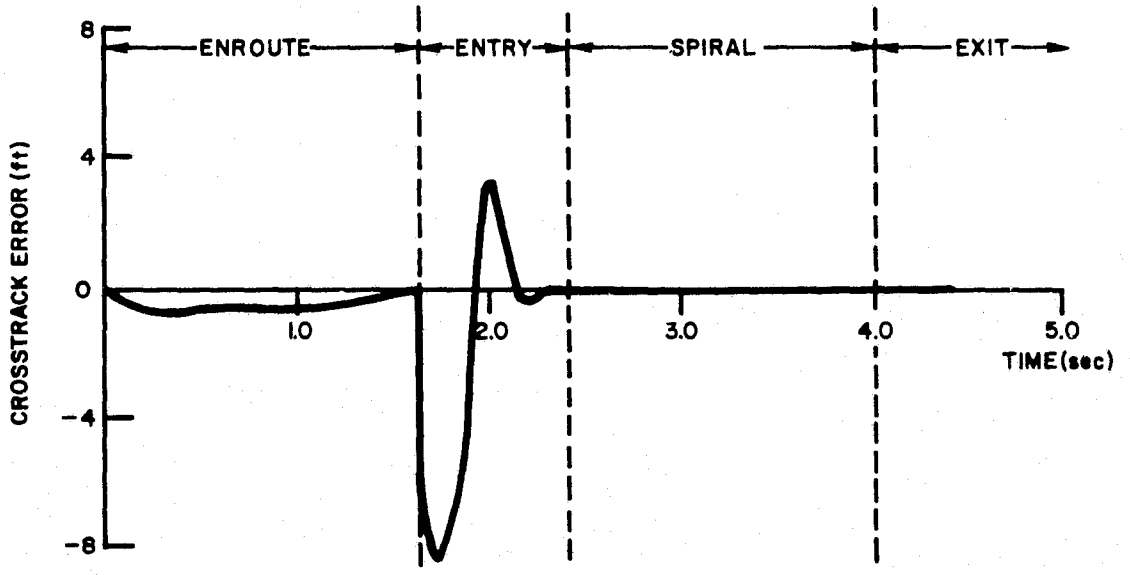
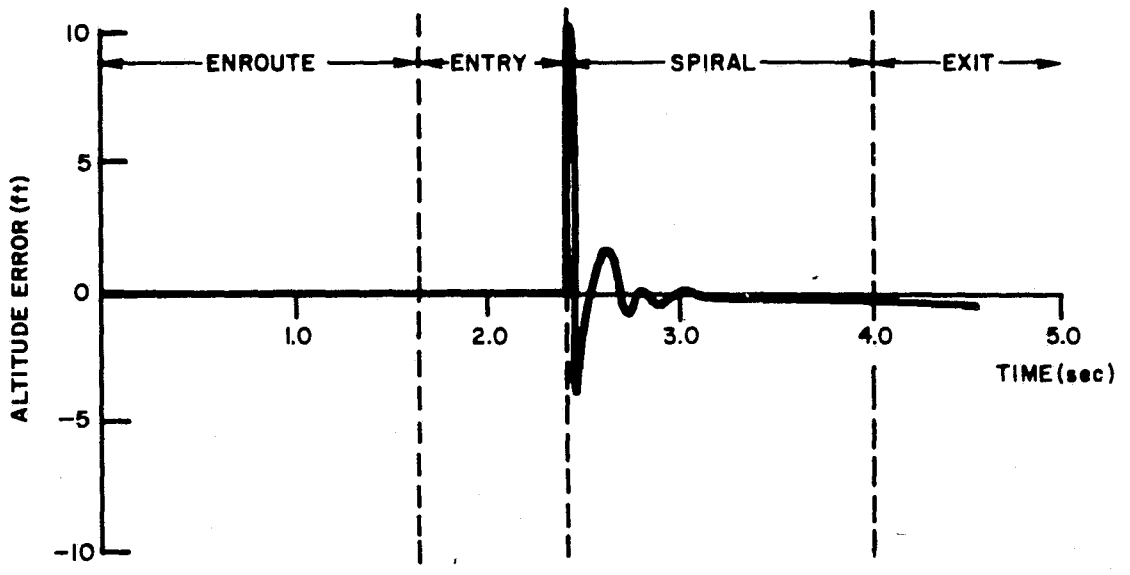


Figure 41. Initial Along-track Error of 1 nm.

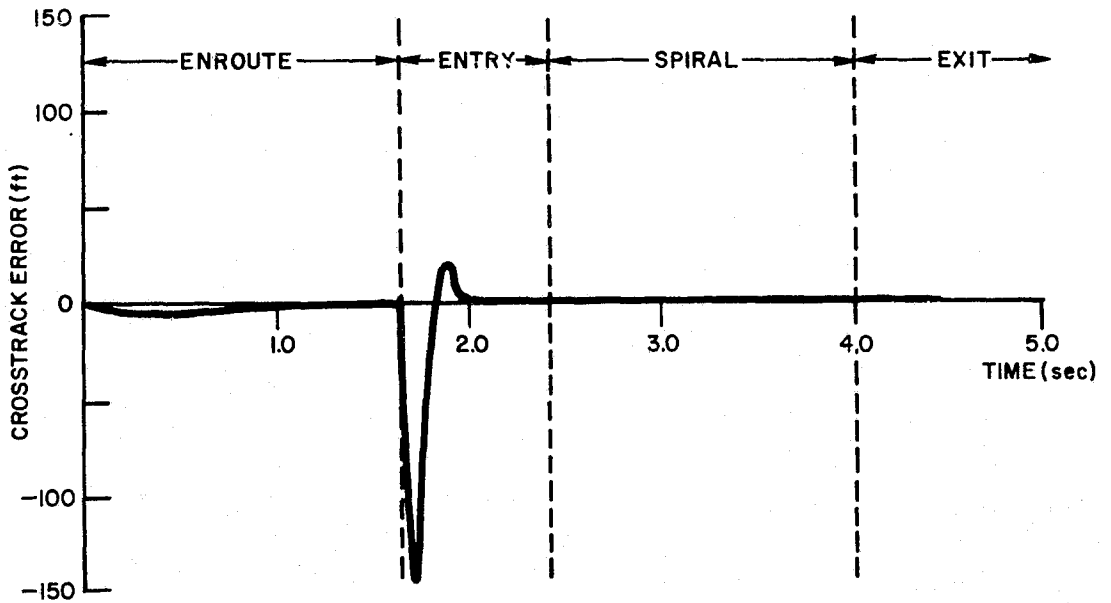
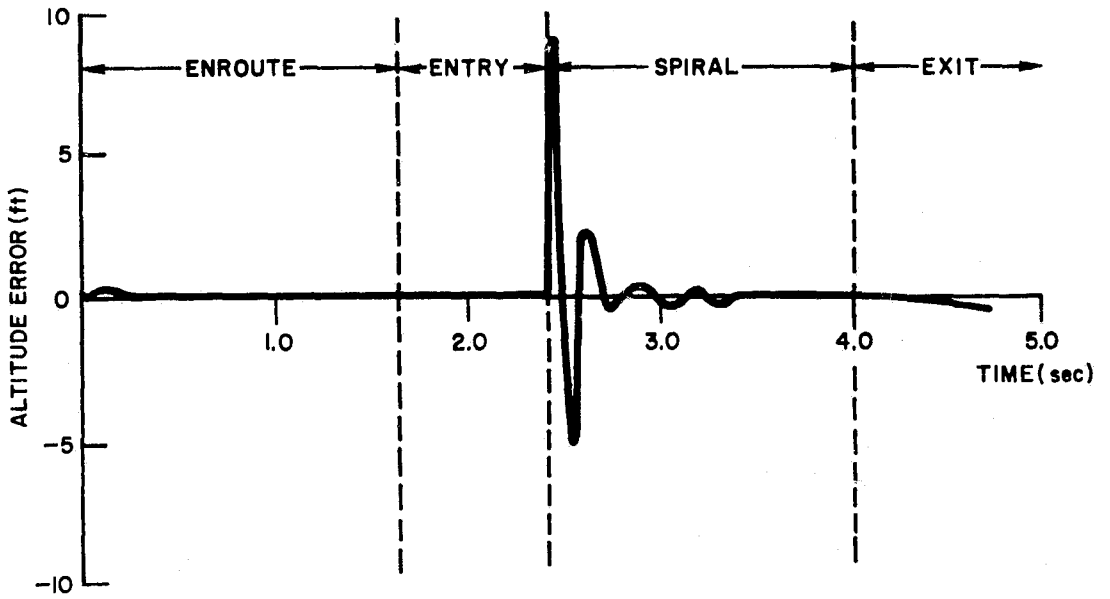


Figure 42. Initial Groundspeed Error of 20 kts.

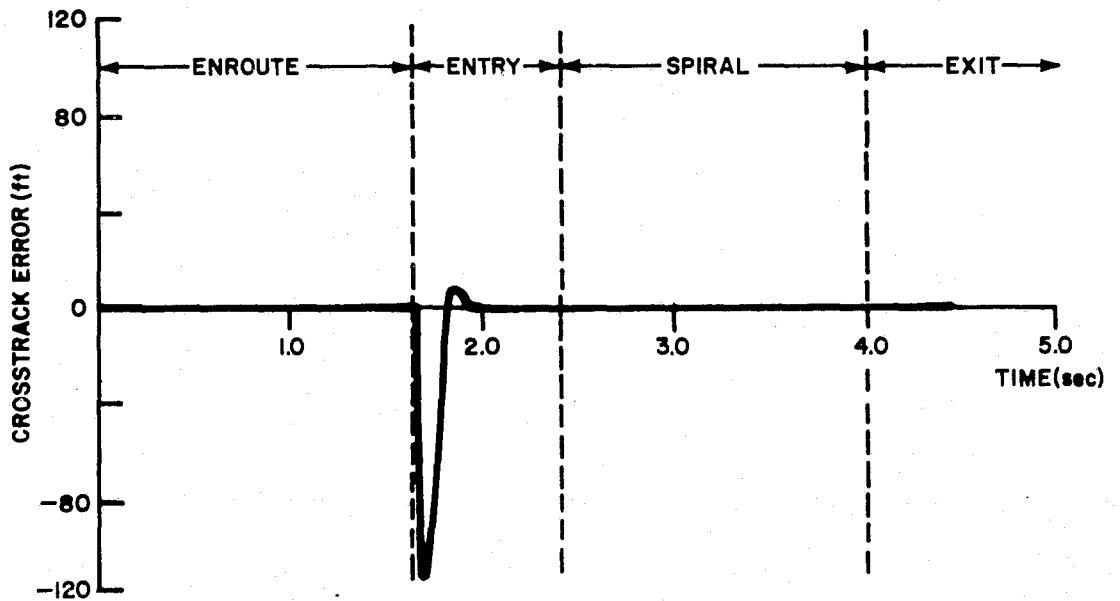
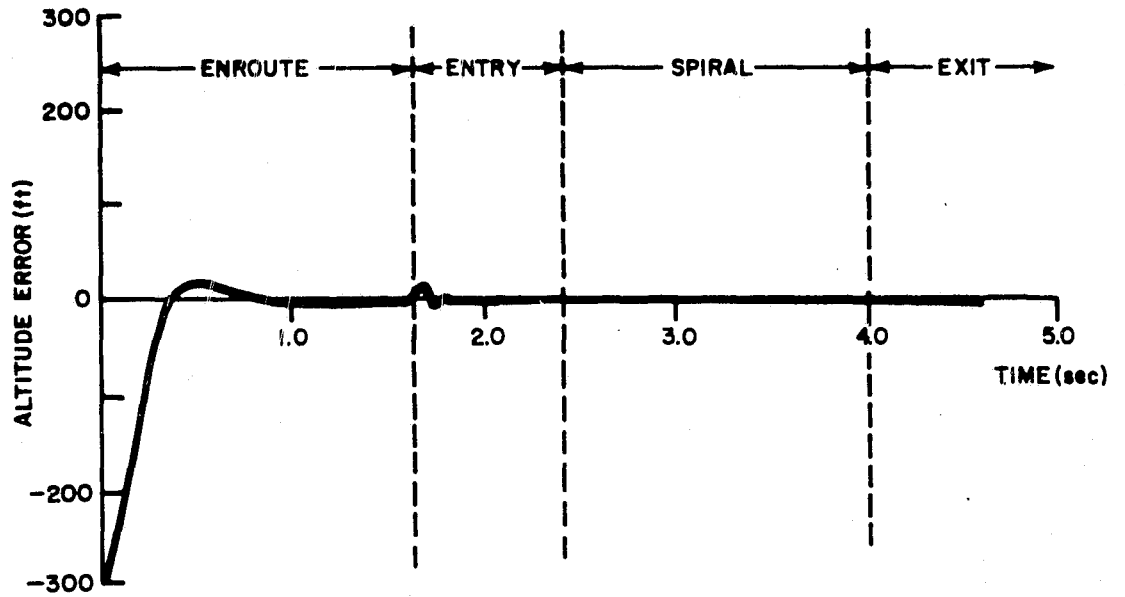


Figure 43. Initial Altitude Error of -300 ft.

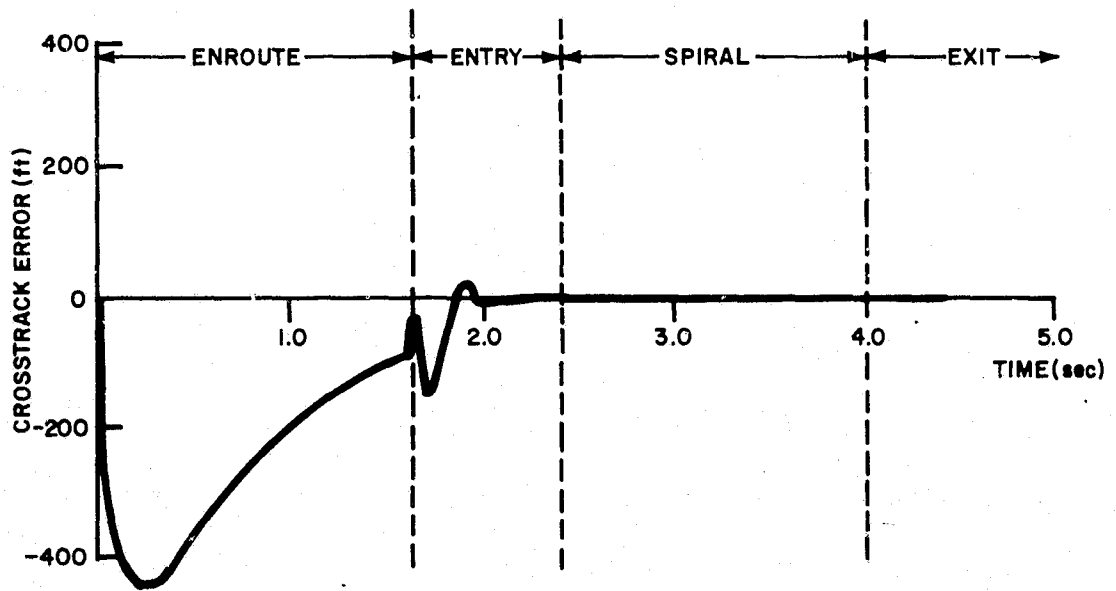
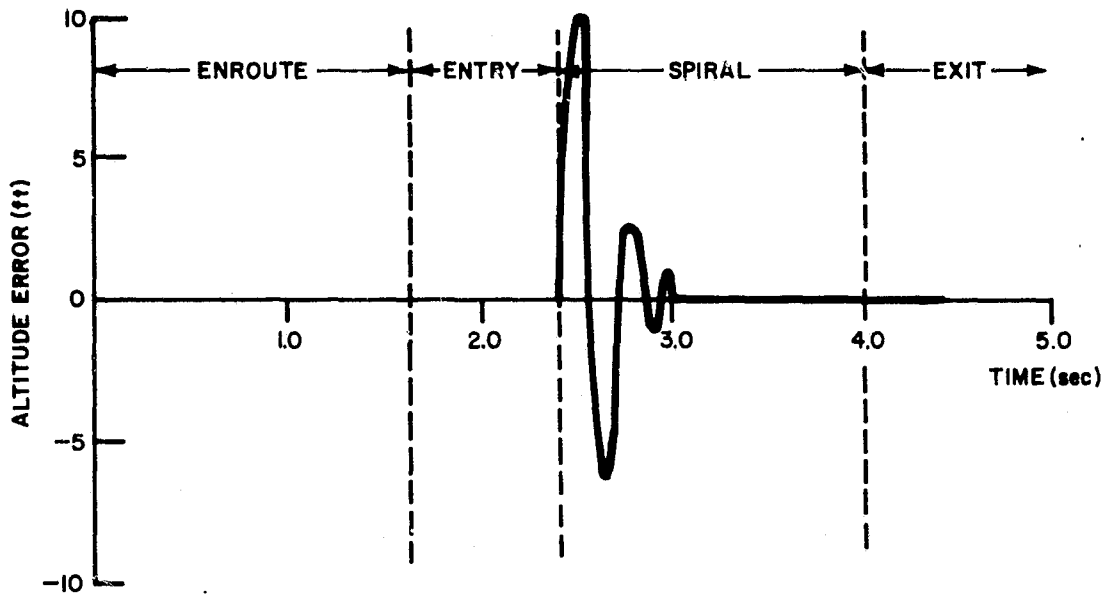


Figure 44. Initial Ground Track Error of -30 deg.

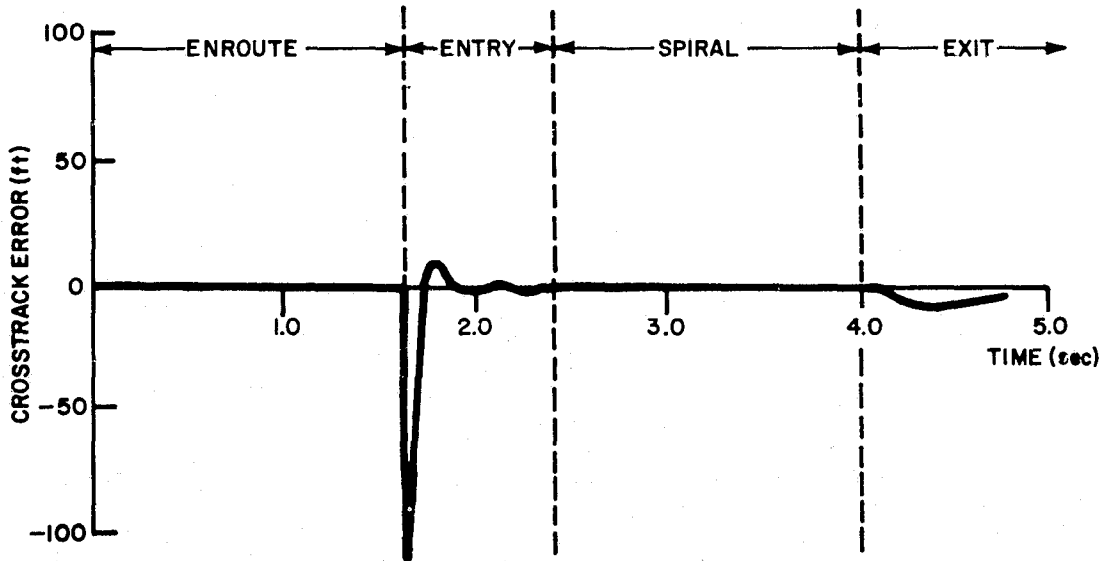
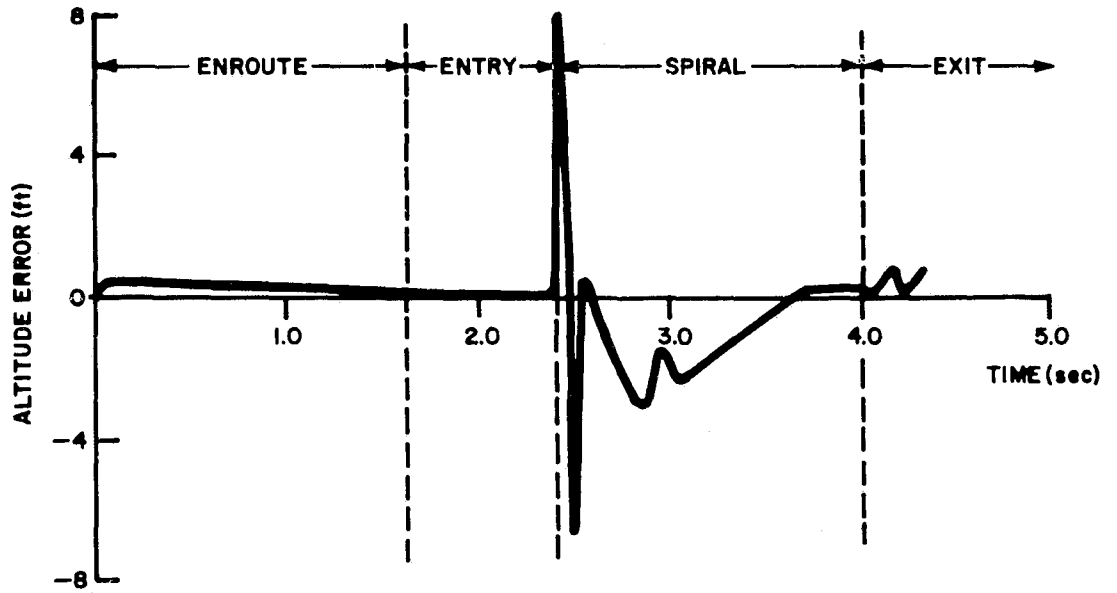


Figure 45. Constant Wind Direction Error of -90 deg.

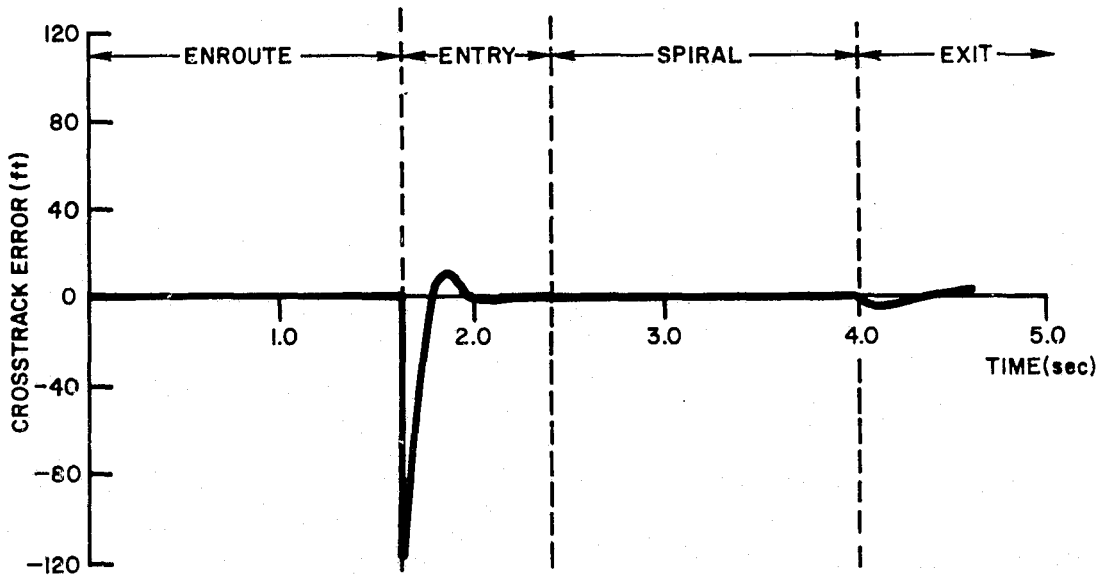
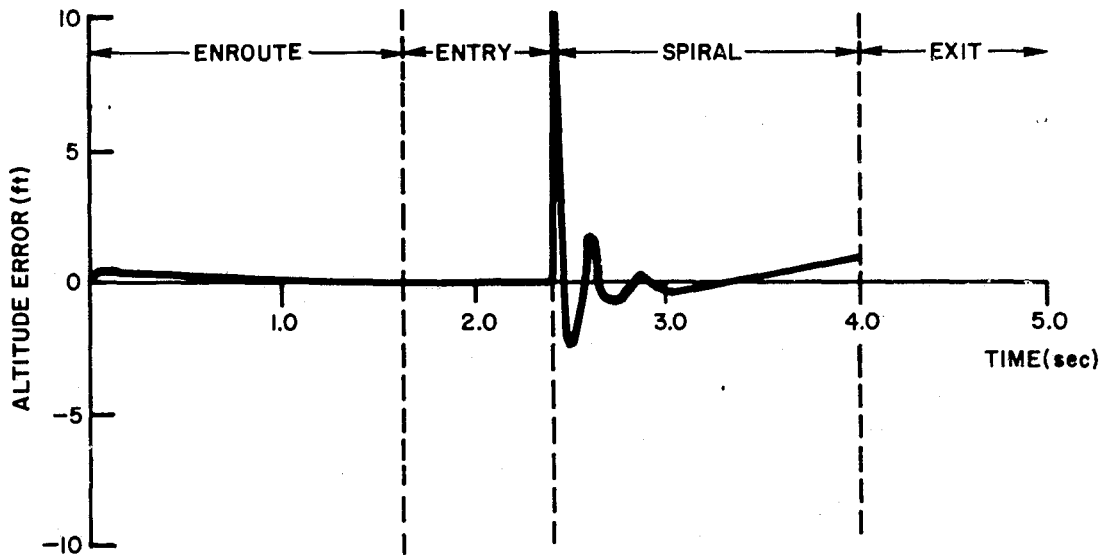


Figure 46. Wind Direction Shear Error of -90 deg/1100 ft.

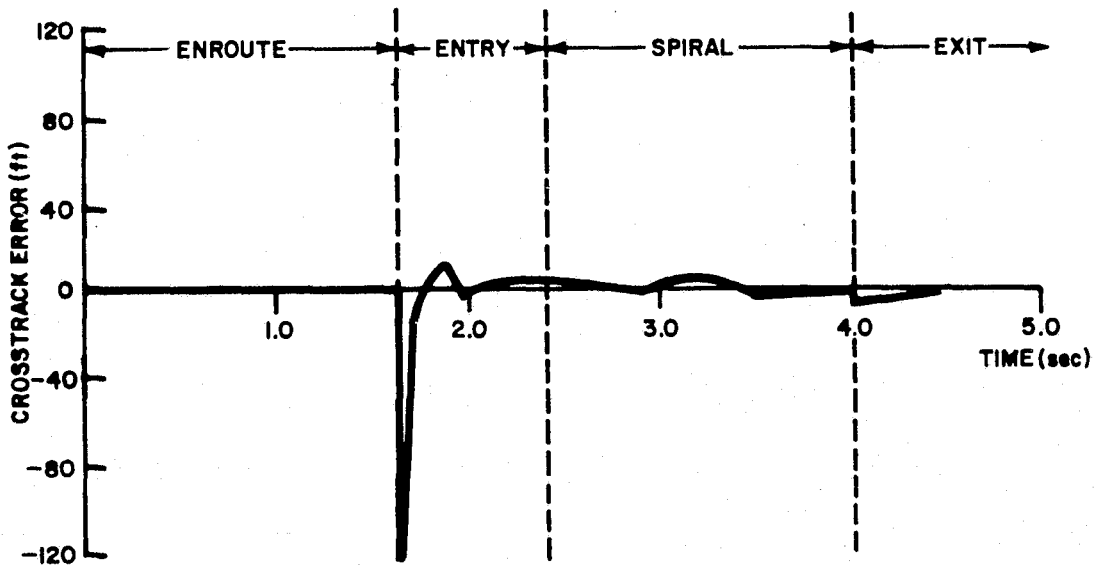
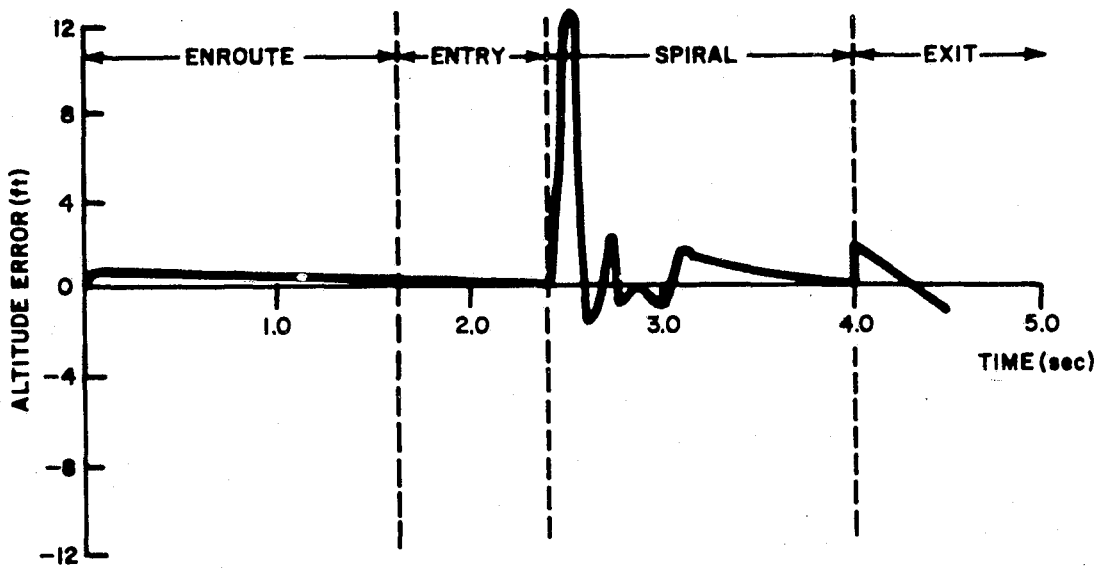


Figure 47. Nominal Wind Speed Error of 15 kts.

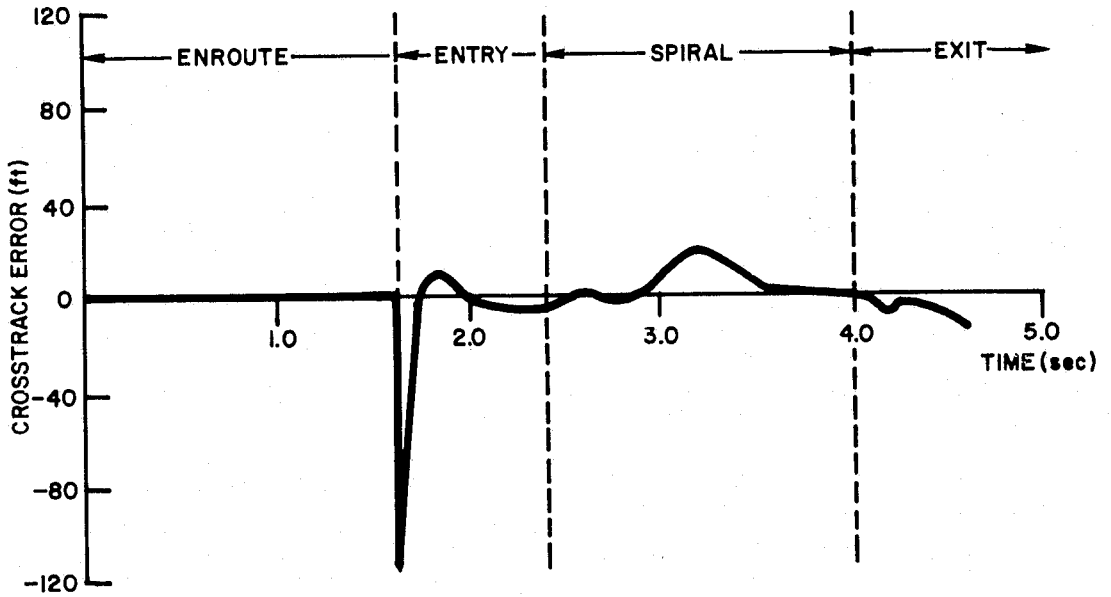
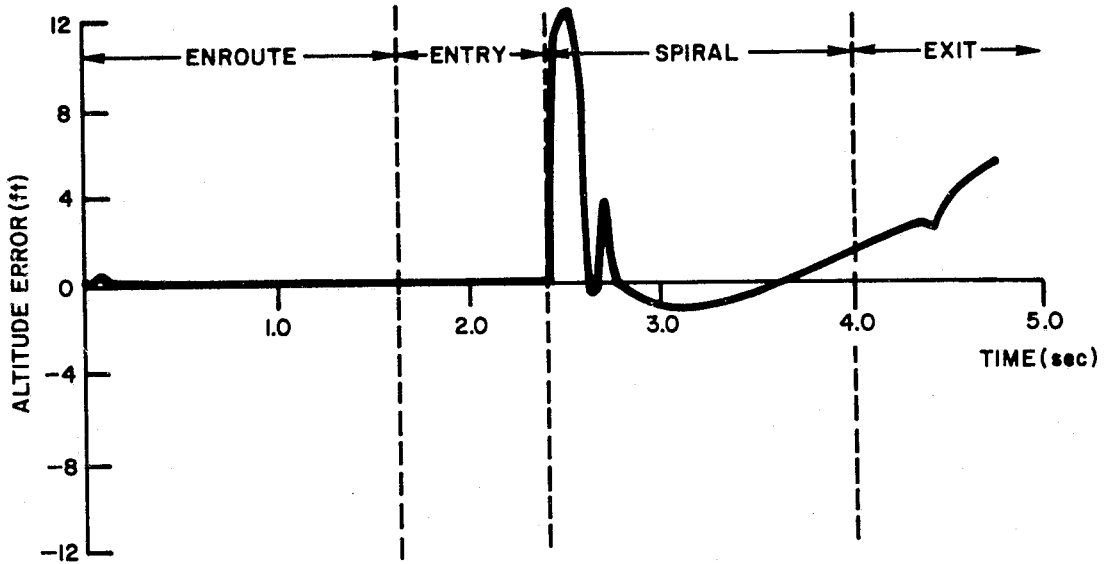


Figure 48. Nominal Wind Direction Error of -90 deg.

SECTION 9 SUMMARY AND CONCLUSIONS

Guidance and navigation requirements of a spiral descent approach concept for commercial VTOL operations have been investigated. The development of the spiral descent as a standard IFR approach procedure is an attractive and feasible means of satisfying several requirements for safe, efficient and independent VTOL operations. Although the spiral descent was first conceived as a means of providing independent IFR operations for VTOL aircraft at conventional airports, the technique is equally applicable to any heliport with airspace restrictions due to other traffic, noise constraints or obstructions.

The spiral descent retains most of the advantages of a vertical descent, but requires less power and fuel, maintains forward airspeed and controllability, and avoids the vortex ring state. The problem with the spiral descent operation is that it presents a difficult guidance and navigation task, particularly in a wind. The steady-state turn introduces an additional integration into the guidance and control loop, making it more difficult to stabilize.

The effect of the wind on the spiral descent is to require a continuous variation in the rotorcraft bank angle and heading rate to remain on the desired path. The choice of maintaining constant airspeed rather than constant groundspeed during the descent was made for several reasons: the descent airspeed can be selected for fuel economy; large airspeed variations could place the rotorcraft in unsafe flight regimes; and continually-varying longitudinal accelerations would be necessary to maintain constant groundspeed.

The basic concept adopted for the spiral approach guidance is that of a feedback system to keep the rotorcraft close to a prespecified nominal path. To simplify the analytical formulation, particularly for 3-D guidance, the spiral turn angle was used instead of time as the independent variable. For 4-D guidance, the nominal time must be computed as a function of the turn angle, which was shown to require the solution of an elliptic integral of the second kind. A truncated series expansion of the elliptic integral, keeping only the first two terms, was found to provide an accuracy of better than 0.3% in approximating the nominal time calculation.

The nominal spiral is based on constant radius, constant airspeed, constant rate of descent, and steady predicted winds. The controlled states are radial position, heading, airspeed, altitude and time (for 4-D guidance); the guidance outputs are commanded values of bank angle, longitudinal acceleration, and vertical speed. For passenger safety and comfort, the guidance commands must be limited to reasonable levels.

A linear perturbation analysis was used to select a satisfactory set of guidance gains for preliminary evaluation of the guidance concept. For 4-D guidance, time errors can be corrected by airspeed adjustments and/or by small changes in the radius. However, the latter technique couples the longitudinal and lateral guidance loops, and somewhat destabilizes the 3-D lateral response. Consequently, the feedback gain term providing bank corrections to timing errors was omitted from further analysis. The resulting guidance gains were used as initial values in the interactive nonlinear simulation. An iterative evaluation produced an improved set of gains, along with additional modifications to the guidance scheme.

As expected, the guidance system performance was found to be extremely sensitive to errors in the predicted wind used for the nominal calculations. Consequently, a wind estimator will be an essential element of the guidance system, both for 3-D and for 4-D guidance. The updated wind estimates are used to revise the nominal calculations of bank angle and heading during the descent. However, for 4-D approaches, the nominal time calculation uses the original wind prediction to maintain proper spacing between aircraft.

Two approaches were investigated for providing the onboard wind estimates. A Kalman filter was formulated using the linearized state equations with the guidance loops closed. The north and east wind components were each modeled as exponentially-correlated random processes (first-order colored noises). The two wind estimate equations must be augmented to the state equations, giving a 7th order error state vector. To implement the estimator, a 7 x 7 error covariance matrix must be propagated.

In lieu of the Kalman filter approach, a simplified wind estimator was developed by using the off-nominal values of bank angle and heading angle to indicate errors in the tangential and radial wind components, respectively. The simplified estimator requires the specification of a characteristic angle, over which the wind estimates are averaged. In a descent through a constant wind, initial errors in the estimate will be reduced to $1/e$ over the characteristic turn angle; in a constant shear, the wind estimate will lag the actual wind by approximately the characteristic angle. Simulation results have verified the performance of the simplified wind estimator, using a characteristic angle of 90° .

A phase plane analysis was used to analyze the behavior of the bank guidance loop for large errors in radial position and/or heading. In such situations, the bank angle is constrained and the system response is nonlinear. For initial spiral offsets greater than 1200-1500 feet, the bank guidance law will command a continuous maximum bank angle, resulting in a tight circular turn which never intercepts the desired path. To ensure spiral capture, the bank guidance law was modified to produce a constant nominal intercept angle for arbitrarily large radial errors. An intercept angle of 60 degrees was found to be satisfactory with the interactive simulation.

The transitions from the enroute guidance mode to the spiral, and from the spiral to hover and touchdown, are critical phases which must be accomplished smoothly. For the present study, these transition paths have been defined as straight flight segments tangent to the nominal spiral. For consistency with the spiral itself, the independent variable has been selected as along-track distance in place of time. The nominal entry transition assumes constant altitude and constant deceleration to the nominal spiral airspeed, while the exit transition assumes a constant rate of descent. The guidance laws for the transition segments are nearly identical to those during the spiral, with the addition of a nominal deceleration term in the acceleration loop. The bank guidance loop is modified to ensure capture in the same manner as in the spiral. Simulation results have verified the performance of the transition segment guidance algorithms.

Two digital simulation programs were developed for analyzing and evaluating the spiral guidance concept. An inhouse, interactive simulation, containing a simple model of the vehicle dynamics and no navigation errors, was used to verify the guidance and wind estimator algorithms and to study guidance parameter adjustments.

This simulation was especially valuable in providing a clear understanding of the entire spiral guidance problem.

The second simulation is a modification of Program VALT, and was used to evaluate the performance of the complete spiral guidance concept for a typical approach to New York City's Kennedy International Airport. The VALT simulation includes both the enroute guidance and spiral guidance algorithms, a general model of the deterministic and random wind inputs, stochastic models of the various navigation sensors, and a Kalman filter for generating the navigation system outputs. The VALT simulation was exercised for a number of parametric variations to evaluate the performance of the spiral guidance concept. Initial condition errors can produce significant errors in the navigation system due to nonlinear effects, as well as timing errors for 4-D guidance. Wind errors give essentially the same results as the interactive simulation; the simplified estimator determines the winds with a delay equivalent to the characteristic turn angle. Variations in the guidance parameters verify the analytical results obtained with the linearized system model.

In summary, the investigation has demonstrated that the spiral guidance technique is technically feasible for commercial VTOL operations. Wind errors have a very important effect on the guidance system performance. Consequently, a wind estimator will be required for the spiral approach to adjust the nominal path appropriately. Finally, the spiral guidance algorithms and models are general, and can be applied easily to various rotorcraft and landing sites.

SECTION 10

RECOMMENDATIONS FOR ADDITIONAL RESEARCH

During the course of this study, several areas have been identified in which additional research is needed to further evaluate the feasibility of the spiral approach guidance concept for commercial VTOL operations. These subject areas are outlined below.

10.1 SPIRAL GUIDANCE FLIGHT TEST PROGRAM

A full-scale flight evaluation of the spiral guidance technique should eventually be conducted as part of the VALT flight test program. In anticipation of this, a detailed flight test plan should be prepared to integrate the spiral guidance tests with the other planned experiments. This is especially important in the present VALT organization since several research groups comprising a variety of technical disciplines will be involved in planning, conducting and evaluating the flight test program.

A preliminary outline of the major elements to be considered in the spiral guidance flight evaluation is presented in the following subsections.

10.1.1 PURPOSE OF TEST

- Verify conclusions of computer simulation and analytic studies by actual flights under automatic control
- Evaluate ability of human pilot to fly manual spirals using flight director commands
- Obtain pilot evaluation of operational procedures
- Check for possible disorientation due to vertigo
- Determine any impact of spiral on passenger comfort

10.1.2 TEST EQUIPMENT AND FACILITIES

- VALT CH-47 helicopter test bed including measurements of position, altitude, groundspeed, vertical speed, airspeed, heading, bank angle and software
- Attitude autopilot
- Flight director

- Timely wind soundings
- Ground tracking radar
- Test pilots - hooded subject plus safety pilot
- Flight test support facilities
- Post-flight data reduction

10.1.3 FLIGHT PROCEDURES

Fly a large matrix of spirals with following variations:

- Automatic and manual control
- Various rates of descent from level to 1500 ft/min
- 3-D and 4-D guidance algorithms
- Various test pilots
- Various wind conditions including shear and turbulence if practicable
- Various initial conditions to evaluate capture logic
- Various radii of spiral
- Various speeds
- With and without wind estimate or variations of guidance gains

10.1.4 DATA OBTAINED

- Ground-based measurements of position and velocity versus time
- Airborne measurements of airspeed, heading, altitude, attitude and accelerations
- Wind estimates based on balloon soundings
- Guidance system commands
- Test pilot Cooper ratings

10.1.5 DATA ANALYSIS

- Reduce flight data with plots and statistics of results
- Attempt to demonstrate that flight results were predicted by preliminary analysis
- Explain differences between analysis and flight results
- Compare manual and automatic results
- Assess practicability of spiral descent as operational technique
- Recommend procedures, parameter values, limitations, etc., based on combined results of analytic and flight evaluations.

10.2 GUIDANCE FOR SPIRAL EXIT AND LANDING

Work on spiral descent guidance under the present contract has shown the advantages and feasibility of this VTOL approach technique. The spiral enables a VTOL aircraft to avoid obstacles and noise sensitive areas, to operate independent of CTOL traffic patterns, and continue to maintain reasonable airspeed for increased safety. It allows the VTOL vehicle to descend into confined air space with effective glide slope angles that are relatively shallow. Exit from the spiral occurs nominally at 60 knots at an altitude from 200 to 400 feet and is followed by deceleration and landing. The exit and landing phase needs additional study to determine the placement of the spiral relative to the landing pad.

Present studies have been limited to landing along a tangent to the spiral (see Figure 49). However, alternate concepts, such as landing inside of the spiral, along the spiral, or outside the spiral are feasible and could be advantageous for some

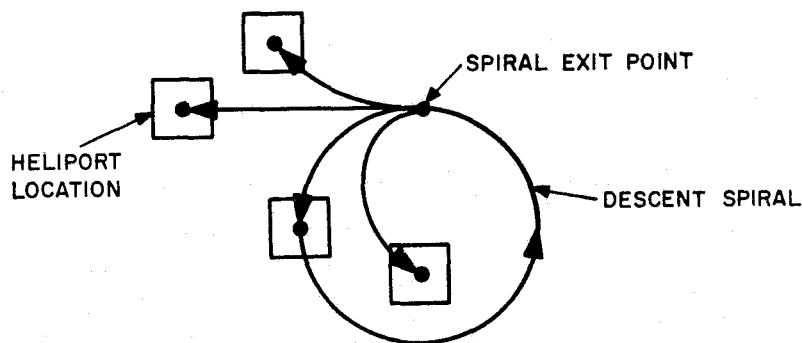


Figure 49. Possible Heliport Locations Relative to the Descent Spiral.

heliports. A related question to be considered is whether there should be only one spiral for several landing pads or a dedicated spiral for each pad. Factors which influence these decisions are:

- Geography of the landing area
- Available navigation coverage
- Operational flexibility
- Magnitude of the necessary maneuvers
- Possibility of pilot vertigo
- Difficulty of the guidance and control tasks
- Location of CTOL air traffic patterns
- Location of noise sensitive areas

Guidance of the VTOL vehicle must undergo a transition from an airspeed control mode during approach to a hover mode prior to landing. The airspeed control mode is characterized by coordinated turns using roll to control the direction of the airspeed vector; whereas, the hover mode is characterized by heading control through the yaw channel with pitch and roll used to maintain ground position and velocity. The transition will normally occur after exit from the spiral during the deceleration for landing. To accomplish this transition, a description of the nominal path to each available landing pad must be formulated, along with a guidance scheme to maintain that path during the transition. The scheme then should be evaluated to determine its performance in the presence of winds, guidance errors, and parameters in the guidance algorithms.

10.3 WIND ESTIMATION IN THE VALT FLIGHT PROGRAM

The present onboard computer software configuration for the Langley VALT flight program guidance logic uses a flight-path-following system that seeks to null cross-track position error and cross-track ground speed error. The position is measured by a ground tracking radar, and the ground speed is derived from the position measurements. In an operational system, ground speed information would not generally be available from the ground. Although onboard inertial navigation systems or Doppler radars could be used to provide the ground-referenced velocity, both of these equipments are relatively expensive compared to more conventional air data and vehicle attitude measurements.

Flight-path following without ground speed information substitutes heading error for cross-track ground speed error. A wind estimate or integration in the feedback path of the cross-track position error is required to prevent a steady-state position offset. Wind estimation is preferable since heading changes introduce a variable cross-track wind component, even when the wind velocity is constant relative to the ground. The present VALT flight computer software can be modified to utilize the same wind estimator developed here for spiral descent guidance. The nominal flight path developed for the flight program consists of patched elliptical arcs which can degenerate into circles and straight lines. Although the ASI wind estimator was developed here for use along circular segments, the concept can be extended to handle elliptical arcs. This would give the VALT flight guidance system an additional capability for wind estimation without ground speed measurement, and consequently would provide more accurate tracking when only air data and attitude information are available. This, in turn, would lead to a more realistic assessment of the requirements for inertial navigation or Doppler radar.

Consequently, an evaluation should be made of the performance of the present onboard computer guidance logic for the VALT flight program in the absence of ground speed information. A wind estimator compatible with the guidance logic utilized on elliptical flight paths should be designed using measurements of position, attitude and airspeed but without ground speed information. Existing computer programs could be modified to simulate the wind estimation scheme when operating along elliptical arcs. The simulation results would predict the performance comparison between the existing VALT flight guidance logic with ground speed information available, as opposed to the modified logic without ground speed information but with the new wind estimator. Flight experiments could test the validity of conclusions drawn from the computer simulation.

REFERENCES

1. Hoffman, W. C.; Hollister, W. M.; and Howell, J. D.: Navigation and Guidance Requirements for Commercial VTOL Operations, NASA CR 132423. Aerospace Systems, Inc., ASI-TR-74-17, January 1974.
2. Sokolnikoff, I. S.; and Redheffer, R. M.: Mathematics of Physics and Modern Engineering, McGraw-Hill, New York, 1958.

PRECEDING PAGE BLANK NOT FILMED